INFORMATION TO USERS

This manuscript has been reproduced from the microfilm master. UMI films the text directly from the original or copy submitted. Thus, some thesis and dissertation copies are in typewriter face, while others may be from any type of computer printer.

The quality of this reproduction is dependent upon the quality of the copy submitted. Broken or indistinct print, colored or poor quality illustrations and photographs, print bleedthrough, substandard margins, and improper alignment can adversely affect reproduction.

In the unlikely event that the author did not send UMI a complete manuscript and there are missing pages, these will be noted. Also, if unauthorized copyright material had to be removed, a note will indicate the deletion.

Oversize materials (e.g., maps, drawings, charts) are reproduced by sectioning the original, beginning at the upper left-hand corner and continuing from left to right in equal sections with small overlaps.

Photographs included in the original manuscript have been reproduced xerographically in this copy. Higher quality 6" x 9" black and white photographic prints are available for any photographs or illustrations appearing in this copy for an additional charge. Contact UMI directly to order.

ProQuest Information and Learning
300 North Zeeb Road, Ann Arbor, MI 48106-1346 USA
800-521-0600

MULTIBEAM SMART ANTENNA SYSTEMS FOR WIRELESS COMMUNICATIONS

By

XIAOMING YU, M.Eng.(Tsinghua University)
B.Eng.(Shanghai Jiaotong University)

A Thesis
Submitted to the School of Graduate Studies
in Partial Fulfilment of the Requirements
for the Degree
PhD

McMaster University

MULTIBEAM SMART ANTENNA SYSTEMS FOR WIRELESS COMMUNICATIONS

PHD (1999)
(Electrical and Computer Engineering)

MCMASTER UNIVERSITY
Hamilton, Ontario

TITLE: **Multibeam Smart Antenna Systems for Wireless Communications**

AUTHOR: Xiaoming Yu
M.Eng.(Tsinghua University)
B.Eng.(Shanghai Jiaotong University)

SUPERVISOR: Dr. John Litva

NUMBER OF PAGES: xii, 123

ABSTRACT

Smart antennas have emerged as one of the key technologies in wireless communications. This thesis focuses on developing algorithms and structures that can be applied to one of the most important types of smart antennas – the multibeam smart antenna - in order to improve the quality and capacity of both existing and future wireless networks. A large database, consisting of vector channel measurement data using an 8-element circular antenna array is analyzed to investigate the underlying characteristics of the multibeam smart antenna in practical propagation environments. Extensive vector channel simulations are also conducted, including the innovative work on the simulation of smart antennas in Frequency Division Duplexing(FDD) systems. Based on the data analysis and simulation results, two multibeam smart antenna algorithms, one for reception and one for transmission, are proposed. Significant performance and capacity improvements can be achieved using these two algorithms. The proposed multibeam smart antenna reception algorithm for DS-CDMA system is expected to have important application in both existing and the third generation CDMA systems, while the proposed multibeam smart antenna transmission algorithm can be used in FDD wireless networks to solve the downlink problem.

ACKNOWLEDGEMENT

I would first and foremost like to express my sincere thanks and deep appreciation to my supervisor, Dr. John Litva, for his guidance, support, and encouragement throughout this work. I am grateful to Dr. David Conn and Dr. Paul Jessop, the members of my supervisory committee, for their kind assistance and helpful comments.

My fellow members of the Wireless Technology Group at the Communications Research Laboratory have helped me in many ways. I would like to express my deep appreciation for their help, support, and friendship. I would also like to thank the staff of the Communications Research Laboratory and the Department of Eletrical Engineering and Computer Engineering for their help and collaborations.

Last, but not least, special thanks to my wife, Li, for her love, inspiration and support.

Contents

List of Figures

List of Tables

Chapter 1

Introduction

The use of radiated electromagnetic waves enables us to communicate with other people or vehicles that move around on land, on the sea, in the air, or in outer space. Early wireless devices, such as car phones, were bulky, pricey, and rarely worked beyond their limited geographic coverage areas. Over the years, wireless technology has improved by leaps and bounds, making it possible for today's wireless devices to be remarkably convenient, economical, and popular. In recent years, the global wireless business has seen an annual increase of 20 to 30%. In 1995, there were about 82 million wireless subscribers worldwide. At the end of 1997, there were 340 million – a four-fold increase. According to some projections there will be up to approximately 1.45 billion wireless subscribers by the year 2010, extending to nearly a fifth of the world's population [1].

With the rapid development of wireless communications, techniques for enhancing the performance of the present systems are ever more hotly pursued. Today's wireless system designers are faced with a number of challenges, such as the complicated time-varying communications channel, limited spectrum, limited capabilities of batteries, etc. With the recent introduction of Personal Communications Service (PCS) systems which aim at providing communications *anywhere anytime*, service quality, coverage and data rates far exceeding those of the current wireless infrastructure are required.

It is expected that many technologies, which include advanced multiple access methods and various sophisticated signal processing techniques, will be used to meet such diverse requirements. Current wireless modems mainly use temporal signal processing techniques such as digital modulation and demodulation, channel/source coding and decoding, equalization and diversity combining, etc. However, one main drawback of such temporal processing methods is that they do not effectively address the co-channel interference problem, which places a major limitation on the quality and capacity of wireless networks. Co-channel interference signals usually arise from different geographical locations: therefore one way to reduce co-channel interference is to use spatial processing. By adding another dimension, namely, space, to signal

processing, one can dramatically improve the quality and capacity of current wireless communications systems.

As was pointed out in [2], time domain processing techniques have virtually been squeezed down to their last one-tenth of a decibel in terms of performance improvement. Spatial processing is truly the last frontier in terms of the rewards that can be achieved in improving the performance of wireless communications systems.

1.1 Spatial Processing – the Last Frontier

The smart antenna, or adaptive beamforming concept, is a technology that was initially developed for sonar and radar applications [3, 4, 5, 6, 7, 8]. A smart antenna system is an antenna system that has signal-processing capability and can change its radiation pattern automatically in response to the signal environment in order to improve radio link performance. It provides a means to separate desired signals from interfering signals even if they are co-located in the same frequency band. In addition to interference suppression, signal-fading reduction and signal strength enhancement can also be achieved by the spatial and time processing capability of the smart antenna.

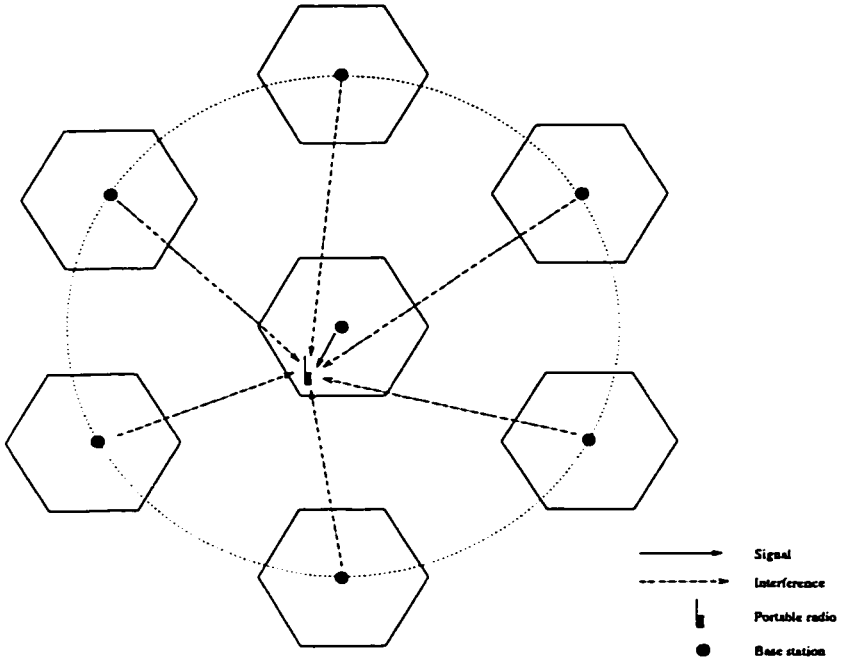

Figure 1.1: First tier of interference in a cellular system with cluster size of 7

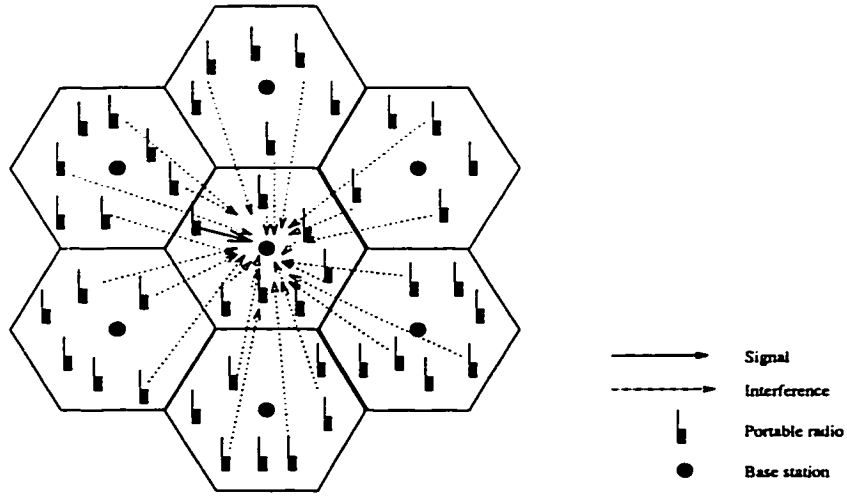

Figure 1.2: Co-channel interference in a CDMA system

In a cellular scenario, co-channel interference usually arrives with a larger angle spread than the desired signal. Figure. 1.1 shows the first tier of co-channel interference in a cellular system that has a cluster size of 7. CDMA systems are different from the situation illustrated in Figure. 1.1. In CDMA systems, many users share the same wideband channel within the same cell by using different spreading codes. Since they use the same channel at the same time and are randomly located within the same cell, the angle spread of the interference that one user experiences is larger than that for the desired signal. This is illustrated in Figure. 1.2. In most cases, it is reasonable, as a first order approximation, to assume that the interference is spread over 360^0 in azimuth.

Smart antennas can be used in cellular radio networks to improve signal quality and to increase capacity. [1] Smart antenna systems are applicable to analogue FDMA, digital TDMA as well as CDMA systems. The use of smart antennas offers a number of benefits [9, 10, 11, 12]:

- Reducing co-channel interference (CCI) by generating antenna pattern nulls pointed in the direction of co-channel interference sources. [2]

[1] When considering smart antennas for wireless communications, we usually consider deploying the smart antenna at the base station site. There are two main reasons for this deployment strategy: cost and size constraint. The cost of using a smart antenna at the mobile side would be prohibitively expensive; the size of a smart antenna makes it unsuitable to be used at the mobile stations in most cases.

[2] CCI reduction is particularly important as it allows the frequency re-use distance (or cluster size) to be reduced, thus improving capacity. Ultimately, it may even be possible to re-use frequencies within a single cell. This is commonly referred to as Space Division Multiple Access (SDMA).

- Improving coverage and power efficiency by utilizing the available directional antenna gain.
- Reducing inter-symbol interference (ISI) through multipath rejection. [3]
- Reducing the undesirable effects of fast fading caused by multipath propagation by way of antenna array processing.
- Assisting users in location finding through the use of antenna arrays.

It is commonly agreed that there are two approaches that can be used when applying smart antennas to wireless communications: adaptive smart antennas and multibeam smart antennas [13, 14]. Depending on the operational environment and factors such as cost, one type may be preferred over the other.

Adaptive smart antennas are more flexible and have the potential of offering better performance than multibeam smart antennas. However, they also face a number of challenges:

- High computational complexity – The adaptive array signal processing techniques that adaptive smart antennas use to determine the optimum weight coefficients are complicated, especially in vehicular communication systems where the desired and interference signals vary rapidly due to fading.
- High tracking requirements – Small changes in spatial angle distributions of signals often result in big changes in weight coefficients to meet the optimality requirements. If adaptive algorithms do not track the vector channel well enough, the antenna's performance may degrade [15].
- Downlink problem – It is difficult to find an optimal set of weights for transmitting signals from the base station to the mobile station for an adaptive smart antenna in FDD systems.

The multibeam smart antenna is easier to implement and more robust. In recent years, there has been increased interest, both from academia and industry, in applying multibeam smart antennas for the purpose of increasing the capacity and quality of wireless networks [16, 17, 9, 18, 19, 10, 20, 21]. Our research on multibeam smart antennas also shows two additional advantages over adaptive smart antennas:

1. The tracking problem associated with multibeam smart antennas is easier to solve due to the fact that the angles-of-arrival (AOAs) of multipath signals changes slowly with time.
2. Effective downlink transmitting algorithms can be developed for multibeam smart antennas.

[3] The effective delay spread of the channel can be reduced to support higher bit rates without the use of an equalizer.

1.2 Focus of Research

The focus of this thesis is to carry out research on multibeam smart antenna algorithms and structures which can be used in micro/pico-cells for the current (2G) and next generation (3G) wireless systems. In particular, the following goals are to be achieved:

- To develop multibeam smart antenna algorithms that are suitable for the downlink transmission in Frequency Division Duplexing (FDD) systems.
- To develop multibeam smart antenna algorithms for improving the future third generation (3G) wireless systems, particularly, multibeam smart antenna algorithms which can greatly improve the performance of the proposed wideband CDMA systems.
- To extend our understanding of vector multipath channels in micro/pico-cell environments by analyzing the results from vector channel sounding and computer simulations.

1.3 Thesis Overview

Following the introduction in Chapter 1, Chapter 2 is devoted to the study of the wireless channel with the emphasis on vector channel characterization. Chapter 3 presents wireless standards and their impact on the structures and algorithms of the smart antenna. Chapter 4 describes multibeam smart antenna structures and diversity combining algorithms. Chapters 5 and 6 present the results of the research on multibeam smart antenna algorithms using both practical data and computer simulation. In Chapter 5, an effective downlink transmission algorithm is developed and its performance improvements are evaluated and analyzed. In chapter 6, a multibeam smart antenna multiuser detection (MSAMD) algorithm is developed and analyzed. The thesis concludes with a summary of the findings of this thesis in Chapter 7.

1.4 Contributions

The contributions made by this thesis include:

1. Developed an effective downlink multibeam smart antenna algorithm for FDD systems. Provided both analysis and simulation results of the performance improvements.
2. Conducted innovative research on using vector channel models to simulate Frequency Division Duplexing(FDD) smart antenna systems. Successfully applied

the Geometrically Based Single Bounce (GBSB) model to the simulation of multibeam smart antenna downlink transmission in FDD systems.

3. Proposed the use of multibeam smart antennas to reduce the computational complexity of current multiuser detection scheme[22, 23].

4. Proposed the partial decorrelation detection algorithm[22].

5. Developed a partial decorrelator based multibeam smart antenna multiuser reception algorithm which can improve both the performance and capacity of CDMA systems[24, 22].

6. Designed and implemented (with Zhaonian Li and Chen Wu) a multibeam microstrip smart antenna array which is suitable for the current 1.9 GHz PCS wireless networks[24, 25].

7. Analyzed the effects of the propagation environment and parameters such as signal bandwidth and antenna beamwidth, on the operation of multibeam smart antennas using practical vector channel data.

8. Designed and calibrated the Talaris vector channel sounding system (with other members of the Wireless Technology Group). Collected vector channel propagation data in both indoor and outdoor environments.

Chapter 2

The Wireless Channel

The wireless channel places a fundamental limitation on the performance of wireless communication systems. The existence of multipath, i.e., signals that travel along different propagation paths, with different time delays, attenuations and phases, gives rise to a highly complex, time-varying transmission channel in which the smart antenna must operate. In order to decide on the optimum method for applying smart antenna systems, a deep understanding of the wireless channel is essential. In particular, the wireless channel has to be characterized with regard to both its spatial and temporal characteristics, i.e., vector channel characteristics.

This chapter focuses on the fundamentals of propagation in wireless communication. The wireless channel is usually studied in terms of both its large-scale effects and small-scale effects. The large-scale effects involve the variation of the mean received signal strength over large distances or long time intervals, whereas small-scale effects involve the fluctuations of the received signal strength about a local mean, where these fluctuations occur over small distances or short time intervals.

This chapter begins with Section 2.1 in which the fundamentals of radio wave propagation, such as basic propagation mechanisms and the free space propagation model are reviewed. Large-scale and small-scale fadings are discussed in Sections 2.2 and 2.3. The emphasis is placed on small-scale fading rather than large-scale fading. The reason is that smart antennas are usually designed to mitigate the effects of co-channel interference and fading based on small-scale channel characteristics. Section 2.4 describes vector channel models. Up to the present, the wireless channel modeling has been mainly focused on temporal models. The reason is that radio technologies employed in the past have been largely based upon time and frequency domain processing. With the introduction of spatial processing, especially smart antenna technology, vector channel models become important. Although several vector channel models have been introduced recently [26, 27], much work remains to be done.

2.1 Fundamentals of Radio Wave Propagation and Channel Characterization

2.1.1 Free Space Propagation Model

If the transmitting antenna is free from any obstructions, wave propagation is described by the free space propagation model. In free space, a radio wave propagates spherically from its source, so that the total radiated power is distributed equally over the surface of a sphere whose radius is equal to the distance between the transmitter and receiver. The power density at a point on the sphere with radius of R is

$$S = \frac{G_t P_t}{4\pi R^2} \tag{2.1}$$

where G_t is the gain of the transmitting antenna, P_t is the transmitted power.

The power intercepted by the receiver antenna is equal to the power density multiplied by the effective area of the antenna, i.e.,

$$P_r = S \times A_{eff} \tag{2.2}$$

where A_{eff} is the effective area. Antenna theory shows that this area is related to the antenna gain in the direction of the received signal by the expression [28]

$$A_{eff} = \frac{G_r \lambda^2}{4\pi} \tag{2.3}$$

where G_r is the gain of the receive antenna, and λ is the wavelength.

Eqns. (2.1),(2.2) and (2.3) combined gives the path loss L as

$$L = \frac{P_r}{P_t} = \frac{G_t G_r \lambda^2}{16\pi^2 R^2} \tag{2.4}$$

or in decibels for which L is usually expressed as

$$L_{dB} = 32.4 + 20\log R + 20\log F - 20\log G_t - 20\log G_r \tag{2.5}$$

Where F is the frequency expressed in MHz and the unit of R is km.

Although radio wave propagation in wireless communications usually cannot be considered as free space propagation because of natural and man-made obstructions, as well as the effect of the atmosphere and ionosphere, the free space model is a useful abstraction. It is a place to start when developing a model for propagation in practical environments.

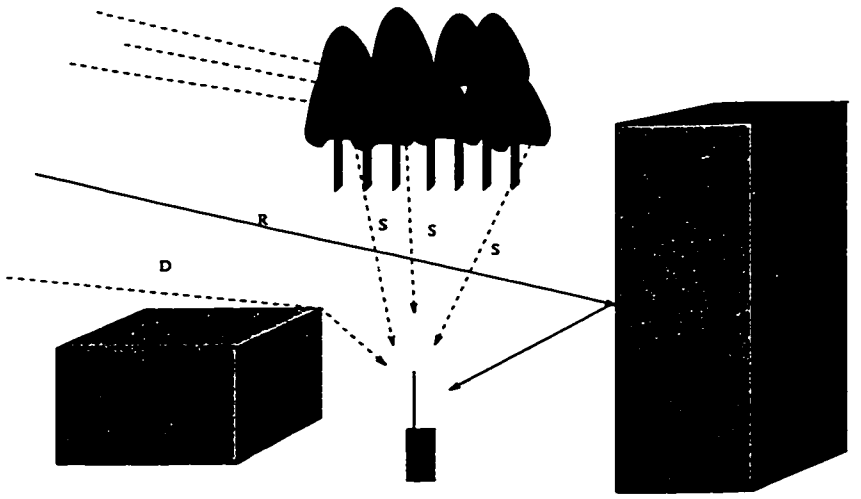

Figure 2.1: Three basic propagation mechanisms

2.1.2 Basic Propagation Mechanisms

The mechanisms governing radio wave propagation are complex and diverse. They are generally characterized into three basic forms, namely, reflection, diffraction, and scattering. Figure. 2.1 illustrates these three basic mechanisms, where paths labeled with R denote reflection, D and S denote diffraction and scattering respectively.

Reflection occurs when a radio wave impinges upon an object which has very large dimensions compared to the wavelength of the radio wave. Both man-made and natural objects produce reflections; building surfaces and the ground are common examples.

Diffraction occurs when there are objects with sharp edges obstructing the path of a radio wave. Based on Huygen's principle, secondary waves are formed behind the obstruction even though there is no line-of-sight (LOS) path connecting the transmitter and receiver. Diffraction happens most frequently in non-line-of-sight (NLOS) situations where there is no direct path between the transmitter and the receiver.

Scattering occurs when there are objects on the order of or smaller than the radio wavelength in the propagation path. Scattering also occurs on large *rough* surfaces. Scattering causes radio energy to be radiated in many different directions. Trees and lamp posts are common objects giving rise to scattering in wireless communications.

These three mechanisms, alone or combined, depending upon the situation under consideration, can be used to explain both large-scale and small-scale wireless channel characteristics. For example, if the mobile station has a LOS path to the base station in addition to the direct path, reflection and scattering are usually

important factors; while if there is no LOS to the base station, diffraction and scattering are most likely to dominate the propagation. As the mobile station moves over a few wavelengths, the instantaneous received signal power will fluctuate rapidly giving rise to small-scale fading. When the transmitted signal is a narrowband signal, [1] the received signal can usually be modeled as a random signal with Rayleigh distributed amplitude and uniformly distributed phase. As the mobile station moves over larger distances, the local average of the received signal power will gradually decrease although the rate of change is much slower. The local average of the received signal power is usually computed over 5 to 40 wavelengths in order to average out the small-scale fading.

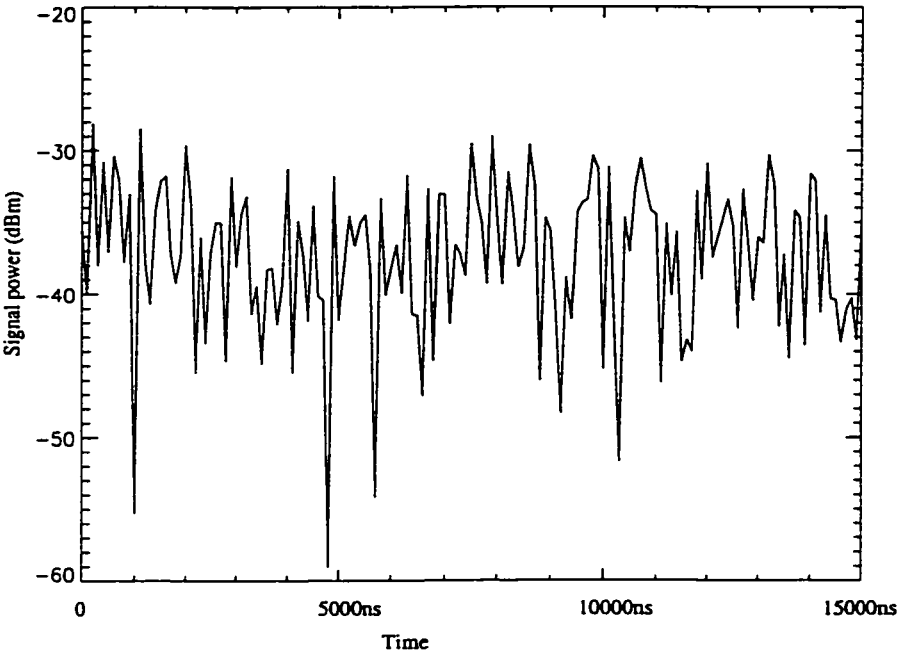

Figure 2.2: Fading signals received at the mobile station during a measurement on the McMaster Campus

Figure. 2.2 illustrates large-scale and small-scale signal fading taken from the measurements carried out on the McMaster Campus. The sampling rate is $10MHz$, and the result shown is obtained when the mobile radio moves at pedestrian speed.

[1] When its bandwidth is smaller than the coherent bandwidth of the channel, we view the signal as narrowband. See Section 2.3.3 for a complete treatment of the concept of channel coherent bandwidth.

2.1.3 Multipath Fading

In wireless communications, a radio wave usually propagates along a number of different paths before it reaches the receiver. In a typical scenario, there is often no direct line-of-sight (LOS) propagation between the transmitter and the receiver. Even if there is a LOS path, multipath still occurs due to reflection and/or scattering from the ground and surrounding objects. Propagation is mainly by way of the combination of reflection, diffraction, and scattering, although one or two of them may be dominant depending on the practical situation.

Multipath creates fading effects. Multiple versions of the transmitted signal arrive at the receiving antenna with random amplitudes, phases, time delays, and angles-of-arrival (AOAs). These multipath components are combined *vectorially* at the receiver, thereby causing the received signal to be distorted or to fade. It has been noted that the vectorial sum of as few as six sine waves with independently fluctuating random phases will give a resultant fluctuating wave whose envelope closely follows Rayleigh statistics and whose phase is uniformly distributed [29]. If there is relative motion between the receiver and transmitter, each multipath wave also experiences a frequency shift which is called a Doppler shift. The Doppler shift is directly proportional to the velocity of the motion and the cosine of the angle between AOA of the multipath and direction of the relative movement.

Three most important multipath fading effects are [30]:

1. Rapid changes in signal strength over small travel distances or time intervals.
2. Random frequency modulation due to varying Doppler shifts on different multipath signals.
3. Time dispersion (echoes) caused by multipath propagation delays.

2.1.4 Two-Stage Wireless Channel Characterization

Wireless channels are usually characterized by using a two-stage process. Although the wireless channel is non-stationary, it usually can be assumed to be stationary over a short time interval. Based on this, a two stage characterization is used to obtain the statistical description of the channel [30].

At the first stage, the channel is characterized over a period of time or the equivalent geographical area, which is small compared to the variations that occur on the channel. The small variations, which are usually called small-scale fadings, are due to the fact that the major features of the environment, which give rise to the channel characteristics, the significant scatterers, for example, remain basically unchanged over this small time interval. This, in effect, gives a time interval or equivalent geographical area in which the mean signal strength remains essentially constant.

At the second stage, the characteristics of much larger geographical areas or time intervals are obtained by extending or extrapolating the characteristics of the small-scale statistics in the first stage.

Over the years, there has been some confusion about which term one should use to describe large-scale and small-scale fading. Some authors have used the terms "slow fading" and "fast fading" to describe large-scale and small-scale fading. In this thesis, the terms "large-scale fading" and "small-scale fading" are used. The terms "slow fading" and "fast fading" are only used to describe the relationship between the time rate of changes in the wireless channel and the transmitted signal. We are mainly concerned with studying small-scale fading and its counter-measures since this is the purview of smart antennas. In what follows, only one section is devoted to large-scale fading, the rest of the chapter deals mainly with small-scale fading: its types and models, in particular, those aspects related to the smart antenna.

2.2 Large-Scale Channel Characterization

Large-scale fading characterization is concerned with predicting the mean signal strength as a function of the transmitter-receiver (T-R) separation distance (d) over T-R separation of hundreds, thousands, or millions of meters. In this section, the widely-employed and easy-to-use log-distance path loss model is presented first, followed by log-normal shadowing as a supplement. More sophisticated models which take into account site-specific information are also referenced. The log-distance path loss model has been shown historically to be a very good first-cut for predicting the distance dependency of the received power in a wireless system.

2.2.1 Log-Distance Path Loss Model

Path Loss is defined as the local average of the received signal power relative to that of the transmitted signal. In a realistic wireless channel, the free-space model does not apply. Both outdoor and indoor propagation measurements indicate that average received signal power decreases logarithmically with distance. A general path loss model that has been demonstrated useful over the years is to use a parameter, n, to denote a similar power law relationship between the received power and distance as in Eqn. (2.6). This model takes into account the decrease in energy density suffered by the electromagnetic wave due to spreading, as well as the energy loss due to the interaction of the electromagnetic wave with the propagation environment. The path loss, L, in decibels can be expressed as (the gains of the transmitting and receiving antennas may be implicitly included or excluded in these power quantities)

$$L(x) = L(x_0) + 10n \log(x/x_0) \tag{2.6}$$

where x is the distance between the transmitter and receiver, $L(x_0)$ is the path loss at a know position of x_0. x_0 is usually a close-in point in the far field of the transmitting antenna so that the near-field effects are eliminated from the path loss prediction. Typically, x_0 is 1 km for large urban mobile systems, $100m$ for microcell systems, and $1m$ for indoor systems [31]. The path loss exponent, n, depends on the propagation environment. As we can see, $n = 2$ corresponds to free space propagation. Table 2.1 shows some typical values for path loss exponents in various environments [30].

Table 2.1: Typical values for path loss exponent in various environments

Environment	Path Loss Exponent n
Free Space	2
Urban area cellular radio	2.7 to 3.5
Shadowed urban cellular radio	3 to 5
In building line-of-sight	1.6 to 1.8
Obstructed in building	4 to 6

2.2.2 Log-Normal Shadowing

The log-distance model in Eqn. (2.6) does not account for the fact that the path losses at different geographical locations at the same distance from a fixed transmitter exhibit a natural variability due to differences in local surroundings, blockage or terrain over which signals travel. This variability is random and found to be log-normally distributed, i.e., it follows a Gaussian distribution (with values in dB) about the distance-dependent mean path loss predicted in Eqn. (2.6)with a standard deviation L_σ dB. This phenomenon is referred to as *log-normal shadowing* [30, 32, 33]. Eqn. (2.6) can thus be modified to include the log-normal shadowing effect as

$$L(x) = L(x_0) + 10n\log(x/x_0) + L_\sigma \tag{2.7}$$

where L_σ is a zero-mean Gaussian distributed random variable (in dB) with standard deviation σ (in dB). Eqn. (2.7) thus gives a complete path loss model for a random location x_0, using $L(x_0)$,n, and σ. For a particular environment, these parameters can be computed from measured data covering a wide range of distances and locations.

2.2.3 Other Models

Although extremely useful for quick estimation of link performance, Eqn. (2.7) combines all propagation effects into two parameters - the path loss exponent n and

standard deviation σ. Considering the various different wireless communication environments that one might encounter, it is unavoidably an oversimplification in some circumstances. More sophisticated models have been developed to take into account other important factors that may vary from site to site, such as terrain, urban clutter, antenna heights, and diffraction. For outdoor propagation, some of the most widely used models are as follows: Longley-Rice, Durkin, Okumura, Hata, COST-231, Walfisch and Bertoni, Wideband PCS microcell [34, 35].

2.3 Small-Scale Channel Characterization

This section discusses the small-scale characterization of radio wave propagation. After introducing the channel impulse response, a discussion on the various parameters used to characterize the wireless propagation channel is embarked upon. Various types of fading, including "fast", "slow", "flat", and "frequency selective", are defined. The time dispersive nature of the wireless propagation channel, which limits the maximum unequalized data rate attainable, will also be discussed. In addition, parameters that are of particular importance to smart antennas, such as the joint angle-of-arrival (AOA), time delay spread and Doppler spread profile, are also described.

2.3.1 Impulse Response of a Multipath Channel

The wireless channel, to a large extent, can be characterized as a time-variant linear system. Like any other linear time-variant or time-invariant system, it can be described by its impulse response, which is defined as the response of the channel when a unit impulse or $\delta(t)$ function is applied to it.

In wireless communications, as with most other communication systems, we are mainly concerned with passband signal transmission. A bandpass system can be represented with an equivalent complex low-pass system [36]. If we assume the channel to be time-invariant, its baseband impulse response, $h(\tau)$, can be expressed as [30]

$$h(\tau) = \sum_{i=1}^{N} A_i e^{j\theta_i} \delta(\tau - \tau_i) \tag{2.8}$$

where A_i is the voltage amplitude, θ_i is the phase shift, and τ_i is the time delay of the ith arriving signal. This shows that the received signal is the sum of a series of time-delayed, phase-shifted, attenuated versions of the transmitted signal. If the channel is time-variant, then A_i,θ_i, and τ_i are also functions of time for which Eqn.(2.8) can be re-written as

$$h(t,\tau) = \sum_{i=1}^{N(t)} A_i(t) e^{j\theta_i(t)} \delta(\tau - \tau_i(t)) \tag{2.9}$$

where a time index has been added to A_i, θ_i, and τ_i to emphasis their dependencies on time.

$h(\tau)$ or $h(t,\tau)$, can be directly measured using wideband channel sounding techniques. A_i, θ_i, and τ_i may be used as parameters to create small scale channel models for system design and simulation.

2.3.2 Time Dispersion Parameters

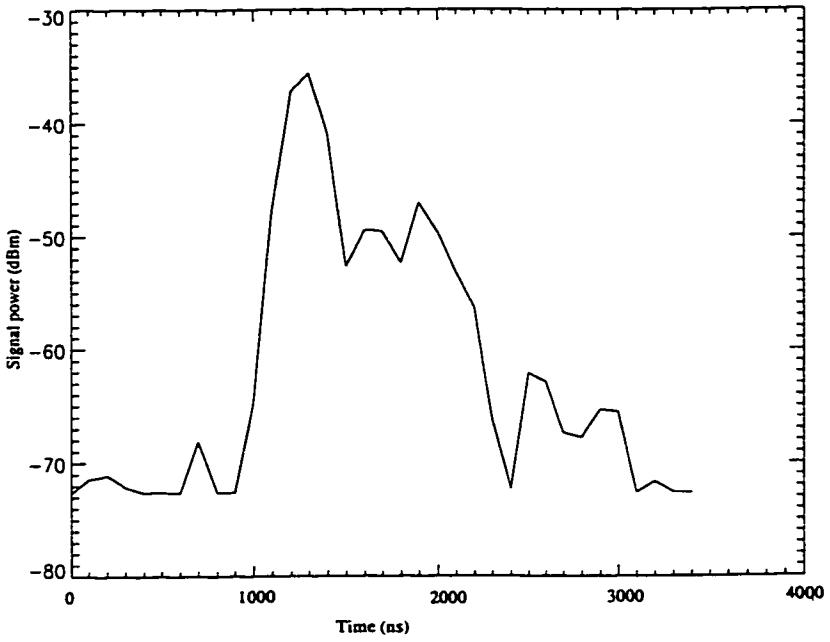

Figure 2.3: Impulse response measured on the McMaster campus (outdoor)

In a wireless environment, a transmitted signal usually travels along multiple paths before it is received at either a base station or a mobile station. The different paths introduce different time delays which result in a time-dispersive wireless channel. The degree of time-dispersiveness is closely related to the nature of the propagation environment under consideration. Figures. 2.3 and 2.4 show two channel impulse responses from our measurement data, where the sampling rate is 10 MHz for both figures. Figure. 2.3 is a typical outdoor impulse response for the McMaster Campus, while Figure. 2.4 is a typical indoor result for measurements taken in the Communications Research Laboratory at McMaster University. As we can see, Figure. 2.3 shows much more time-dispersiveness than Figure. 2.4. To quantify the time

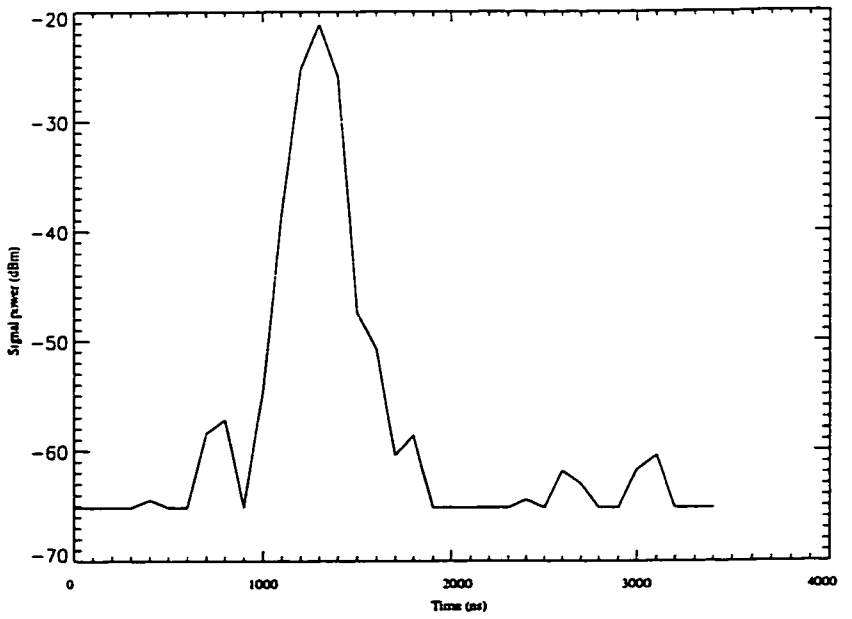

Figure 2.4: Impulse response of the Communications Research Laboratory (indoor)

dispersiveness of wireless channel, three parameters are usually used: *mean excess delay, rms delay spread*, and *maximum excess delay.*

To define these three parameters, the *power delay profile* of the channel has to be defined first. If we denote the channel impulse response as $h(\tau)$, the power delay profile of the channel is defined as $p(\tau)$ which is the spatial average of $|h(t)|^2$ over a local area. In real practice many snapshots of $|h(t)|^2$ are averaged over a local area to provide one multipath power delay profile. The mean excess delay, $\bar{\tau}$, is the first moment of $p(\tau)$ and is defined to be

$$\bar{\tau} = \frac{\sum_k p(\tau_k)\tau_k}{\sum_k p(\tau_k)} \tag{2.10}$$

The rms delay spread, σ_τ, is the square root of the second central moment of $p(\tau)$ and is defined to be

$$\sigma_\tau = \sqrt{\bar{\tau^2} - \bar{\tau}^2} \tag{2.11}$$

where

$$(\bar{\tau^2}) = \frac{\sum_k p(\tau_k)\tau_k^2}{\sum_k p(\tau_k)} \tag{2.12}$$

τ_k is measured relative to the first detectable signal arriving at the receiver with $\tau_0 = 0$. The maximum excess delay (X dB), τ_x, is defined to be the time delay during which $p(\tau)$ falls to X dB below the maximum of $p(\tau)$.

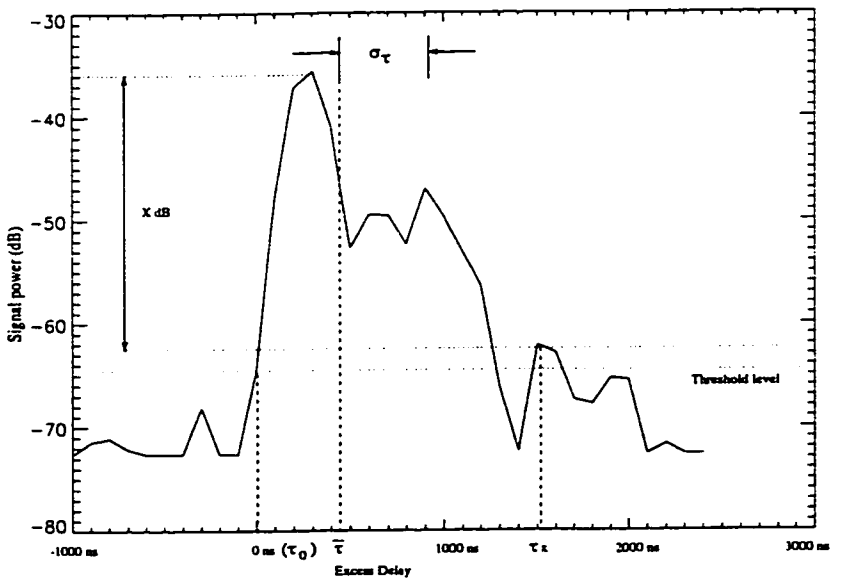

Figure 2.5: An example of power delay profile, rms delay spread, mean excess delay, and maximum excess delay (X dB)

Fig.2.5 shows an example of power delay profile, rms delay spread, mean excess delay, and maximum excess delay (X dB).

2.3.3 Coherence Bandwidth

Coherence bandwidth is a statistical measure of the range of the frequencies over which the channel can be considered "flat". A "flat" channel passes all spectral components with approximately equal gain and linear phase, in other words, coherence bandwidth is the maximum separation over which two frequency components have a strong potential for amplitude correlation [30]. The existence of different time delays in the various paths causes the statistical properties of two narrowband signals with different frequencies or two frequency components of the same wideband signal to be essentially uncorrelated if the frequency separation becomes large.

Coherence bandwidth is related to the rms delay spread. It is defined as the bandwidth over which the frequency correlation function is above 0.9, i.e., the maximum separation in frequency of two components whose correlation remains greater than 0.9. The coherent bandwidth is related to the RMS delay spread according to the approximate formula [30]

$$B_c = \frac{1}{50\sigma_\tau} \tag{2.13}$$

where B_c is the coherence bandwidth. If the cross-correlation of any two spectral components is reduced to 0.5, then B_c is related to the RMS delay spread according to the approximate formula

$$B_c = \frac{1}{5\sigma_\tau} \tag{2.14}$$

While approximate, the essence of these two equations is that the coherence bandwidth bears an inverse relationship to the RMS delay spread.

2.3.4 Coherence Time

Coherence time is a parameter which gives information about the time varying nature of the wireless channel. It is a statistical measurement of the time duration over which the channel impulse response is essentially invariant.

Relative motion between the transmitter and receiver impresses Doppler shifts upon the frequencies of the transmitted signal, which means that the received signal will be a frequency shifted version of the transmitted signal. The frequency shift, f_d, is given by

$$f_d = \frac{v}{\lambda} cos(\theta) \tag{2.15}$$

where

v = the magnitude of the relative velocity between the transmitter and receiver

λ = wavelength of the transmitted signal

θ = angle-of-arrival of the received signal relative to the direction of motion

In most wireless communication systems, where the relative transmitter-receiver velocity varies with time, f_d will also vary with time. The frequency of the received signal thus will appear to vary with time. As a result, the Doppler shift tends to introduce a FM modulation into the signal. For instance, a continuous-wave (CW) signal of frequency f_c , which is transmitted over a mobile radio channel, will spread out over the bandwidth $[-f_m + f_c, f_m + f_c]$, where f_m is the maximum Doppler shift suffered by the signal. The direction of arrival of energy determines the exact Doppler shift.

The coherence time of a wireless channel is the time over which the channel impulse response can be considered stationary. The same signal received at different points within a time period equal to or less than the coherent time, is likely to be correlated in amplitude. The coherence time, T_c, is inversely proportional to f_m, the maximum Doppler shift suffered by the signal. If T_c is defined as the time over which the time correlation function is above 0.5 then [30]

$$T_c = \frac{9}{16\pi f_m} \tag{2.16}$$

2.3.5 Flat Fading

Multipath delay spread leads to fading and time dispersion. Depending on the relationship between the signal bandwidth (or symbol period) and rms delay spread, different transmitted signals will undergo two different types of fading, namely, flat fading and frequency selective fading.

Flat fading happens when the wireless channel has a constant gain and linear phase response over the bandwidth of the transmitted signal. Since the channel satisfies a non-distortion transfer function [36], the received signal preserves the same spectrum of the transmitted signal except for a scaling factor and a constant phase shift which are caused by the channel. Due to the time-variant nature of the wireless channel, the scaling factor and phase shift are usually time-variant too. The strength of the received signal thus changes in time with fluctuations in channel gain.

Flat fading can also be viewed from the time domain. In a flat fading channel, the reciprocal bandwidth of the transmitted signal is much larger than the multipath time delay spread of the channel. Since the bandwidth of the transmitted signal is small compared to the channel flat fading bandwidth, flat fading channels sometimes are also referred to as narrowband channels.

Flat fading conditions can result in errors in wireless systems. The probability of error depends on the distribution and duration of these fades as well as the data rate. Referring back to the measurement at McMaster campus as shown in Fig. 2.2, we can see deep fades of 20dB or $30dB$ are not uncommon. The most common type of flat fading channel model is *Rayleigh Channel* in which the channel is assumed to introduce a Rayleigh distributed amplitude variation on the received signal. If we denote the amplitude as r, the Rayleigh distribution can be described as

$$P(r) = \begin{cases} \frac{r}{b} e^{-\frac{r^2}{2b}}, & r \geq 0, b > 0 \\ 0, & r < 0 \end{cases} \tag{2.17}$$

If there is a very strong multipath component as in the case of line-of-sight, the distribution becomes Rician instead of Rayleigh. The Rician distribution is given by

$$P(r) = \begin{cases} \frac{r}{b} e^{-\frac{r^2+s^2}{2}} J_0(rs/b), & r \geq 0, b > 0 \\ 0, & r < 0 \end{cases} \tag{2.18}$$

where s^2 is the mean power of the strong component and $J_0()$ is the modified zeroth order Bessel function of the first kind.

2.3.6 Frequency Selective Fading

If the channel does not have constant gain and linear phase over the transmitted signal bandwidth, the signal will undergo another kind of fading which is called

frequency selective fading. The term frequency selective fading comes from the fact that the gain of the channel is a variable for the different frequency components of the transmitted signal.

If we look at this from the time domain perspective, the impulse responses of such channels have multipath delay spreads which are greater than the reciprocal of bandwidth of the transmitted signal. Intersymbol interference occurs due to fact that the multiple versions of the transmitted signal are received and the delays are greater than the inter-symbol period (T_s). As a parallel development in the flat fading case, the frequency selective fading channel is sometimes also referred to as *wideband channel*, since the bandwidth of the transmitted signal is wider than the coherent bandwidth of the channel.

As a summary, the conditions under which the signal undergoes flat fading or frequency fading is given in Table. 2.2. It only occurs when B_s, the signal bandwidth, is greater or much smaller than B_c. For cases when B_s is neither greater nor much smaller than B_c, the situation is not as straightforward. It depends on the type of modulation carried by the transmitted signal. A common rule of thumb is that a channel is frequency selective when $\sigma_\tau > 0.1T_s$ [30].

2.4 Vector Multipath Channel Models

The propagation environment provides the signaling condition that the smart antenna must exploit to improve system performance. To properly design, analyze, and develop smart antenna systems, channel models that incorporate spatial characteristics, i.e., vector channel models, must be used. Such channel models incorporate one more dimension, namely *space*, into the modeling of the wireless channel.

The challenge and task of vector channel modeling for smart antennas is to develop a realistic channel model that can be used to efficiently and accurately simulate the performance of a smart antenna system. In what follows, traditional channel models, such as the Clarke model, which deal mainly with narrowband systems, are first presented. These traditional models provide only information about the signal power level distribution and Doppler shifts of the received signals. As wireless systems move towards greater bandwidth, the traditional models are becoming inadequate.

Table 2.2: The condition under which the signal undergoes flat fading or frequency fading (B_s:signal bandwidth, B_c: coherent bandwidth, T_s: symbol period, σ_τ: rms delay spread)

$B_s << B_c$ or $T_s >> \sigma_\tau$	flat fading
$B_s > B_c$ or $T_s < \sigma_\tau$	frequency selective fading

Recent research in vector channel modeling has been more focused on jointly modeling the channel in terms of signal power level, multipath delay and angle-of-arrival (AOA) [37, 38, 39, 40, 41, 26]. Multipath channel models can essentially be grouped into two classes: statistical models and deterministic models. Statistical models use statistical parameters that describe the phenomenon of multipath propagation within a given error. They are simple to use, but relatively coarse. The deterministic models are environment-specific. They characterize a specific multipath propagation environment and reveal more details concerning the physical propagation in that particular environment.

2.4.1 Vector Channel Impulse Response

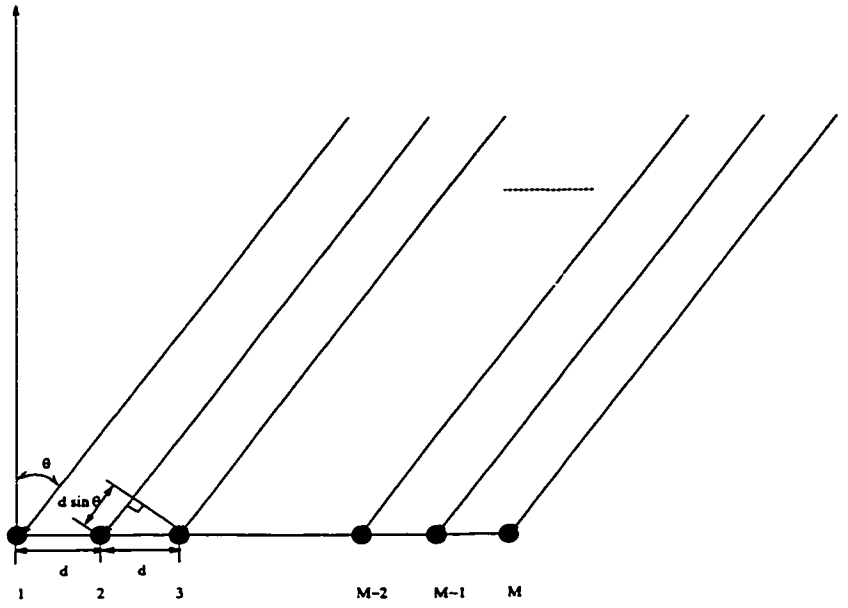

Figure 2.6: An M-element array

We begin vector channel modeling by first introducing the vector channel impulse response. Suppose there are a total of K users that are communicating via the same channel with a base station equipped with an M-element antenna array as in Fig. 2.6. The vector channel impulse response of the M-element array to user k is defined as

$$\mathbf{H}_k(t,\tau) = [h_{1,k}(t,\tau), h_{2,k}(t,\tau), \ldots, h_{M,k}(t,\tau)]^T \tag{2.19}$$

where $h_{m,k}(t,\tau)$ is the impulse response of the mth antenna element to user k and T denotes the transpose of a matrix or vector.

Let us assume there are L_k multipaths for user k. Associated with each path l of user k, the signal component will experience a different path environment, which in turn determines the amplitude $A_{l,k}$, carrier phase shift $\phi_{l,k}$, time delay $\tau_{l,k}$, and angle of arrival $\theta_{l,k}$. In general, each of these signal parameters will be time-variant.

The channel impulse response in Section 2.3.1 can be extended to vector channel impulse responses which will be used in vector channel modeling. As shown in Section 2.3.1, the channel impulse response for an individual user can be represented as

$$h_k(t,\tau) = \sum_{l=1}^{L_k(t)} A_{l,k}(t) e^{j\phi_{l,k}(t)} \delta(\tau - \tau_{l,k}(t)) \tag{2.20}$$

Eqn. (2.20) does not consider the angle-of-arrival distribution of the multipath components which need to be included to yield the vector channel impulse response.

If the inverse of signal bandwidth is large compared to the travel time across the array, [2] $[A_{1,k}, \ldots, A_{L_k,k}]^T$, the complex envelope vector of the signals received by different antenna elements from a certain path, are identical except for phase and amplitude differences which depend on the angle-of-arrival of the path, the array geometry and the antenna element pattern. Assume each antenna has an omni-directional radiation pattern, the effects of the angle-of-arrival and array geometry can be absorbed into an m-dimensional *array response vector* which can be expressed as

$$\begin{aligned} \mathbf{a}(\theta) &= [a_1(\theta), a_2(\theta), \ldots, a_M(\theta)]^T \\ &= [1, e^{j2\pi d_1/\lambda}, \ldots, e^{j2\pi d_M/\lambda}]^T \end{aligned} \tag{2.21}$$

where $d_m(\theta)$ is obtained by subtracting the distance between the signal source and the first element from that between the signal source and the mth element, and λ is the wavelength. $\mathbf{a}(\theta)$ is also referred to as *steering vector* in the literature. [3] The vector channel impulse response can be written as

$$\mathbf{H}_k(t,\tau) = \sum_{l=1}^{L_k(t)} \mathbf{a}(\theta_{l,k}) A_{l,k}(t) e^{j\phi_{l,k}(t)} \delta(\tau - \tau_{l,k}(t)) \tag{2.22}$$

In Eqn.(2.22), each multipath component has its own complex amplitude, phase, and angle-of-arrival. The distribution of these parameters is very much dependent upon the type of environment. If we denote the signal bandwidth and the

[2] This is also commonly referred to as narrowband signal in array processing, not to be confused with the general narrowband definition. It is generally true for the conditions under which smart antennas are used. For example, the inverse signal bandwidth of Global System for Mobile (GSM) is 5μ seconds, whereas the travel time across an array of several meters, which is in the order of tens of wavelength at $900MHz$ or $1.9GHz$, is only a few nano-seconds.

[3] Please refer to Section 4.1.1 for details on the array response vector.

maximum time delay as B and τ_{max} respectively, a very important special case of Eqn. (2.22) is $B\tau_{max} << 1$. Under this situation, Eqn. (2.22) can be simplified as

$$\mathbf{H}_k(t,\tau) = \mathbf{U}_k(t)\delta(\tau) \tag{2.23}$$

Where $\mathbf{U}_k(t) = (\sum_{l=1}^{L_k(t)} \mathbf{a}(\theta_{l,k})A_{l,k}(t)\exp j\phi_{l,k}(t))$. In other words, the channel for the kth user can be explicitly characterized by a complex variable $\mathbf{U}_k(t)$.

2.4.2 Clarke's Model

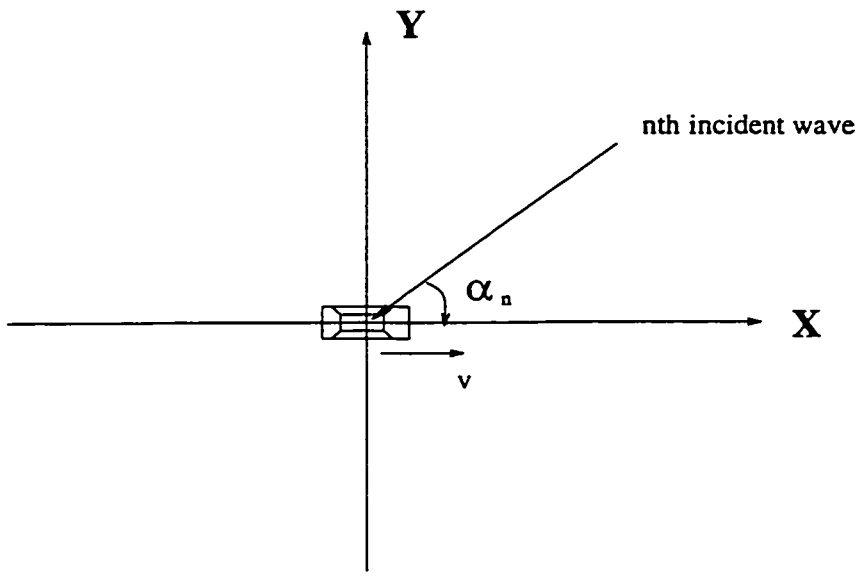

Figure 2.7: Clarke's model

Clarke's Model describes the statistical characteristics of the amplitude and phase of a signal received at a mobile station. It is one of the earliest models that incorporate angle-of-arrival information. The two key AOA assumptions are as follows: [42]

1. Only the azimuth angle is important: the elevation angle can be neglected.
2. The AOA is uniformly distributed in azimuth over $[0, 2\pi]$.

Although the AOA assumptions are rather simple compared to the models we will introduce later in this chapter, Clarke's model successfully explains the Rayleigh fading phenomenon.

As shown in Figure. 2.7, a mobile station travels at a velocity of v in the x-direction relative to the transmitter. The waves that are incident on the mobile are

assumed to be comprised of N multipath signals which are distributed in the azimuth plane. In addition to the two AOA assumptions, the amplitude and phase of each wave are assumed to be statistically identical with phase uniformly distributed over $[0, 2\pi]$. For the nth wave arriving at the mobile station at an angle of α_n relative to the x axis, the Doppler shift is given by

$$f_n = \frac{v}{\lambda} cos\alpha_n \tag{2.24}$$

where λ is the wavelength of the incident wave.

The vertically polarized plane waves arriving at the mobile have E and H field components as [30]

$$E_z = E_0 \sum_{n=1}^{N} C_n cos[2\pi(f_c + f_n)t + \phi_n] \tag{2.25}$$

$$H_x = -\frac{E_0}{\eta} \sum_{n=1}^{N} C_n sin\alpha_n cos[2\pi(f_c + f_n)t + \phi_n] \tag{2.26}$$

$$H_y = -\frac{E_0}{\eta} \sum_{n=1}^{N} C_n cos\alpha_n cos[2\pi(f_c + f_n)t + \phi_n] \tag{2.27}$$

where E_0 is the real amplitude of average local E-field, C_n is a real random variable representing the variation in the amplitude of the nth wave, η is the free space impedance of 377Ω, ϕ_n is the random phase uniformly distributed over $[0, 2\pi]$. If the probability density functions (PDF) of C_n, α_n, and ϕ_n are independent of n, and N is sufficiently large, E_z, H_x, and H_y can be approximated by random Gaussian variables. Eqn.(2.25) can be written as

$$E_z = T_c(t) cos(2\pi f_c t) - T_s(t) sin(2\pi f_c t) \tag{2.28}$$

where $T_c(t)$ and $T_s(t)$ are uncorrelated zero-mean Gaussian random processes given by

$$T_c(t) = E_0 \sum_{n=1}^{N} C_n cos[2\pi f_n t + \phi_n] \tag{2.29}$$

and

$$T_s(t) = E_0 \sum_{n=1}^{N} C_n sin[2\pi f_n t + \phi_n] \tag{2.30}$$

The envelope of E_z is given by

$$|E_z(t)| = \sqrt{T_c^2(t) + T_s^2(t)} \tag{2.31}$$

It can be shown that $|E_z(t)|$ has a Rayleigh distribution given by Eqn. (2.17). [4]

[4] Please refer to [30] for details.

Although it includes phase information for each of multipath signals, Clarke's model does not consider time delay information, so it is inherently a narrowband model. Clarke's model is a two-dimensional model that assumes multipath signals only arrive in the azimuthal plane. It is obvious that in the real world, signals would arrive with different elevation angles. However, the waves that make the major contributions do indeed travel approximately in the horizontal plane. That is, to a first-order approximation, the elevation angle of the waves can be assumed to be zero. This is also evident from the fact that Clarke's model successfully explains the envelop and phase of an observed narrowband signal in a wireless communications environment.

2.4.3 Geometrically Based Single Bounce (GBSB) Model

Clarke's model assumes incident waves are uniformly distributed over $[0, 2\pi]$ in azimuth. From the point of view of scatterer distribution, this is equivalent to assuming that they are distributed in a circle, which is centered at the mobile station. It is obvious that the real propagation environment rarely resembles this simplified model. To improve this, the geometrically based single bounce (GBSB) model was proposed by Liberti and Rappaport [43, 44]. It defines a spatial scatterer density function instead of simply assuming that the scatterers are uniformly distributed. By placing the spatial scatterers according to a predefined (simulated or extracted from propagation measurements) density function, the AOA, TOA and the signal amplitude are determined.

Another characteristic of the GBSB model is that it assumes every incident wave is the result of a single bounce from a scatterer. Although this a simplification of the real situation, it has been shown to be successful in many cases [43]. As is also evident from our simulation results which are presented in Chapter 5, it captures many characteristics in our simulation of the smart antenna in Frequency Division Duplexing (FDD) systems even though it is too coarse in some cases. The single bounce assumption can be a merit or shortcoming depending on the problem it deals with.

When we do not have a predefined density function of scatterers, or very little information is available about the distribution of scatterers, one special case of the GBSB model which is called Geometrically Based Single Bounce Elliptical Model (GBSBEM) is very useful. It assumes that the scatterers are uniformly distributed within an ellipse as shown in Fig. 2.8. The base station and the mobile are the foci of the ellipse. The semi-major axis a and semi-minor axis b are given by

$$a = \frac{c\tau_{max}}{2} \tag{2.32}$$

$$b = \frac{1}{2}\sqrt{c^2\tau_{max}^2 - D^2} \tag{2.33}$$

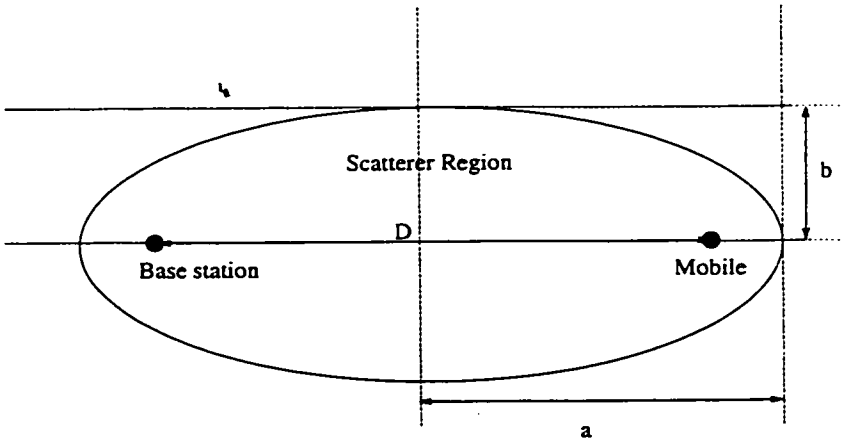

Figure 2.8: The GBSBEM model

where c is the speed of light, and τ_{max} is the maximum TOA to be considered.

Uniformly placing scatterers in an ellipse may be accomplished by first uniformly placing the scatterers in a circle and then scaling each x and y coordinates by a and b respectively. In this case, the joint TOA and AOA density function observed at the base station can be shown to be [43]

$$f(\tau,\theta_b) = \begin{cases} \frac{(D^2-\tau^2c^2)(D^2c+\tau^2c^3-2\tau c^2 DCos\theta_b)}{4\pi ab(Dcos\theta_b-\tau c)^3}, & \frac{D}{c} \leq \tau \leq \tau_m \\ 0 & ,otherwise \end{cases} \tag{2.34}$$

where θ_b is the AOA observed from the base station.

2.4.4 Ray Tracing Model

Unlike statistical models, the ray tracing model is deterministic. It requires detailed knowledge of the physical propagation environment.

Fig. 2.9 shows a simple case of ray tracing in which the received signal is modeled as the sum of multiple reflections of the transmitted signal. The ray tracing model treats electromagnetic waves the same way as light and is thus based on geometric theory of reflection, diffraction, and scattering. Typical ray tracing models require information such as profiles of naturally occurring objects and man-made structures, as well as path loss and delay spread information to produce propagation prediction.

It is felt, though, that the high computational burden and lack of detailed database for terrain and man-made objects make ray tracing models difficult to use except in a very few simple or well controlled cases [41, 45, 46]. Although progress

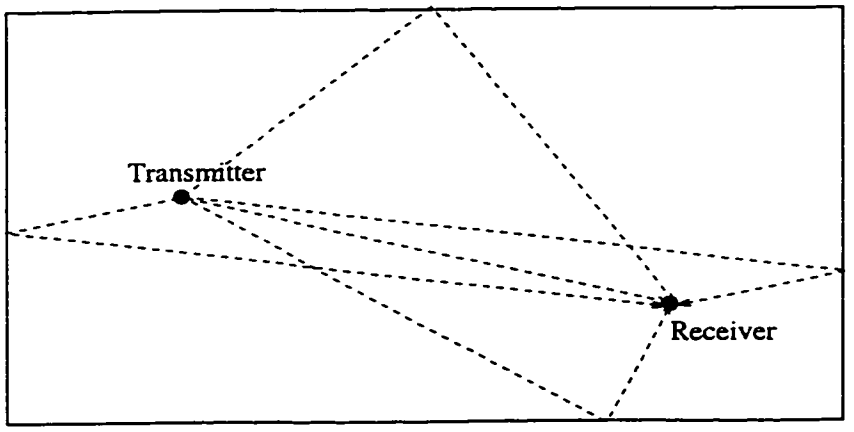

Figure 2.9: An example of ray tracing where the transmitter and receiver are enclosed by a box

has been made in both the ray tracing and computer technology, further development of efficient ray tracing algorithms is still needed before it can be applied to practical environments.

2.4.5 Channel Sounding

Channel sounding refers to the use of measuring equipment (channel sounder) to obtain experimental data from which one can derive a deeper and better understanding of the wireless channel under investigation. Channel sounding is particularly important in the study of smart antennas due to the complexity of the wireless channel. Although a number of vector channel models have been proposed, currently there is not a single vector channel model that is well validated to capture both AOA, time delay, and power of the multipath components. *There is still no substitute for a well-planned-and-executed channel sounding measurement.*

There are basically two kinds of channel sounding measurements: narrowband channel soundings and wideband channel soundings [35]. Narrowband channel sounders excites the channel with a narrowband signal (usually a CW carrier) and measure the variations in both the amplitude and phase of the signal received in a possibly moving receiver. In the early days, wireless communication systems were usually narrowband. With the introduction of digital commutations and the increase in data rate, current wireless systems have evolved more and more towards wideband. Since we are more interested in the joint AOA, TOA and power distribution of the received vector signal, we only address wideband soundings in this subsection. In the rest of this thesis, we refer to wideband channel sounding implicitly when we say "channel sounding".

Channel Sounding Methods

Basically there are three kinds of channel sounding methods: *spaced-tone sounding, periodic pulse sounding*, and *pulse compression sounding*. Examples of these sounding methods can be found in [30, 35, 47].

Spaced-tone sounding is an extension of the narrowband single-tone sounding method. By measuring the channel response to sequentially transmitted tones with a predetermined frequency spacing over the frequency band of interest, a measurement of the channel frequency transfer function can be obtained. This method suffers two drawbacks. First, stepping a synthesizer over a large bandwidth in small steps (the accuracy of the frequency transfer function depends on the step size) is time-consuming. Secondly, no Doppler-shift information can be obtained. Although spaced-tone sounding is attractive in that it requires relative simple equipment, it is usually not preferred.

When a pulse of very short duration is transmitted, the received signal is the convolution of the sounding pulse and the channel impulse response. As can be proven, the received signal will approximate the impulse response provided the pulse duration is short enough. Channel sounding employing a periodic short pulse is called periodic pulse sounding. The actual duration of pulse is determined by the frequency band of interest. To be exact, it should be shorter than the inverse of the frequency band. In order to observe the time varying response of individual propagation path, the repetition rate of the pulse cannot be very long. In other words, it has to be long enough to ensure that all multipath components have decayed between successive pulses while short enough to capture the time-varying nature of the channel. The major difficulty of periodic pulse sounding is the requirement of transmitting a short pulse of high peak power. The high peak power is required to detect the weak multipath signals that are generated by the transmitted pulse. One way of overcoming this is to use a pulse compressing technique.

If a white noise signal $n(t)$ is transmitted, the received signal is

$$y(t) = \int_{-\infty}^{\infty} h(\tau)n(t-\tau)d\tau \tag{2.35}$$

where $h(t)$ is the channel impulse response. And

$$\int_{-\infty}^{\infty} n(t)n^*(t-\tau) = N_0\delta(\tau) \tag{2.36}$$

The correlation of $y(t)$ and $n(t)$ gives

$$\int_{-\infty}^{\infty} y(t)n^*(t-\eta)d\eta = \int_{-\infty}^{\infty}\int_{-\infty}^{\infty} h(\tau)n(t-\tau)n^*(t-\eta)d\tau d\eta \tag{2.37}$$

$$= N_0 h(\tau) \tag{2.38}$$

In practice, genuine deterministic white noise is impossible to generate, one widely used waveform is the pseudo-noise(PN) sequences which are deterministic and

have a noise like character. The 8-element vector channel sounder which is described in Appendix A uses this method.

2.5 Conclusions

In this chapter the wireless channel is studied in detail. The dispersiveness in time, space, and frequency of wireless channels is presented together with the parameters that describe these phenomenon, e.g., coherent bandwidth, coherent time, time delay spread. We then further study vector channel models, in particular, Clarke's model, the GBSB model and the ray tracing model. However, none of the currently existing models can completely satisfy all the needs for adequately simulating smart antennas in realistic propagation environments and much research remains to be done. To supplement the inadequacy of the current vector channel models, channel sounding can be used to provide an understanding and characterization of the wireless channel under investigation.

Chapter 3

Wireless Communication Standards and Smart Antennas

Wireless communication standards have evolved through two generations, namely, first generation analog systems and second generation digital systems. With the introduction of first generation analog FDMA/FM system such as Advanced Mobile Phone Service(AMPS) and Total Access Communication System(TACS), we have seen the widespread deployment of cellular systems. Second generation standards with GSM, D-AMPS, and CDMA (IS-95) as its key members, started the era of personal communications systems (PCS). Wireless systems are now moving towards to a third generation standard. Although fundamentally, smart antenna technology can be incorporated into any of these standards, the implementation in each instance will inevitably be different.

There have been many standards developed for wireless communication up to now. In this chapter, instead of going to lengthy explanation of each standard, we will concentrate on identifying the key underlying differences in these standards which are important to smart antenna technologies.

3.1 Cellular System Fundamentals

Early mobile radio systems used a single high power transmitter mounted on a tall tower to achieve a large coverage area. It was impossible to re-use the same frequencies throughout the large coverage area since the interference would render the system unusable. With the increase in the number of users, new systems were needed to offer higher capacity. But the spectrum is limited and cannot be allocated in proportion to the increasing demand for wireless communications. It has become imperative therefore to build a system which achieves high capacity with a limited radio spectrum. The cellular concept was thus introduced which used many base stations with low power transmitters. Each base station provided coverage to only a small portion of

the service area which is called a *cell*. Each base station is also allocated a portion of the total number of channels available to the entire system. Neighboring base stations are assigned different groups of channels so that the interference between base stations is minimized.

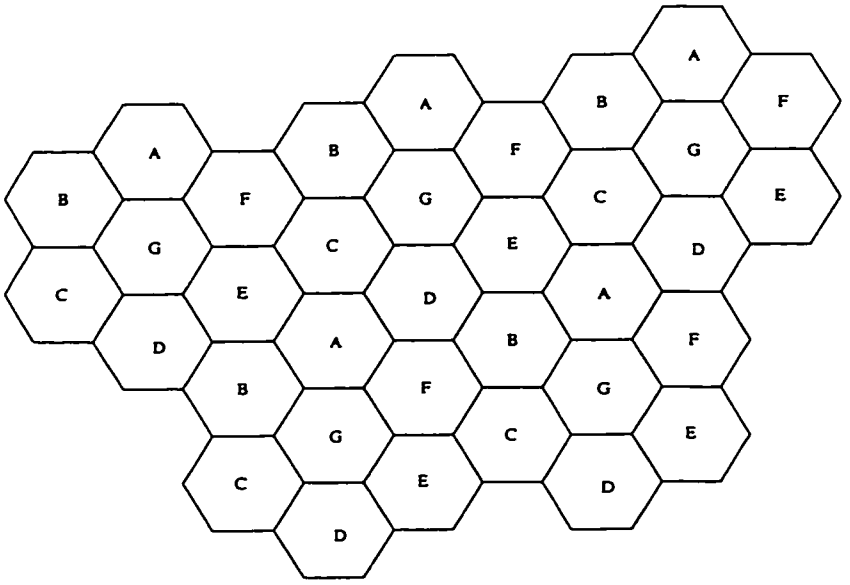

Figure 3.1: Cellular system and frequency reuse

Figure. 3.1 shows a cellular system in which the ideal hexagon cell shape is used. [1] In practice, the cell shape will be very irregular with the boundaries determined by the propagation environment in which it operates. Referring to Fig. 3.1, the available channels are divided into groups and allocated to each cell. A particular group of channels can be reused in cells that are separated by distances large enough that they do not cause interference to each other. Suppose S, the total of channels available, is divided into N groups with each of the cell allocated k channels, we have $S = kN$. The neighboring N cells which use completely S disjoint channels are called a cluster. Since frequency reuse occurs every N cells, the *reuse factor* of a cellular system is defined as $1/N$. Typical values for N are 1,'4, 7, and 12. It can be shown that only a number of values of N are possible with the hexagonal structure which can be expressed as [48]

$$N = i^2 + ij + j^2 \tag{3.1}$$

where i and j are non-negative integers. If we move i cells along any chain of hexagons

[1]Smart antennas are viewed as a space (or space-time) processing technology. Interestingly enough, the cellular concept can also be viewed as a spatial processing technology in the sense that it allows the same frequency reuse at spatially separated regions [2].

and then turn 60° counter-clockwise and move j cells, we will arrive at the nearest co-channel neighbors of the cell from which we started.

When the size of each cell is approximately the same, it can be shown that the co-channel interference is independent of the transmitted power and is a function of the radius of the cell (R) and the distance (D) between the co-channel cells[48]. A parameter Q can be defined which is called the *co-channel reuse ratio* to describe the capacity of a cellular system

$$Q = \frac{D}{R} = \sqrt{3N} \tag{3.2}$$

Q describes the ratio of separation of co-channels relative to the cell size. A smaller value of Q also indicates larger capacity since the cluster size N is smaller.

3.2 FDD and TDD

It is usually desirable to allow the user and the base station to communicate with each other simultaneously. The function whereby the user is able to talk and listen at the same time is called *duplexing*. The user talks and listens to the base station through two links, one is called the uplink or reverse link, which links the user to the base station, the other is called the downlink or forward link, and links the base station to the user. There are basically two ways of providing duplexing: frequency division duplexing (FDD) and time division duplexing (TDD). In an FDD system the two links use different carrier frequencies, while in a TDD system the two links operate on different time slots at the same frequency. In TDD systems the time interval between the two time slots is small, and the two links appear as simultaneous to the user, as in the case of FDD. Figure. 3.2 illustrate these two methods.

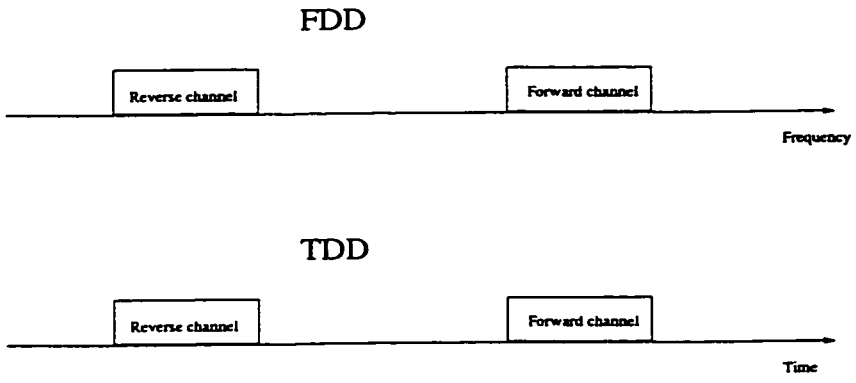

Figure 3.2: FDD and TDD

There are several trade-offs between FDD and TDD methods. In FDD the

frequencies for the two link must be carefully coordinated with out-of-band users occupying the spectrum between the two frequencies. Also there is a need of a frequency separation wide enough for the use of inexpensive frequency duplexers. TDD requires more coordination in time and synchronization, which makes it unsuitable for use in cells of large size due to the round trip time delay inherent in TDD systems.

The implementation of smart antennas in the uplink for the two duplexing methods are similar, but fundamental difference occurs in the downlink. The filtering coefficients (or weights) of smart antennas for FDD are different if the frequency separation is wider than the channel coherent bandwidth. Although the wireless channel is time-variant, the downlink filtering weights for TDD are expected to be very much correlated with the uplink weights provided that the time interval of duplexing is small enough compared to the channel coherence time. FDD systems usually use duplexing frequency separation of tens of MHZ which is much wider than the coherence bandwidth of most wireless channels. This makes it more difficult for FDD systems to implement the smart antenna on the downlink than TDD systems. In Chapter 5, we will address this problem and come up with an effective algorithm to deal with it.

3.3 Multiple Access Methods

Multiple Access refers to the scheme that allows many mobile users to simultaneously share a finite radio spectrum resource without interfering with one another. Frequency division multiple access (FDMA), time division multiple access (TDMA), and code division multiple access (CDMA) are the three major multiple access methods used in wireless communication systems. Figure. 3.3 illustrates the differences among these three multiple access methods by plotting frequency, time, and code as the three axes.

3.3.1 Frequency Division Multiple Access (FDMA)

FDMA is the multiple access method that was adopted for the first generation wireless system, e.g. AMPS. Compared with TDMA and CDMA, it is relatively simple to implement and bandwidth inefficient. With the introduction of digital wireless systems, FDMA is gradually being replaced by other forms of multiple access techniques.

FDMA divides the available frequency block into frequency bands as shown in Figure. 3.3. Usually a pair of frequency bands, one for receive and the other for transmit, are used together for a single user. This pair of frequency bands is usually called a *channel*. The channels are assigned to users who request service. Each user communicates with the base station via a different channel and thus avoids interference. Once a voice channel is assigned, the base station and the mobile transmit simultaneously and continuously.

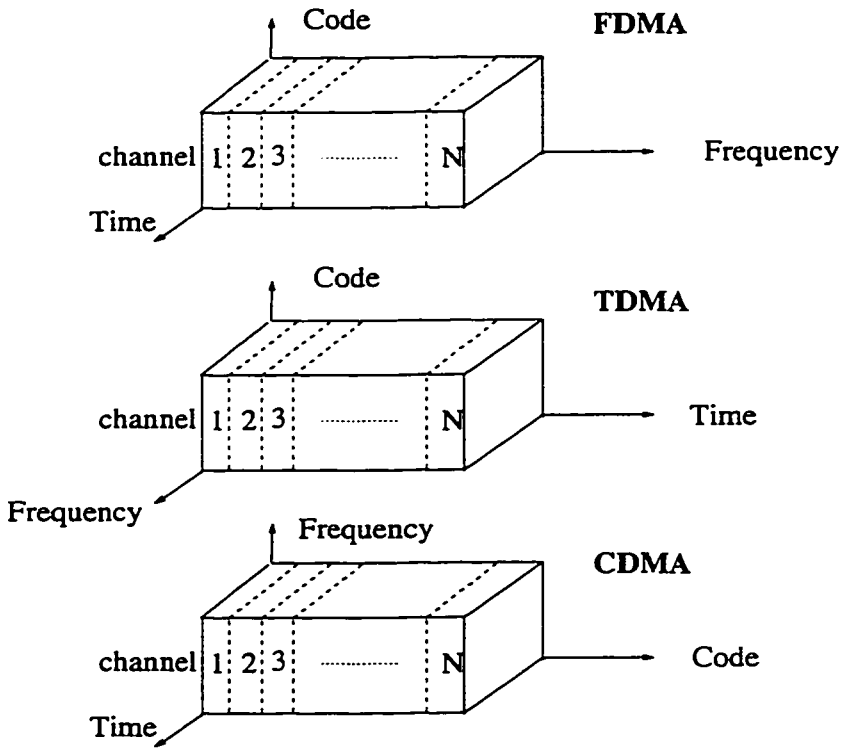

Figure 3.3: Three common multiple access methods

Since each channel carries only one user, FDMA is usually implemented as a narrowband system. FDMA can be used in either analog or digital systems. For example, AMPS is a $30KHz$ analog modulation system. Equalization is usually not needed in FDMA systems since the symbol time is much larger than the average delay spread due to its narrow bandwidth.

Although FDMA is relatively simple to implement, it suffers a number of serious drawbacks. In addition to its inefficient use of bandwidth (compared to other methods), it is also expensive to implement. Since only one user can be allocated for each carrier, and costly bandpass filters are needed to eliminate spurious radiations at the base station, the radio equipment used by one user at the base station cannot be shared with other users as in TDMA and CDMA.

3.3.2 Time Division Multiple Access (TDMA)

In TDMA systems, several users time-share a common carrier frequency to communicate with the base station. Each carrier frequency, i.e., channel, is divided into frames and time slots as shown in figure. 3.4. A channel is time-divided into frames, with preamble, an information message and trailing bits in each frame. One frame

consists of N slots. In each slot, there are trail bits, synchronization bits, and guard bits in addition to the information data bits. The guard bits in the frame and slot structures are used for receiver synchronization.

Each user is allocated one or more timeslots within a frame in both the downlink and uplink. The uplink and downlink can be on the same frequency in which case TDD is used, or different frequencies in which FDD is used. In general, TDMA/FDD systems intentionally induce several time slots of delay between the two links so that duplexers are not required in the subscriber unit.

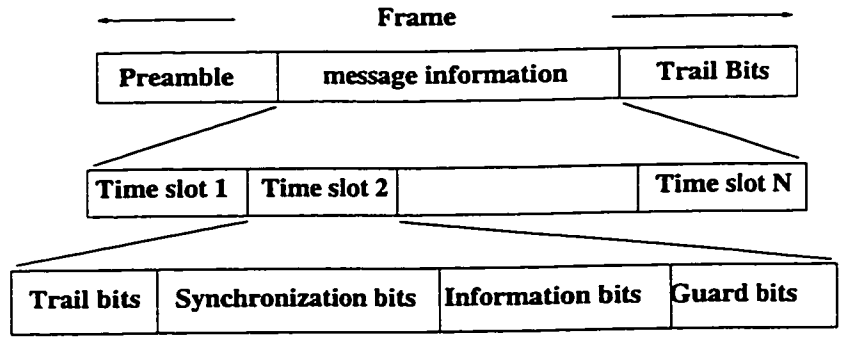

Figure 3.4: A general TDMA structure

Since N users can share the same carrier, one common radio equipment can be shared among them at the base station, thereby reducing the cost. The data rate for each user is also very easily changed by allocating multiple time slots. Multiple users can share the same channel, thereby increasing the symbol rate. TDMA usually requires some form of equalization in order to combat the intersymbol interference problem. The degree of equalization needed depends on the symbol rate and channel coherent bandwidth as discussed in Section 2.3.3.

Data transmission for each user is not continuous. Since each user has a $1/N$ duty cycle with a total of N users in one channel, TDMA signals have a periodically pulsating power envelope. This presents a challenge to designers of portable RF units. Frequency and time slot assignments also entails extra complexity in TDMA systems.

3.3.3 Code Division Multiple Access (CDMA)

CDMA is based on spread spectrum communications, which were originally developed for military applications. Spread spectrum communication uses transmission bandwidth that is much wider than the bandwidth of the original information signal. There are a number of way of achieving this; frequency hopping (FH) and direct sequence (DS) are the two most widely used methods. In FH, the information signal is

broken into bursts and each burst is transmitted at a different frequency. The current CDMA system, i.e., IS-95 standard family, however, is based on DS spread spectrum.

In DS-CDMA systems, the information signal is multiplied by a code sequence which is called the spreading sequence or signature waveform. The code sequence has a chip rate much higher than the information bit rate. The resultant signal thus has approximately the bandwidth of the spreading sequence, which is usually much wider than the original information signal. If each user uses a code sequence that is orthogonal to those of other users, it is possible for them to share the same carrier frequency without causing serious interference to each another. Upon detection of each user signal, the received signal is correlated with the code sequence for that particular user in order to decode the original message signal. All other user signals appear as noise due to the orthogonality of the code sequences.

Perfect orthogonality among all the users cannot be realized in the real world, thus the power of each user has to be strictly controlled to allow multiple users to use the same carrier frequency at the same time in CDMA systems. Otherwise, strong signals will yield higher noise power after the decorrelation for weak signals and make them difficult to detect.

CDMA systems have a number of unique features. The reuse factor of CDMA is one, i.e., all neighboring cells are co-channel cells. The capacity of a CDMA system depends on the noise level that can be tolerated in the system, rather than a hard number such as in the case of TDMA or FDMA. Since data rates are usually high, and many multipath components have time delays greater than the chip rate, a RAKE receiver can be used to improve reception by collecting multiple time delayed versions of the transmitted signal [49].

3.3.4 Comparison of FDMA, TDMA, and CDMA

Although it is generally agreed that TDMA and CDMA are more efficient and less costly to implement than FDMA, it is very hard to make an objective comparison between TDMA and CDMA. This is also one of the reasons that some of the current second generation wireless systems use TDMA while others use CDMA. TDMA is a better understood technology than CDMA, however, with more widespread use of CDMA technology, this situation is changing. It seems, for the present, CDMA is gradually gaining the upper hand. However, the battle of TDMA and CDMA is expected to last well into third generation wireless systems. Table 3.1 gives a comparisons of these three multiple access methods.

3.4 Mobility: High Tier and Low Tier Systems

Wireless communication standards tend to be targeted at two different markets. On the one hand we have lower tier systems with low mobility, low transmission power

Item	FDMA	TDMA	CDMA
Spectrum efficiency	low	high	high
Implementation cost	high	low	low
Modulation scheme	analog/digital	digital	digital
Equalization	not needed	needed	not needed
Power control requirement	low	low	high
Varying bit rates	not possible	possible	possible
Pulsating power envelop	no	yes	no

Table 3.1: A comparison of FDMA, TDMA, and CDMA

(and thus smaller cell sizes), and on the other hand we have high tier systems, which allow high mobility, higher transmission powers and larger cell sizes. Recently, there has been an increasing level of interest in fixed wireless access (FWA) or wireless local loop (WLL) systems. This is an extreme case of low tier system that has almost zero mobility. Systems such as personal access communications systems (PACS), digital European cordless telephone (DECT) and personal handyphone systems (PHS) are examples of the low tier systems, while GSM, IS-54/IS-136, and IS-95 are examples of the high tier system. Interestingly enough, most low tier standards seem to favour TDD which may be attributed to the suitability of the use of TDD in cells with smaller sizes.

Low mobility reduces Doppler Spread which translates into low channel variability, i.e., longer channel coherence time. This makes the channel characteristics easier to estimate and track which in turn requires less computational power for processing spatial-domain algorithms and adapting the weights of a smart antenna. Smaller cell sizes also result in lower delay spreads which reduces the need for time processing. The fact that most low tier standards are tied with TDD also means that downlink problem can be more easily solved in these systems. However, since low tier standards are intended to be used as low cost systems, the challenge of incorporating smart antennas with these systems will consist of finding a solution that improves the systems performance at low cost. The cost issue is less sensitive in high tier systems, however; it also presents a more challenging problem because of the higher channel variability associated with higher mobility. The fact that most high tier standards use FDD presents another major challenge for the use of smart antennas on the downlink.

3.5 Third Generation Wireless Standards: IMT-2000

IMT-2000 stands for International Mobile Telecommunications - 2000. It is an initiative of the International Telecommunications Union (ITU) directed at achieving a worldwide standard for third generation wireless systems. Its goal is to provide wireless access to the global telecommunication infrastructure through both satellite and terrestrial systems, serving fixed and mobile users in public and private networks with integrated voice and data service. It is being developed on the basis of the "family of systems" concept, defined as a federation of systems providing IMT-2000 service capabilities to users of all family members in a global roaming offering.

When third generation systems are deployed, users will not only be able to roam among countries which currently use different technologies but will also be capable of seamlessly moving between multiple networks - fixed and mobile, cordless and cellular. As a result, product life cycle for core network and transmission components should be longer. Network operators, service providers and manufacturers should benefit from increased flexibility and cost effectiveness. Table 3.2 gives a list of the Radio Transmission Technology(RTT) submitted to ITU by June 30, 1998.

While the path of evolution as well as its speed will be governed by market needs, appropriate global standards, as well as the harmonized assignment of suitable spectrum by the various national and regional authorities within the framework of the internationally agreed spectrum allocations in the ITU Radio Regulations, will be the determining factors for a successful implementation of IMT-2000.

IMT-2000 is being developed in recognition of the fact that future wireless access systems will need to provide users with the same high quality and broadband characteristics offered by fixed networks. As wireless becomes a major part of global telecommunications, common network components need to be developed which can provide virtually any desired future service combination composed of wired or wireless access links.

The present work schedule calls for the key choices of Radio Transmission Technology (RTT) associated with IMT-2000 to be made by March 1999, with appropriate ITU recommendations to be completed by the year 2000. Although the finally results of the ITU recommendation will not be known until the year 2000, Table 3.2 shows a clear trend towards CDMA, or wideband-CDMA to be exact, in third generation systems. Among all the proposed RTTs, the European Telecommunications Standard Institute(ETSI), decided to adopt W-CDMA for the FDD mode of UTRA, which is a radio transmission scheme very similar to the one contained in the Japanese proposal. Also, the U.S. is likely to harmonize their activities with the decision made by ETSI. In Korea, wideband CDMA is studied as one of the candidates for the radio transmission technology of IMT-2000. Thus W-CDMA is not only a more competent technology than other systems, but it is also the most

PROPOSAL	DESCRIPTION	ENVIRONMENT				SOURCE
		Indoor	Pedestrial	Vehicular	Satellite	
DECT	Digital Enhanced Cordless Telecommunications	x	x	-	-	ETSI Project (EP) DECT
UWC-136	Universal Wireless Communications	x	x	x	-	USA TIA TR45.3
WIMS W-CDMA	Wireless Multimedia and Messaging Services Wideband CDMA	x	x	x	-	USA TIA TR46.1
TD-SCDMA	Time-Division Synchronous CDMA	x	x	x	-	China Academy of Telecommunication Technology (CATT)
W-CDMA	Wideband CDMA	x	x	x	-	Japan ARIB
CDMA II	Asynchronous DS-CDMA	x	x	x	-	S. Korea TTA
UTRA	UMTS Terrestrial Radio Access	x	x	x	-	ETSI SMG2
NA: W-CDMA	North American: Wideband CDMA	x	x	x	-	USA T1P1-ATIS
cdma2000	Wideband CDMA (IS-95)	x	x	x	-	USA TIA TR45.5
CDMA I	Multiband synchronous DS-CDMA	x	x	x	-	S. Korea TTA
SAT-CDMA	49 LEO sats in 7 planes at 2000 km	-	-	-	x	S. Korea TTA
SW-CDMA	Satellite wideband CDMA	-	-	-	x	ESA
SW-CTDMA	Satellite wideband hybrid CDMA/TDMA	-	-	-	x	ESA
ICO RTT	10 MEO sats in 2 planes at 10390 km	-	-	-	x	ICO Global
Horizons	Horizons satellite system	-	-	-	x	Inmarsat

Table 3.2: IMT-2000 radio transmission technology proposal

promising system to be applied as a global system. Therefore, it is necessary to carry out research into applying smart antenna technology to wideband CDMA for the various wideband CDMA proposals. In Chapter 6 we are going to study the problem of applying multibeam smart antennas to CDMA systems.

3.6 Conclusions and Discussions

In this chapter, various wireless standards, including the third generation standard —IMT2000, which is under world-wide investigation, are discussed with an emphasis on their impact on the smart antenna technology. We also showed how the problem of applying smart antenna algorithms on the downlink differs for FDD and TDD systems. The challenge of downlink smart antenna algorithms in FDD systems is identified which lays a foundation for the work described in Chapter 5.

Chapter 4

Multibeam Smart Antenna Systems and Algorithms

This chapter begins with an overview of antenna arrays and beamforming techniques in Section 4.1, followed by Section 4.2 in which multibeam smart antennas are studied in relation to beam-space beamforming. In Section 4.3, signal combining algorithms that are applicable to the multibeam smart antenna are described.

4.1 Antenna Arrays and Beamforming

A multibeam smart antenna uses multiple directive antenna beams to illuminate the whole coverage area of the base station. The directive beams can be generated by applying a technique called *beamforming*. The term beamforming relates to the function performed by a device or apparatus in which energy radiated by an aperture antenna is focused along a specific direction in space [2]. For example, in a parabolic antenna system, the dish is the beamforming network in that it takes the energy that lies within the aperture formed by the perimeter of the dish and focuses it onto the antenna feed. Energy from the preferred direction is aligned at the feed and summed coherently while energy from other directions is summed incoherently [2].

Although it is possible to use antenna systems such as the parabolic antenna to form a multibeam smart antenna, it is generally more desirable to use antenna arrays. By applying beamforming to an array of antenna elements, one can obtain directional antenna beams at low cost. In addition, the beam patterns formed by an antenna array are very flexible. An antenna array can change its beam patterns if desired, which is a very desirable feature in time-variant wireless environments. As shown in Figure 4.1, the array consists of N antenna elements designed to receive (and/or transmit) signals. The physical arrangement of the array is arbitrary. Linear, circular and planar arrays are some of the most widely used structures. The beamforming network is capable of weighting the signals received at each antenna

element over a wide range of relative amplitude and phase values in order to produce an effective pencil-beam radiation pattern at each output port. The number of ports can be different from the number of antenna elements, usually the number of ports is smaller.

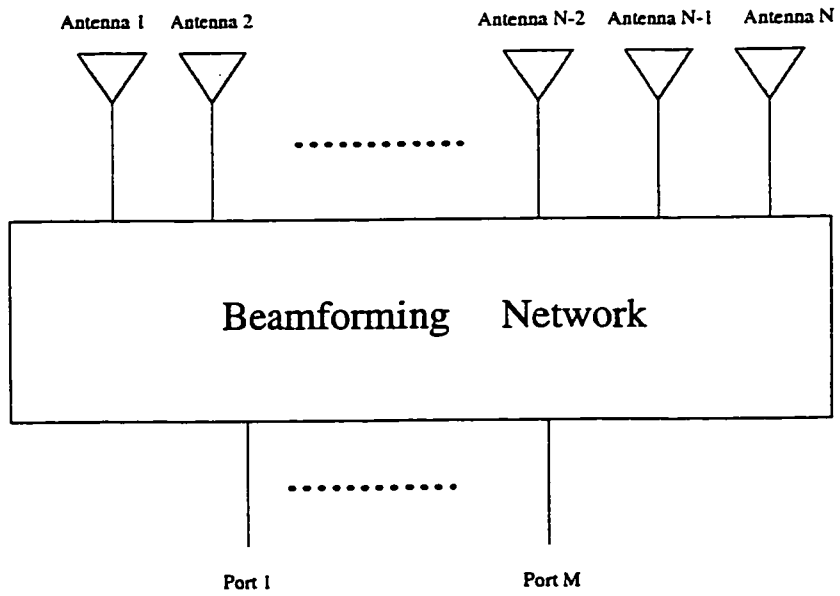

Figure 4.1: Array-beamforming network for a multibeam antenna

4.1.1 Antenna Array Overview

Many applications require antennas that produce narrow concentrated beams with little radiation in other directions. Such directional antennas can be generated by a single antenna such as the parabolic antenna, but a more flexible approach is to use antenna arrays. An antenna array is a collection of more than one identical antennas that are arranged and excited to produce high-gain beams in certain directions [28, 50].

Antenna arrays can have many different configurations, the linear array and the circular array are the most common among them. A linear array consists of n equally spaced antenna elements along a straight line as shown in Fig. 4.2. A circular array consists of n equally spaced antenna elements placed on a circle as shown in Fig. 4.3.

To derive the radiation pattern of a general array and to see how an antenna array can form directional beams, consider N identical antennas, placed within an area of radius r_0 as shown in Fig. 4.4. We place an additional reference antenna,

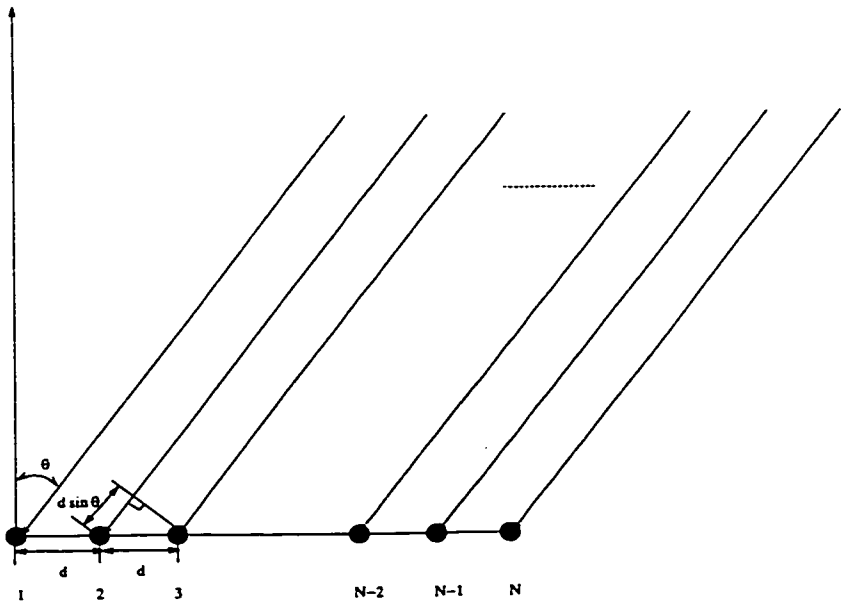

Figure 4.2: A linear array

which has the exact same radiation pattern, at the origin. The electromagnetic field generated by the reference antenna at an observation point (r, θ, ϕ) in the far field of the array is [1]

$$P = I_0 \frac{e^{-jkr}}{r} p(\theta, \phi) \tag{4.1}$$

where k is the wavenumber, I_0 is a complex amplitude, and $p(\theta, \phi)$ is the radiation pattern of the reference antenna. The far field generated by each of the N antenna array elements is similar to Eqn. (4.1), which is

$$P_n = I_n \frac{e^{-jkR_n}}{R_n} p(\theta_n, \phi_n) \tag{4.2}$$

where $n = 1, 2, \ldots, N$, and R_n is the distance between the nth antenna element and the observation point (r, θ, ϕ). Since $r_0 << r$, the following approximation can be used

$$e^{-jkR_n} = e^{-jkr} e^{j2\pi d_n/\lambda} \tag{4.3}$$

where λ is the wavelength, d_n is the projection of $\mathbf{r}_n$ on $\mathbf{r}$. In addition, $1/r_n \approx 1/r$, $\theta_n \approx \theta$, and $\phi_n \approx \phi$. Eqn.(4.2) can be approximated as

$$P_n = I_n \frac{e^{-jkr}}{r} p(\theta, \phi) e^{j2\pi d_n/\lambda} \tag{4.4}$$

[1]The far field of an antenna array is defined as observation points which satisfies $r >> r_0$, where r is the distance between the antenna and the observation point.

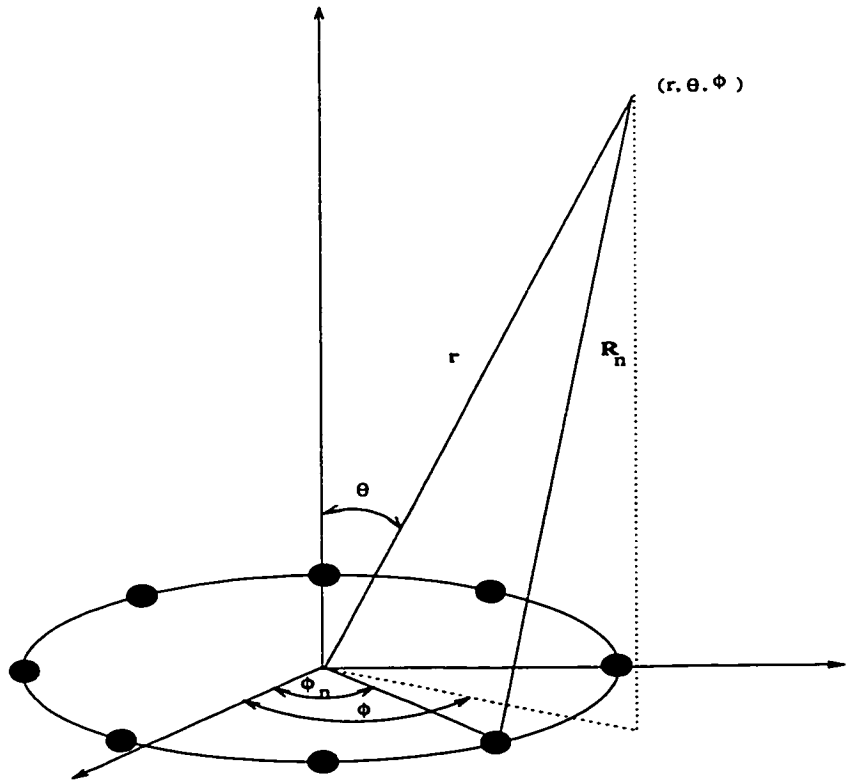

Figure 4.3: A circular array

By the use of the superposition principle, the total field generated by the N element antenna array at the far field is

$$P_n = \sum_{n=1}^{N} P_n = I_0 \frac{e^{-jkr}}{r} p(\theta, \phi) \sum_{n=1}^{N} \frac{I_n}{I_0} e^{j2\pi d_n/\lambda} \tag{4.5}$$

Eqn. (4.5) indicates that the far field of an antenna array is equal to the reference antenna pattern multiplied by a sum called the *array factor* which is $\sum_{n=1}^{N} \frac{I_n}{I_0} e^{j2\pi d_n}$. [2]

[2]In array processing, a frequently used term which is related to the array factor is called *array response vector* or *steering vector*. If we assume the complex weights, $I_0, I_1, \ldots, I_N$ are equal, and the first antenna element is placed in the origin, the array factor for Eqn. (4.5) is

$$\sum_{n=1}^{N} e^{j2\pi d_n/\lambda} = 1 + e^{j2\pi d_1/\lambda} + \ldots + e^{j2\pi d_N/\lambda} \tag{4.6}$$

The vector corresponding to the above array factor, which is $[1, e^{j2\pi d_1/\lambda}, \ldots, e^{j2\pi d_N/\lambda}]$ is called the array response vector. Apparently, the array response vector is a function of both frequency and array geometry, since it is dependent upon λ and d_n.

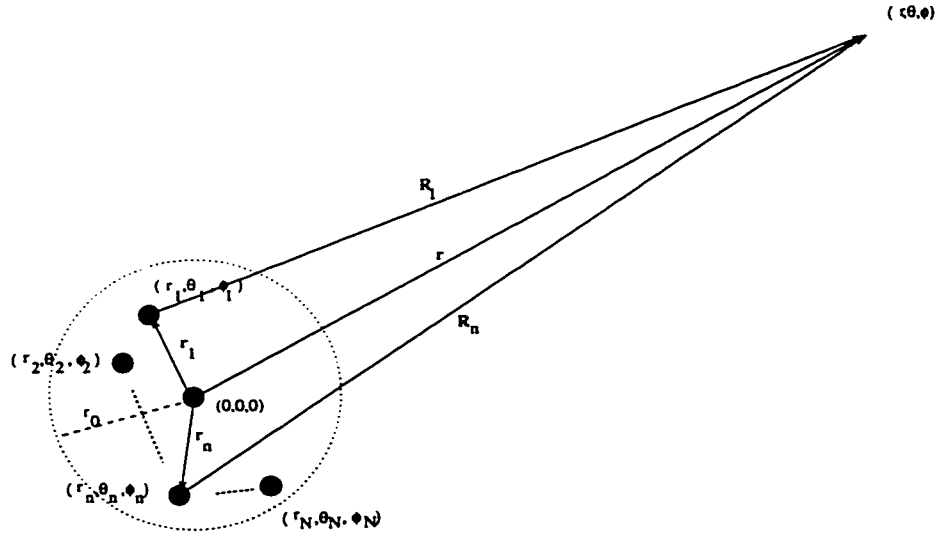

Figure 4.4: A generic array

By adjusting parameters such as N, $\frac{I_n}{I_0}$, d_n, one can obtain various directional antenna beams. To show this, we use the linear array shown in Fig. 4.2. In the case of the linear array, d_n satisfies the following equation:

$$d_n = (n-1)kdcos\theta\frac{\lambda}{2\pi} \tag{4.7}$$

Consider a special case in which the complex amplitudes are equal and the relative phase between adjacent elements is a constant β. Eqn. (4.5) becomes

$$P_n = \sum_{n=1}^{N} P_n = I_0\frac{e^{-jkr}}{r}p(\theta,\phi)\sum_{n=1}^{N} e^{j(n-1)(kdcos\theta-\beta)} \tag{4.8}$$

Fig. 4.5 shows the array pattern of an 8-element linear array which is comprised of omnidirectional antenna elements with a spacing of $\lambda/2$.

4.1.2 Analog and Digital Beamforming

Beamforming can be achieved through either analog or digital methods. Figure 4.6 shows the structure of an analog beamforming network which consists of devices such as power dividers, power combiners, and phase shifters. They are used to adjust the amplitudes and phases of the signals received from each antenna element, thereby forming a desired directional beam. Figure 4.6 shows a single-beam beamforming network. Multiple single-beamforming networks can be used when a

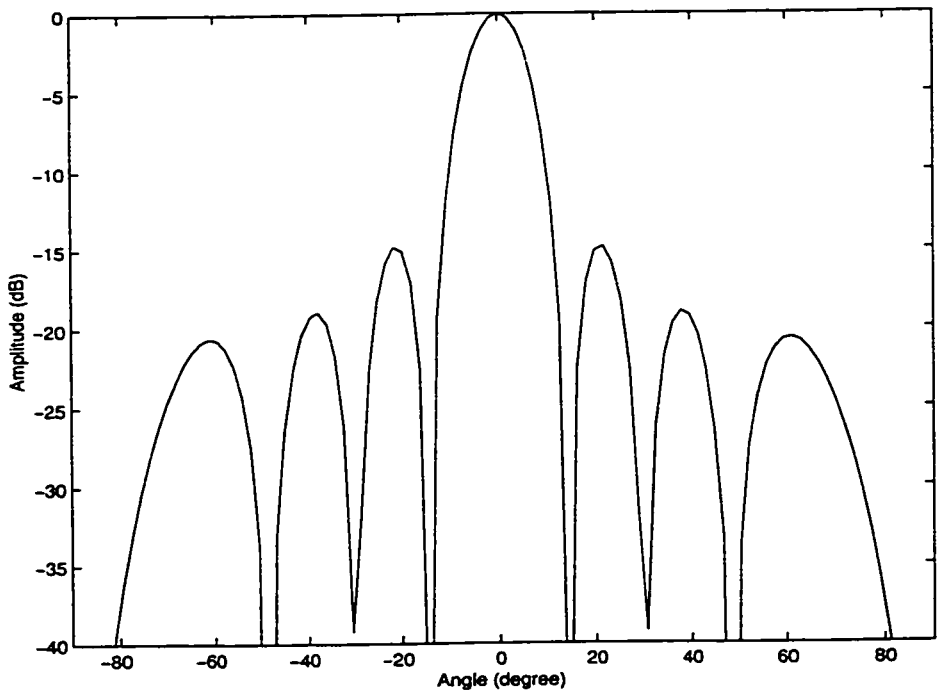

Figure 4.5: The beam pattern of an 8-element linear array

multibeam antenna is needed. By offsetting the desired direction of each single-beam beamforming network, a multibeam antenna can be generated.

Beamforming can also be carried out digitally. Figure 4.7 depicts a generic digital beamforming (DBF) structure. The transceivers are required to perform frequency down-conversion and up-conversion, filtering, and amplification. A/D and D/A converters converts signals in the digital domain into analog domain, and vise versa. Various digital signal processing techniques can be used to form the desired beams. The major advantage of digital beamforming is the fact that RF signals are captured in digital form, enabling a multitude of digital signal processing techniques and algorithms to be used for spatial processing. It also brings great flexibility without any degradation in SNR.

4.2 Multibeam Smart Antenna Structures and Beam-Space Beamforming

There are many possible ways of performing digital signal processing in digital beamforming. One possible way of characterizing various DBF methods is to divide them into two categories: element-space beamforming and beam-space beamforming.

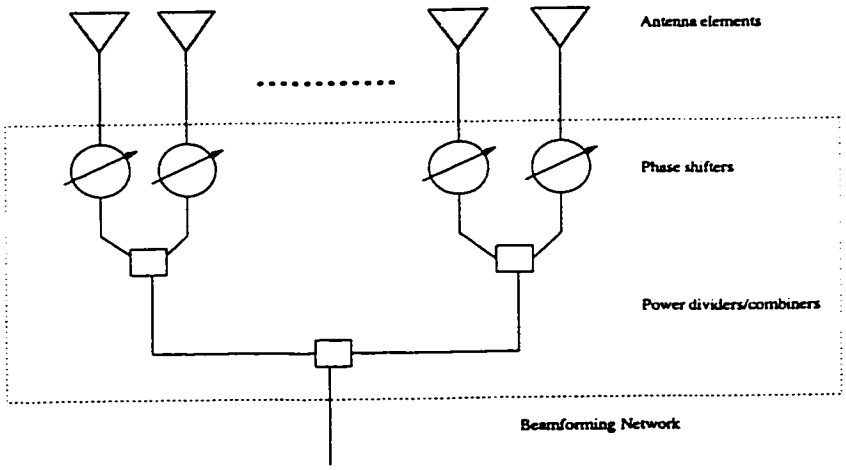

Figure 4.6: An analog beamforming network

Figure. 4.8 shows a simple beamforming structure in element space. In element-space beamforming, one manipulates signals directly from/to the antenna elements by applying weights to the signals to achieve the desired response. In contrast, in beam-space beamforming, the outputs from/to the array elements are first processed by a multiple-beamforming network to form a set of beams. The beam outputs are then weighted and combined to produce the desired output. Figure. 4.9 shows a beam-space beamforming structure.

It can be proven that beam-space beamforming and element-space beamforming are equivalent provided that the number of beams formed in beam-space is equal to the number of elements and the beams formed in the beam-space are all orthogonal [51].

But what is really interesting is the case when $M < N$ as shown in Figure. 4.9, in particular, when $M << N$. Although the capability of an adaptive array to perform a pattern shaping function increases as the number of elements increases, the complexity of the processing circuitry and logic also increases. In addition, the complexity of processing may make it impractical for real-time usage. By using $M << N$, the number of signal ports can be kept tractable while performance close to the element-space processing can be achieved. In many cases, the implementation of smart antennas using beam-space beamforming is simpler.

The structure of multibeam smart antennas can be generalized as shown in Figure. 4.10. The multibeam smart antenna consists of three main components: a multibeam antenna, a beam selection processor, and a combining processor. The beam selection processor reduces processing complexity by reducing the number of beams included in the combining processor. The combining processor validates the beam selection, does combining and other appropriate signal processing.

Comparing Figures 4.10 and 4.9, we can see that multibeam smart antennas

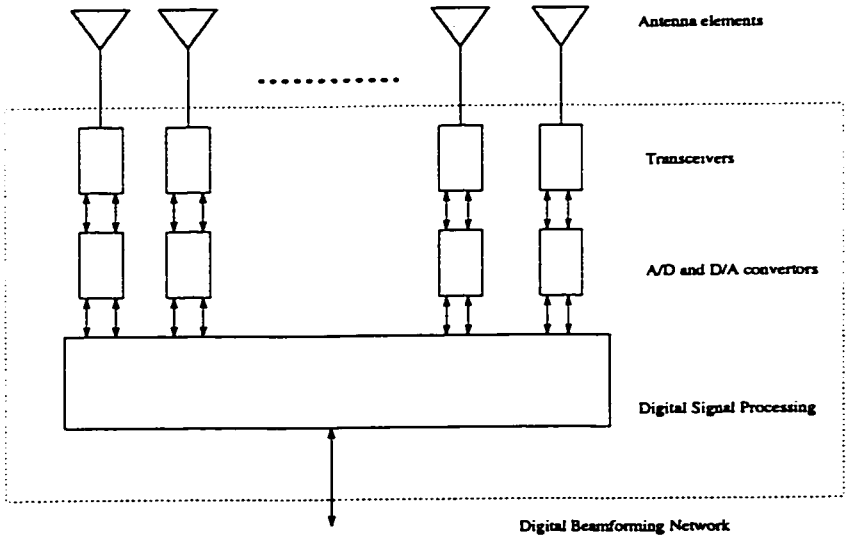

Figure 4.7: A generic digital beamforming network

have close relationship with beam-space beamforming. In fact, multibeam smart antennas can be viewed as a special case of beam-space beamforming.

The adaptive processor determines the operation of beam selection/combining. The information commonly used by the adaptive processor includes: [52]

- The signals received by the antenna array.
- The output of the smart multibeam antenna.
- The structure of the antenna array.
- Feedback signals from the mobiles.
- Network topology.

4.3 Multibeam Smart Antenna Combining Algorithms

From the perspective of diversity, the multibeam smart antenna can be viewed as an extension of angle diversity systems. Most algorithms used for multibeam smart antennas bear their roots in diversity combining algorithms, although the operation of the multibeam smart antenna is usually more complicated.

In wireless communication literature, compared to antenna space diversity, angle diversity has received far less attention. The use of space diversity has long been

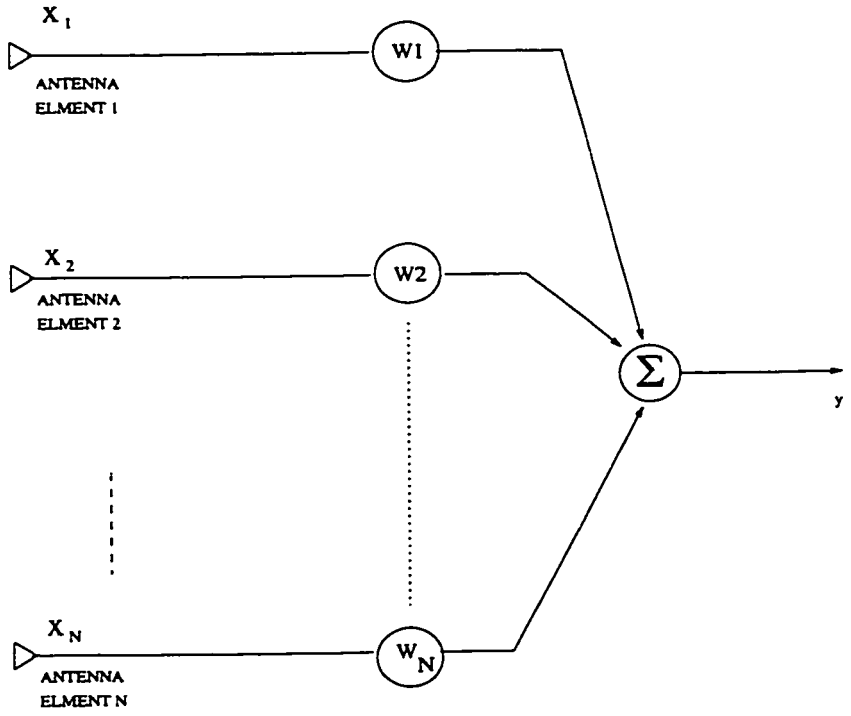

Figure 4.8: A simple beamforming structure for element-space processing

recognized as an effective technique for combating the detrimental effects of channel fading [42, 53, 54]. This is probably due to the fact that classical diversity techniques are usually applied to noise-limited systems. It has not been until recently, with the introduction of cellular technology, that interference-limited system caused by co-channel interference has become very important. The inherent difference in their AOAs distributions makes angle diversity a very attractive candidate for interference cancellation in such systems.

Diversity combining algorithms can be classified into three types, namely, selection combining (SC), equal gain combining (EGC) and maximal ratio combining (MRC) [42]. The structures of these combining methods are similar, the differences (and thus the resultant performance) lie mainly in the mechanism of complex weight generation.

4.3.1 Selection Combining (SC) Algorithm

Selection combining is the simplest of all combining algorithms. Referring to Figure 4.11, the basic idea behind selection combining is to select the single beam with the best *baseband* signal-to-noise-and-interference ratio (SNIR). In practice, however,

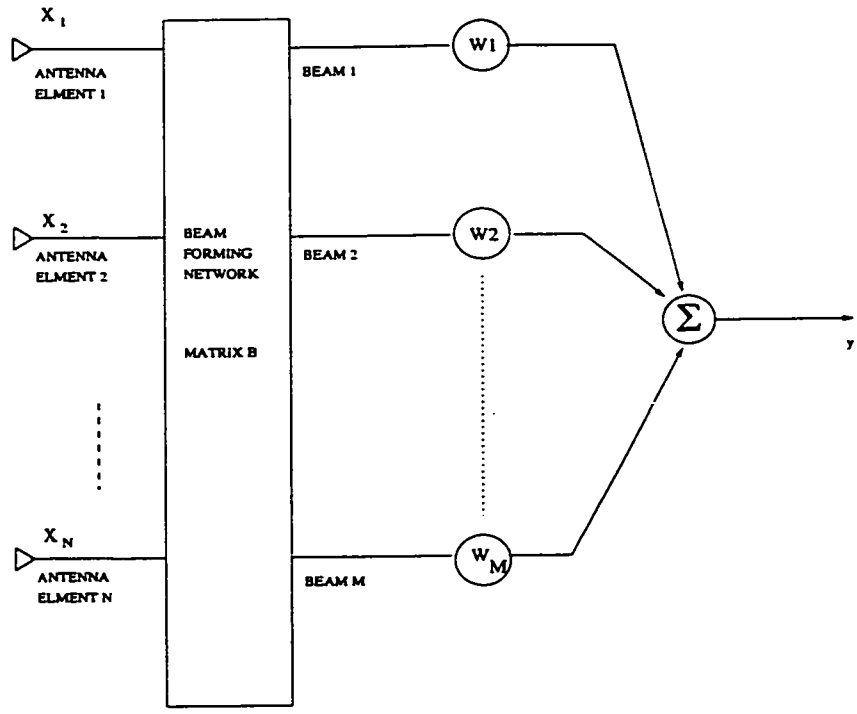

Figure 4.9: A simple beamforming structure for beam-space processing

there are different approaches. For example, the beam with the highest signal-plus-noise power may be selected in certain situations when it is difficult to estimate SNIR.

In a typical wireless communications environment, instead of a single beam, the received signal powers at several beams are often higher than the rest. For selection combining to work well in this kind of environment, the SC algorithm can be generalized to include more than one beam. In this case, *coherent* combining is usually used. By coherent combining we mean that the signal in each beam has to be properly aligned in phase before they are combined. The combining weights are selected using the same method as in maximal ratio combining (MRC) algorithm which is the subject of the next section.

Thomas Eng et al. have studied this generalization of SC algorithm in [55]. Their study shows that algorithms combining the two (or three) strongest branch signals, which is termed as SC2 (or SC3), offer significant improvement over the performance of just selecting the largest signal (SC). When the number of available paths is small, or only a few of the branches have significant signal power, SC2 and SC3 perform close to the maximal ration combining when coherent combining is used. Furthermore, SC2 and SC3 perform better or comparably to EGC if non-coherent combining is used.

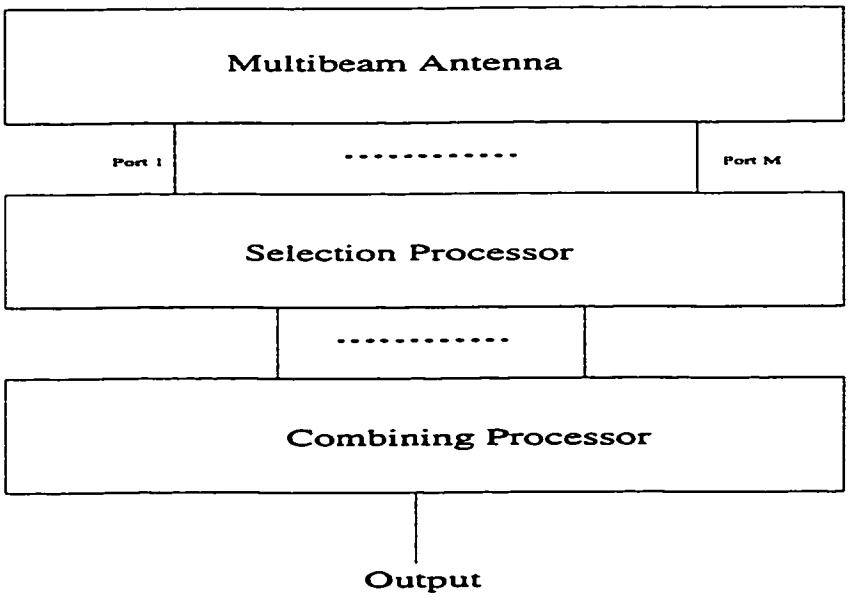

Figure 4.10: A generic multibeam smart antenna structure

4.3.2 Maximal Ratio Combining (MRC) Algorithm

In maximal ratio combining the signal in each beam is cophased and weighted proportionally to the ratio of its signal to noise ratio before they are summed together. Fig. 4.12 shows the signal flow diagram for this method. If we denote the received signal in the ith beam signal as r_i, it includes s_i and n_i, which are the desired signal and noise respectively. That is

$$r_i = s_i + n_i \tag{4.9}$$

If r_i are weighted and combined, the combiner output can be expressed as

$$R = \sum_{i=1}^{M} g_i(s_i + n_i) \tag{4.10}$$

where g_i is the weight applied to each beam. If we denote noise power at each beam to be N_i, i.e., $N_i = E(|n_i|^2)$ ($E()$ represents the expectation of a random variable), and also assume that they are mutually independent, the total noise power in Eqn. (4.10) is

$$N = \sum_{i=1}^{M} |g_i|^2 N_i \tag{4.11}$$

The SNR of the combiner output is then

$$\gamma = \frac{|\sum_{i=1}^{M} g_i s_i|^2}{\sum_{i=1}^{M} |g_i|^2 N_i} \tag{4.12}$$

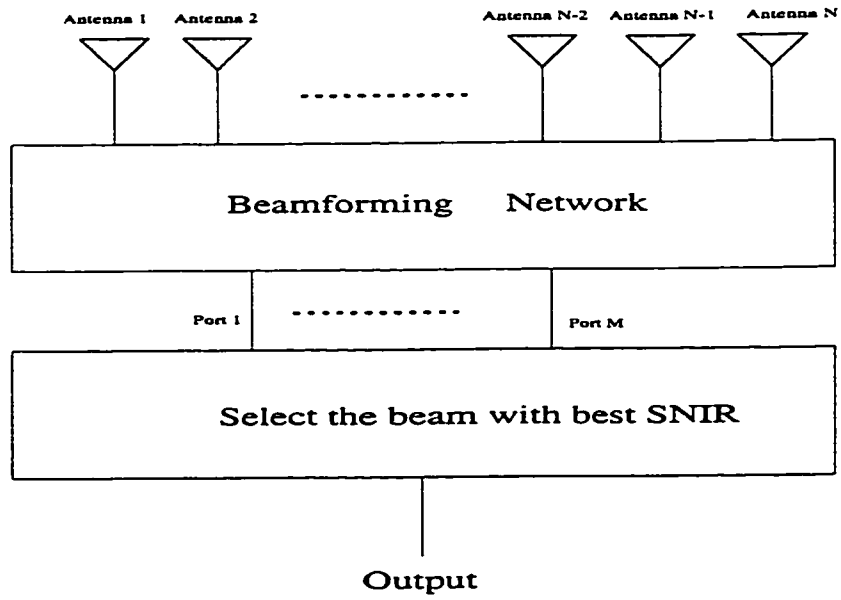

Figure 4.11: The selection combining algorithm

It can be proven that γ is maximized if we choose [29]

$$g_i = K\frac{g_i^*}{N_i} \tag{4.13}$$

Where K is some arbitrary complex constant and * denotes complex conjugate. The maximum value for γ is

$$\gamma = \sum_{i=1}^{M} \frac{|s_i|^2}{N_i} \tag{4.14}$$

which equals the sum of the SNR in each beam.

4.3.3 Equal Gain Combining (EGC) Algorithm

It is not always possible to provide the variable weighting capability required for true MRC. To deal with this kind of situation, one method is to cophase the signals in each of the beams and combine them by setting all the weights to be unity. This is referred to as equal gain combining (EGC).

Denote the signal received by the ith ($i = 1, 2, \ldots, M$) beam as r_i. It can be expressed as

$$r_i = s_i + n_i \tag{4.15}$$

where s_i and n_i are the desired signal and noise in that beam, respectively. The

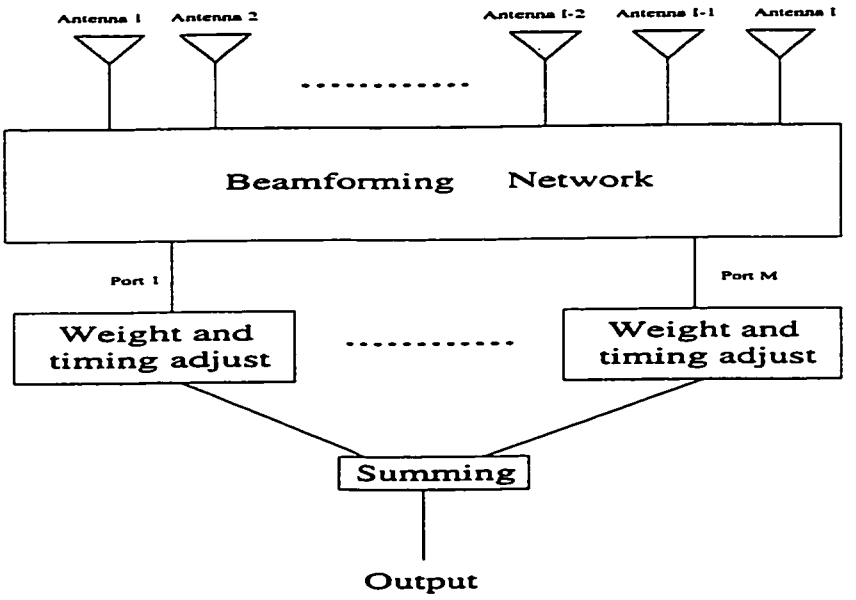

Figure 4.12: The maximal ratio combining algorithm

output from an equal gain combiner is

$$R = \sum_{i=1}^{M} r_i \tag{4.16}$$

The SNR for the equal gain combiner is then

$$\gamma = \frac{\sum_{i=1}^{M} |s_i|^2}{\sum_{i=1}^{M} N_i} \tag{4.17}$$

Equal gain combining algorithm is most effective when the noise levels in all beams are equal. Otherwise, those beams with large noise levels would dominate the output SNR even if the beam itself is weak in terms of signal level. If various beams have unequal noise, one way to equalize the noise would be to use different gains in each beam before combining.

4.3.4 Comparison of Algorithms

Of the three algorithms presented above, the MRC algorithm gives the best performance, however it is also the most complex algorithm to implement since the SINR has to be estimated at each beam. Due to the difficulty and cost involved in the implementation of the MRC algorithm, SC/SC2/SC3 or EGC are usually the algorithms of choice in many situations. The MRC algorithm is more of theoretical curiosity and is often used as a benchmark for other combining algorithms [56]. In real wireless

propagation environments, the angular distributions of signals and interference are very different. Usually, there are a few beams with strong signals and/or strong interference while the rest are relatively weak, both in terms of the desired signal and the interference signals. In this case, SC/SC2/SC3 may be the most cost-effective algorithm.

Chapter 5

Multibeam Smart Antennas for the Down-link Transmission in FDD Systems

5.1 Introduction

Most wireless communication systems today have two links: *uplink* (or reverse link) and *downlink* (or forward link). Radio signals transmitted from base stations travel via the downlink before being received by mobile stations; signals transmitted from mobile stations travel via the uplink before received by the base station. As was mentioned before, practical considerations generally rule out the possibility of using an antenna array on the mobile station side, thus leaving only the base station as a candidate for deploying smart antennas. This makes it difficult to use smart antennas for the downlink. On the downlink, the smart antenna has to decide on what processing should be done *before* the signal is transmitted through the wireless channel to the mobile station. This contrasts the uplink case where the smart antenna can receive the multipath signal first and then do processing as appropriate. In other words, a smart antenna can estimate the channel on the uplink, while it can not do so directly on the downlink. The fundamental question for smart antennas working in the downlink is the following: can it estimate the downlink channel? If yes, how?

The principle of reciprocity implies that downlink and uplink channels are identical if the channels operate on the same frequency and nearly simultaneously in time. In a TDD system, if the duplexing time between reception and transmission is small compared to the coherence time of the channel, both channels are approximately the same for the uplink and downlink, and the base station can use its estimate of the uplink channel and apply it to the downlink channel. In FDD systems, the downlink and uplink channels can potentially be very different due to the large frequency separation of the two channels. S.S. Jeng et al have conducted measurements

on the difference of the uplink and downlink channel in terms of their spatial signatures [57]. [1] Their results show that the spatial signature variation is quite significant even for a small percentage change ($< 5\%$) of the carrier frequency. Most digital cellular standards operating in 800 MHz frequency band, $IS-54/IS-136(TDMA)$, $IS-95(CDMA)$ and GSM, for example, have a frequency separation of 45 MHz while Personal Communications Systems in the 1.9 GHz frequency band have a frequency separation of 80 MHz. The frequency separation, whether 45 MHz or 80 MHz, is large enough to give rise to different values for the complex gain experienced by each multipath at the two frequencies.

Although AOA based algorithms show promise for smart antennas in the downlink, they are restricted by the requirement that they need more antenna elements than the number of multipath components [58]. In this chapter, we investigate the use of multibeam smart antennas for downlink transmission. Our focus is on FDD systems since this is still a major challenge for researchers of smart antennas.

Algorithms for smart antenna systems working on the downlink are still in their preliminary stages of development and much work remains to be done. In dealing with the downlink smart antenna problem, we analyze the large set of practical data we have collected with the 8-element vector channel sounder system. An in-depth understanding is obtained by examining individual cases from the measurements. In addition, numerical simulations are also conducted whenever necessary using the Geometrically Based Single Bounce (GBSB) vector model.

The chapter is organized as follows: First, the downlink system model is presented and major difficulties involved in downlink are identified. Next, the results from measurements and experiments are analyzed. Simulations using the geometrically based single bounce (GBSB) model are carried out to gain further insight into the analysis. A novel multibeam smart antenna algorithm for downlink transmission is then proposed. Its performance improvement is shown and analyzed for a QPSK modulation system.

5.2 Estimating the Downlink: the System Model and General Approaches

The objectives for a smart antenna on the downlink are three-fold:

- to maximize signal power delivered to the desired mobile station.
- to minimize the co-channel interference (CCI) to other mobile stations.

[1] If we denote the array steering vector as $\mathbf{a}(\theta)$, the spatial signature of a source $s(t)$ is defined as $\sum_{l=1}^{L} \mathbf{a}(\theta_l)$, where θ_l is the angle of arrival of the lth multipath and L is the total number of multipath associated with $s(t)$.

- to minimize fading of the signal received by the desired mobile station.

The CCI at the desired mobile station is usually not controlled by the base station in which the smart antenna operates unless some kind of complex multiuser detection scheme is used as will be addressed to in Chapter 6. For the present, we concentrate on the single-user detection scheme in which the CCI is not under the direct control of the referenced base station or the smart antenna system. However, the method used here is also applicable to CDMA systems using multiuser detection.

Smart antennas involve both spatial and temporal signal processing. For this kind of signal processing to be successful the key lies in the estimation of the characteristics of the channel. The effectiveness of both spatial and temporal processing depends on the degree to which the channel can be estimated. There are basically two approaches in dealing with the estimation of the downlink:

1. estimate the downlink *directly* from the uplink.

2. base the estimate on feedback between the mobile station and the base station.

5.2.1 Downlink Channel Estimation in TDD Systems

Time-division duplexing (TDD) systems use time-sharing on a single frequency for both transmission and reception. CT2, DECT, PHP(Personal Handy Phone) and DCS 1800 are some examples of TDD systems [2].

The principle of reciprocity implies that downlink and uplink channels are identical if the uplink and downlink communications use the same frequency and are nearly simultaneous in time. If that happens, the downlink channel will be a scaled version of the uplink channel.

The current trend seems to see TDD techniques applied mostly in low-tier, low mobility wireless systems. Since the channel coherence time is inversely related to the Doppler shift which is proportional to the speed of the relative movement between the base station and the mobile station, the duplexing time between reception and transmission will be small compared to the coherence time of the channel in these low mobility systems. Thus both channels are roughly the same and the base station can use its estimate of the uplink channel for controlling and optimizing the downlink channel.

When applying TDD techniques to higher mobility wireless systems, the task of the downlink channel estimation is still less formidable than in FDD systems. Although the two channels are no longer completely reciprocal, strong correlation can still be expected given the fact that transmission and reception occur at the same frequency.

5.2.2 Downlink Channel Estimation in FDD Systems

Frequency-division duplexing (FDD) is used in many current wireless systems, most prominent among them are systems based on IS-54/IS-136, IS-95, and GSM standards. In FDD systems, the downlink and uplink channels can potentially be very different due to the large frequency separation. The difference in channel arises from the difference in the instantaneous complex path gains, in particular, the relative phases of the signals arriving via different paths vary with changes in frequency. This difference makes it impossible for a smart antenna to reuse the weights of its uplink for its downlink.

Paulraj and Papadias have proposed to divide this estimation problem into four different situations according to the relative time-delays and angle-spreads of the multipath signals [59]. The four situations consist of the following:

1. Zero delay and angle spread: in this condition the channel reduces to a single vector, $a(\theta)$. In this case the uplink and downlink channels are identical up to a scalar factor. If we denote the vector channel impulse responses of the uplink and the downlink channels as $\mathbf{H}_u$ and $\mathbf{H}_d$, respectively, $\mathbf{H}_u = c\mathbf{H}_d$, where c is a scalar. [2]

2. Zero angle spread, nonzero delay spread.

3. Zero delay spread, nonzero angle spread.

4. Finite delay and angle spread.

While the first three situations are more or less ideal situations, the last one is more frequently encountered. It is of more practical value, but is also the most difficult to deal with.

As was shown in Chapter 2 the vector channel impulse responses of both the uplink and downlink can be expressed as

$$\mathbf{h}(\tau) = \sum_{l=1}^{L_q} \mathbf{a}(\theta_{lq}) A_{lq} e^{j\phi_{lq}} \delta(\tau - \tau_{lq}) \tag{5.1}$$

While it is arguable that the amplitude of A_{lq} is the same for both uplink and downlink; the total number of paths L_q, time delays τ_{lq} and angles-of-arrival (angles-of-departure in the downlink) θ_{lq} are expected to be the same. This may suggest that AOA based algorithms are better positioned for smart antennas in the downlink. If the delay and AOA can be jointly estimated in the uplink, the same information can be used in the downlink processing. However, a fundamental difficulty here is that all AOA estimation techniques currently available are based on the key assumption that

[2] Both $\mathbf{H}_u$ and $\mathbf{H}_d$ satisfy Eqn.(5.1).

the number of signal wavefronts, including cochannel interference signals, must be less than the number of antennas in the array [58]. In a typical wireless communication environment, there are usually a large number of multipath signals, therefore, it would be too costly to apply these AOA estimation techniques because it would require too many antenna elements.

Another approach is feedback. Paulraj and Papadias suggested a feedback approach in which a training signal is transmitted individually by each element of the base station antenna array to the mobile station [59]. The estimation of the channel from each base station antenna to the mobile station can be solved using methods such as Least Squares. Once the channel for each antenna is estimated, the total vector channel can be determined. In [60], another feedback approach is proposed. In this approach, the base station transmits probing signals separately from each element on the downlink frequency, each mobile station measures its own response to the probing signal and feed the information back to the base station. Based on the feedback, the downlink channel is estimated, thereby deriving the weights that can be used by the smart antenna for the downlink. However, this approach requires the interruption of normal information transmission when the base station transmits probing signals.

While the feedback approach may seem feasible, it suffers a number of drawbacks. Feedback algorithms need information to be transmitted back from the mobile station to the base station, occupying additional bandwidth which reduces the system capacity. It also requires a complete re-design of current protocols. With the increase of demand for wireless communications, the system capacity is becoming one of the most important issues with respect to future systems. It is very desirable that we develop algorithms which estimate *directly* the downlink channel from the information obtained on the uplink channel, and require no additional bandwidth. The multibeam smart antenna is a possible solution to this problem. A multibeam smart antenna can measure the channel characteristics at the receive frequency and decide on appropriate actions when transmitting on the downlink frequency. For example, it may decided to transmit on the beam that has maximum received signal power. Although this is a fairly good first estimate in some cases, this is clearly not adequate in most practical situations, especially in highly built-up urban areas. In the rest of this chapter we will explore options and expand on the idea of transmitting on the beam with maximum received power, thereby devising a novel transmission algorithm for multibeam smart antennas.

5.3 Estimating the Downlink in Multibeam Smart Antenna Systems

5.3.1 Uplink and Downlink Relation: Measurement Results

A series of experiments were designed by the Wireless Technology Group, McMaster University to investigate the channel characteristics at PCS transmit and receive frequencies and the possible relationship between them. Extensive measurements and experiments were carried out at several outdoor sites on the McMaster University campus and surrounding areas. Several indoor measurements have also been conducted inside the Communications Research Laboratory at McMaster University.

The FDD experiment was set out as follows: A transmitter with a dipole antenna was used to repetitively transmit a 255-bit PN sequence with a chip rate of 5MHz at two frequencies at the same time. While transmitting, the transmitter was in motion, carried about at walking speed. An 8-element circular antenna array, which we named Talaris, receives the signals and samples them at a 10 MHz clock rate. The sampled signals were first stored in a Sun Sparc workstation and later multiplied offline by 8 pre-calculated vector weights, which emulate an 8-beam multibeam antenna. This effectively provided us with a database that would be received using an 8-beam (multibeam) antenna.

A. The Power Distribution on the Uplink and Downlink

When considering the application of a multibeam smart antenna to the downlink problem, the first question one has to answer is: does the signal power distribution in each beam at the transmit frequency bear any relationship with that of the receive frequency?

To answer this question, the large amount of data from the FDD measurements are processed and further analyzed. The signal received at each beam is correlated with the transmitted PN sequence to yield the corresponding channel impulse response. Fig. 5.1 shows the impulse response of each beam at one time instant for a particular outdoor measurement site. The impulse response of an omni-directional antenna, measured simultaneously with the multibeam antenna, is also plotted at the lower right part of Fig. 5.1 (labeled as omni) for the purpose of comparison. Generally, depending on the environment, there will be a marked difference in the energy received on the different beams. One thing worth noting is that the output of each beam has a finite number of multipath components, although the number of multipath signals is much smaller than is the case for the omni-directional antenna.

Denote $p_{ti}(nT)$ and $p_{ri}(nT)$ as the average power of the impulse response of the ith beam at $t = nT$ for transmit and receive frequencies, respectively, where

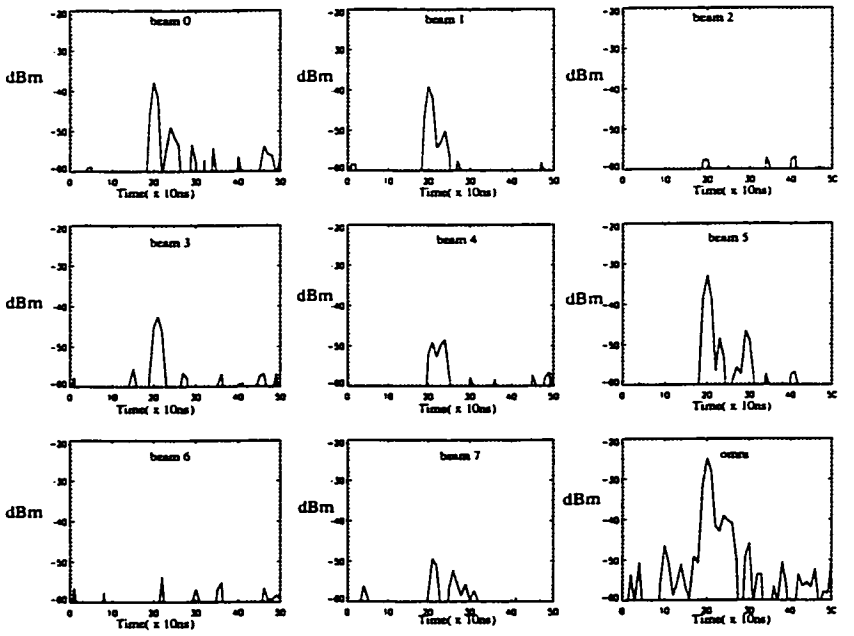

Figure 5.1: Impulse responses of multibeam antenna and omni directional antenna

$i = 0, 1, \ldots, 7$. We rank the average powers of all the beams at the transmit frequency ($p_{ti}(nT)$) in descending order and denote $K_{ti}(nT)$ as the rank for the ith beam. Similarly, we rank $p_{ri}(nT)$ in descending order and have $K_{ri}(nT)$ as the rank for the ith beam at the receive frequency. $K_{ri}(nT)$ and $K_{ti}(nT)$ are generally random variables. To investigate the relation between $K_{ri}(nT)$ and $K_{ti}(nT)$, the conditional probability $P\{K_{ti}|K_{ri}\}$ obtained from our measurement database is analyzed. Figure. 5.2 plots $P\{K_{ti}|K_{ri}\}$ at one outdoor measurement site, where $i = 0, 1, \ldots, 7$. The transmit and receive frequencies are 1.94 GHz and 1.86 GHz respectively.

Figure. 5.2 suggests that there is statistically strong correlation in the power distributions at the two frequencies. In Fig. 5.2, $P\{K_{ti} = 0|K_{ri} = 0\}$ and $P\{K_{ti} = 1|K_{ri} = 0\}$ are 82% and 9% respectively, which suggest if we select to transmit on the beam with the maximum received signal power, 82% of the time we end up with the best choice while 9% of the time it is the second best. Similar results are found in all our measurements, including the indoor environment, although, generally the values for $P\{K_{ti} = 0|K_{ri} = 0\}$ and $P\{K_{ti} = 1|K_{ri} = 0\}$ are lower for indoor environments. Fig. 5.3 shows another outdoor site and Fig. 5.4 shows an indoor site respectively.

B. Simulations and Explanation

The measurement results presented above have important implications. It

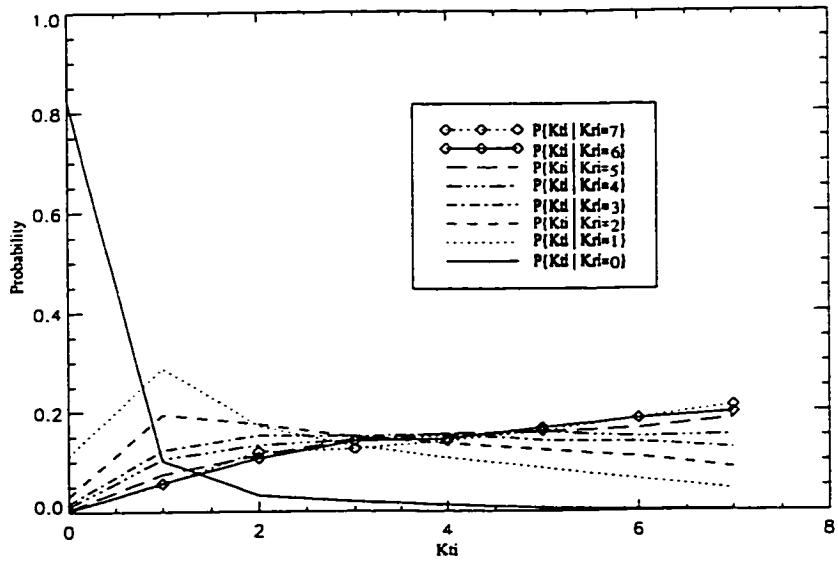

Figure 5.2: The relationship between the power levels of the transmit and receive frequencies at outdoor site I

suggests that there is strong correlation between signals on the uplink and the downlink in the same beam of a multibeam antenna. When one considers that there are still many multipath components in each beam output, we need to explain why the correlation exists at the two frequencies.

In analyzing the Talaris measurement data, two important phenomena are observed. One is that the impulse responses of strong beams typically have a few strong peaks within a continuum of lower intensity scatterer contributions; this is especially true in the strongest, or second strongest beam. The impulse responses in weak beams, on the other hand, usually contain a large amount of multipath signal components which none of them dominates. The other is that each peak in a beam impulse response typically consists of a number of signal components with very close time delays. This suggests that there are strong scatterers physically located close together (or in a "cluster"). This clustering phenomenon is also observed in experimental data published in the literature [61].

With the above two observations in mind, our explanation is based on the theory of wave interference. Let us further assume that there is a one-to-one correspondence between the plane waves traveling on the uplink and the downlink. That is, for each traveling wave at the receive frequency, there is another corresponding traveling wave at the transmit frequency that has the same time delay and angle-of-arrival (angle-of-departure to be exact in the transmit frequency). In addition, their

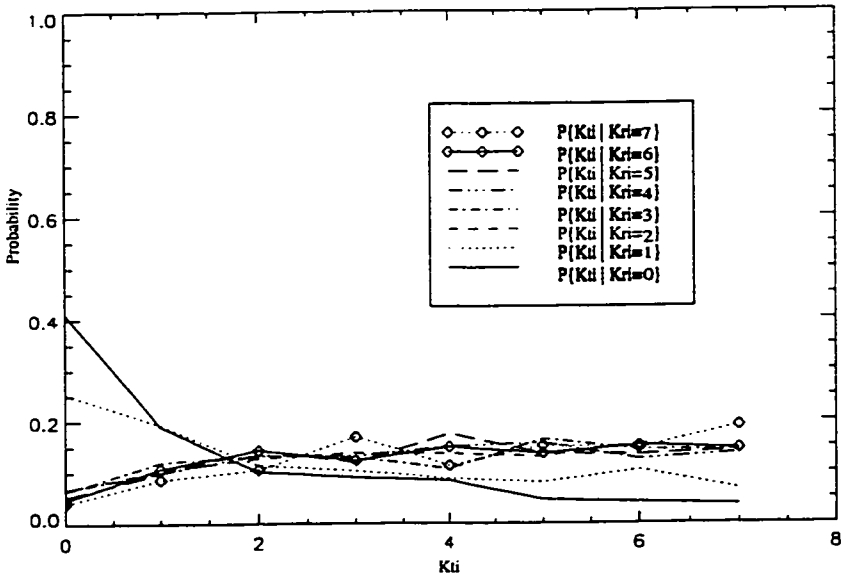

Figure 5.4: The relationship between the power levels of the transmit and receive frequencies at an indoor site

simulate multibeam antenna reception at the two frequencies using the Geometrically Based Single Bounce (GBSB) model [30]. The GBSB model is a geometrically based wave propagation model that treats each multipath component as a wave bounced from a single scatterer (See Chapter. 2 for details on this model). Clustered scatterers are assumed in the simulation. The cluster size is assumed to be 40m. The number of clusters is selected to vary from 6 to 20, which is similar to the environment we encountered in our 8-element antenna array measurements. The number of scatterers in each cluster is a randomly generated integer in the range of $[5, 10]$. In addition, the distance between the receiver and transmitter is 500m. Path loss exponent of 3.5 with a deviation of 5dB is assumed. An 8-beam multibeam antenna, which has exactly the same beam patterns as the ones used in the Talaris measurements, are used. Figure 5.5 shows a typical simulation layout.

Figure. 5.6 shows an example of the simulation results using the layout as shown in Fig. 5.5. Comparing Fig. 5.6 with Figs. 5.2, 5.3, and 5.4, we can see the strong correlation in two frequencies which we discovered in measurement indeed exists in our simulation, although $P\{K_{ti}|K_{ri}\}$ is larger for $K_{ri} \neq 0$ in the simulation. The discrepancies may due to the fact that the GBSB model only simulates single bounce waves. For $K_{ri} = 0$, the beam consists of mostly strong multipath components and can be expected to contain many single bounce waves. For $K_{ri} \neq 0$, however, the corresponding beams contain more multiple bounce waves. The GBSB model may not have captured the underlying physics of multiple bounce components received by

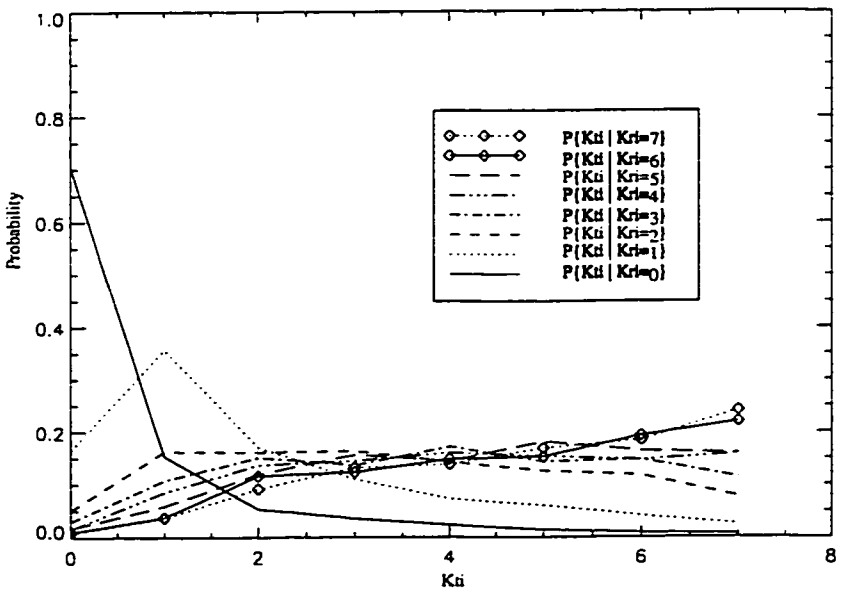

Figure 5.3: The relationship between the power levels of the transmit and receive frequencies at outdoor site II

amplitudes are the same, but their phases are uncorrelated. [3] Under these assumptions, the resultant signal power on the downlink would be correlated with that of the uplink for the same beams when there are very few unresolved multipath components, or if the powers of the unresolved multipath components account for only a small portion of the total signal power. The reason is that the unresolved multipath components add *vectorially* and thus contribute to the de-correlation effect between the signal powers of the downlink and uplink in the same beam. Since the powers of the unresolved multipath components are usually low in the strongest or the second strongest beam, even though there may be quite a few of them, the signal power on the downlink usually "tracks" that of the uplink most of the time. For the weak beams, however, the multipath components may add constructively at the receive frequency but destructively at the transmit frequency, or vise versa, since there are usually many unresolved multipath components which none of them is dominant. The exact statistics of the relation between the downlink and uplink, of course, are dependent on a number of factors. As we will show later, the propagation environment, signal bandwidth, and multibeam antenna patterns all play important roles.

To show how the above assumption captures the essence of our findings, we

[3]The assumption that their amplitudes are the same is reasonable considering the fact in our measurements the difference of wavelengths at these two frequencies, namely 1.86 GHz and 1.94 GHz, is only less than 5%. Considering the underlying physics of propagation, this can be expected to be a good assumption.

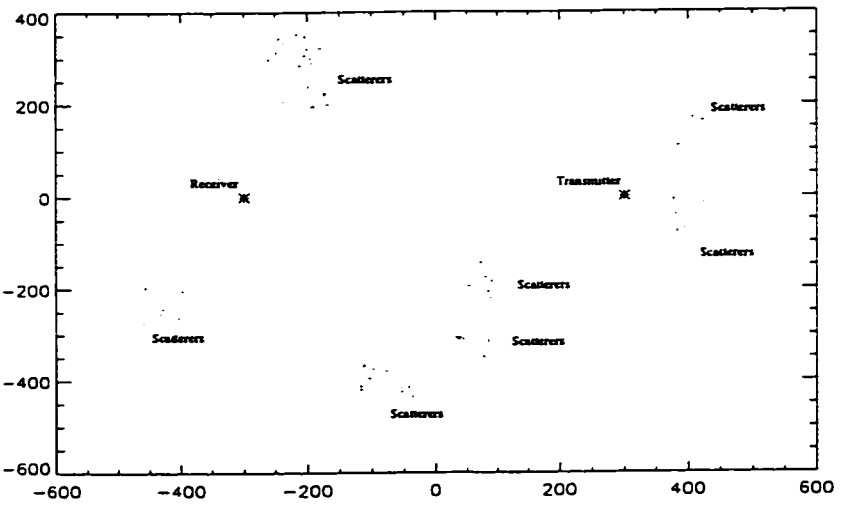

Figure 5.5: An example of simulation layouts

those beams that well.

5.3.2 Beamwidth Effect

Table 5.1: Correlation coefficients between the powers at the receive frequency and transmit frequency based on Talaris measurements (receive frequency: 1.86GHz, transmit frequency: 1.94GHz)

Location	Condition	45^o beamwidth	90^o beamwidth	120^o beamwidth	360^o beamwidth
Outdoor 1	NLOS	0.878	0.601	0.527	0.473
Outdoor 1	LOS	0.828	0.712	0.675	0.572
Outdoor 1	Average	0.810	0.718	0.605	0.547
Outdoor 2	NLOS	0.801	0.705	0.596	0.547
Outdoor 2	LOS	0.801	0.709	0.654	0.597
Outdoor 2	Average	0.815	0.698	0.633	0.574
Indoor	Average	0.413	0.359	0.255	0.253

If the explanation presented in last section is to be believed, we can expect the correlation between the power levels of the same beam on the uplink and the downlink to increase with a decrease in the beamwidth of the multibeam antenna. This follows from the fact that the narrower the beamwidth the fewer the number of

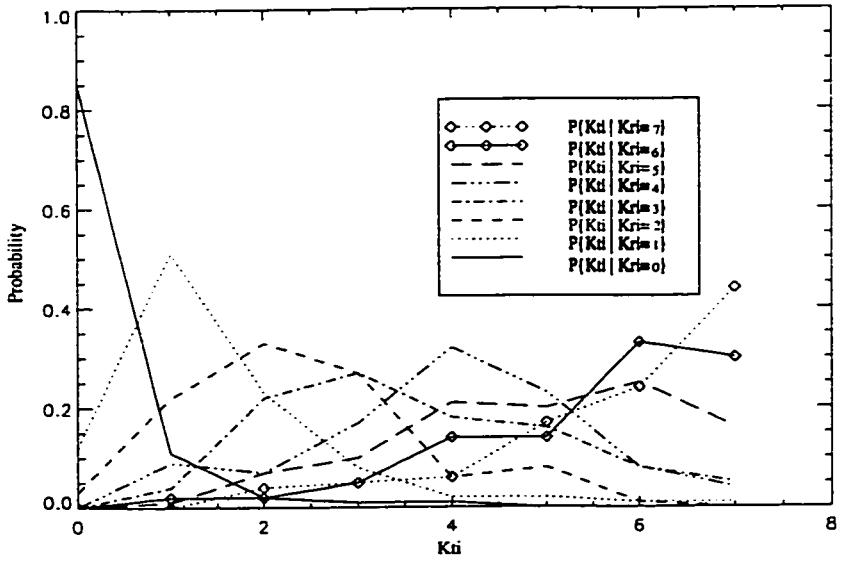

Figure 5.6: An example of simulation results for Fig. 5.5

multipath components that an antenna will receive. With the number of dominant components reduced, the correlation between the receiving and transmit frequencies can be expected to be stronger. This is indeed true. Table. 5.1 shows the correlation between the power of the outputs of the beam with maximum receiving power at the two frequencies using multibeam antennas with different 3dB beamwidths.

It is apparently desirable to achieve high correlation between the receive and transmit frequencies from the point of view of multibeam smart antenna transmission algorithms. The multibeam smart antenna would be able to transmit on the beam with the maximum received power if the correlation between the power distribution of the two frequencies is 100%.

To achieve higher correlation among the two frequencies and thus make the downlink multibeam smart antenna problem easier, one can use multibeam smart antenna systems that have a greater number of beams. As indicated in Table. 5.1, the narrower the beamwidth, the higher the correlation. However, care must be taken in using this approach. In our measurements and simulations, we found that the curve of correlation versus number of beam tended to fall off as the number of beams increases. For example (except for the indoor case) in Table. 5.1, the correlation coefficients increase approximately 10% in going from 360° beamwidth (omni-directional) to 120° beamwidth. Considering the dramatic decrease in the beamwidth, the increase of the correlation coefficients is not that significant. The extreme seems to happen in the indoor case where there is significantly less improvement.

We obtained similar results in our simulations using the GBSB model. In

each simulation run, we keep the same cluster size as shown in Fig. 5.5; as well, we keep the other parameters fixed and only change the beamwidth of the multibeam antenna to see the change in the correlation coefficients. We use an approximation of the multibeam antenna in the simulation. The approximate beam pattern for the mth beam $g_m(\theta)$ is shown in Fig. 5.7. It satisfies the following

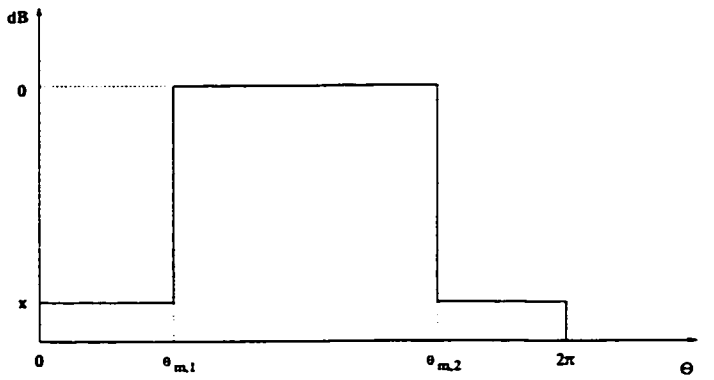

Figure 5.7: First order approximation of a practical multibeam antenna

$$\|g_m(\theta)\|^2 = \begin{cases} 0dB, & \theta_{m,1} < \theta < \theta_{m,2} \\ xdB, & otherwise \end{cases}$$

where $m = 1, 2, \ldots, M$, $[\theta_{m,1}, \theta_{m,2}]$ is the main lobe (main beam) area of the mth beam. x is the sidelobe level.

Fig. 5.8 shows the simulation results for typical micro-cell environment. The simulation was carried out using the following parameters: a cluster size of $80m$, a receiver and transmitter distance of $500m$, 15 clusters, 8 scatterers per cluster, path loss exponent equal to 3.5 (with a deviation of $5dB$), and sidelobe level of -16dB. As can be seen the increase of correlation between the two frequencies is not that significant for number of beams larger than 20.

From the perspective of downlink transmission, the optimum number of beams a multibeam samrt atenna should have will depend very much upon the environment in which the smart multibeam antenna operates. The narrower the multipath components spread in angle, the larger the optimum number of beams will be.

5.3.3 Signal Bandwidth Effect

As was stated before, smart antenna systems are expected to operate in different wireless systems, having different bandwidths, with the objective of improving

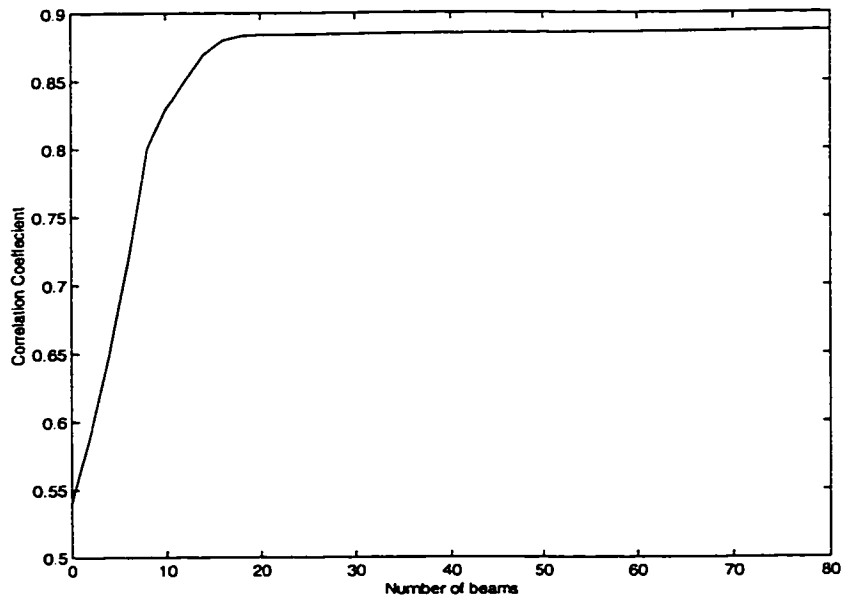

Figure 5.8: Antenna beamwidth versus two frequency power correlation: simulation results

the system capacity and quality. In this section, the effect of bandwidth on the correlation relationship between the receive and transmit frequencies is addressed.

To show the bandwidth effect on the relationship between the power distributions at the two frequencies, the same set of data which was used to plot Fig. 5.2 is processed to reflect the change in signal bandwidth. The result is shown in Fig. 5.9. As we can see from Fig. 5.9 that the probability peak (at $P\{K_{ti} = 0|K_{ri} = 0\}$) decreases with the system bandwidth, indicating a decrease in the correlation at the two frequencies for the beam with maximum power. Another thing worth noticing is that the tail of the curve for $P\{K_{ti}|K_{ri} = 0\}$ rises with the decrease in system bandwidth. This indicates that the intuitive downlink algorithm in which we select to transmit only at the beam with the maximum received power will perform more poorly when the system bandwidth is narrow.

The bandwidth effect is consistent with the fact that the number of multipath components which cannot be resolved on reception increases with the decrease in signal bandwidth. These effects are also observed in simulations using the GBSB model. Figure. 5.10 shows the simulation for the same conditions as Figure. 5.6. Again the agreement is good for $K_{ri} = 0$, relatively poor for other values of K_{ri}.

The bandwidth effect gives us more insight into the results presented in Section. 5.3.1. We have seen the correlation at two frequencies is much lower for indoor environments than for outdoor environments. The bandwidth effect clearly shows

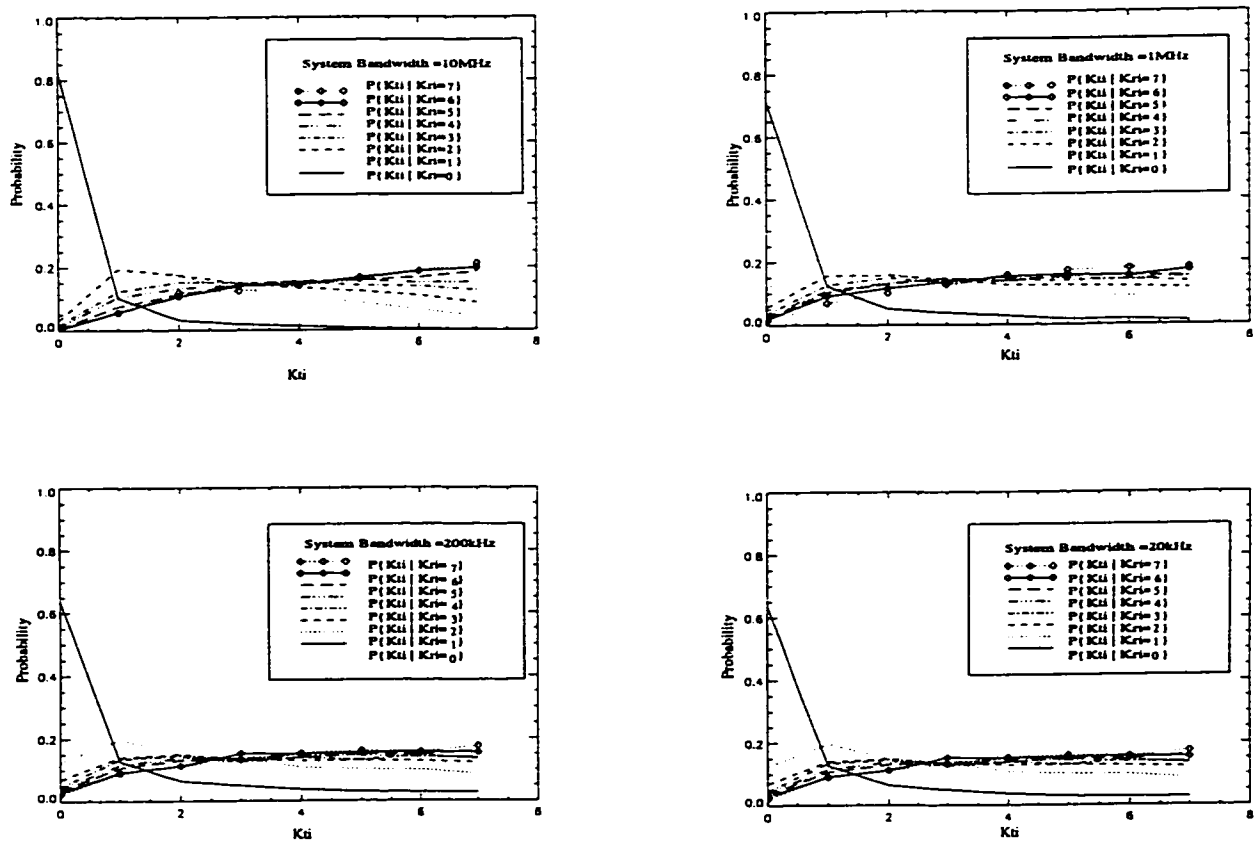

Figure 5.9: The effect of bandwidth on the power distribution relationship at two frequencies : measurement results

the tendency for de-correlation among the distribution of beam powers at the two frequencies with an increase in the number of unresolved multipath components. In an indoor environment, the number of multipath signals is usually higher than for an outdoor environment. In addition, the delay spread is usually an order of magnitude smaller than for an outdoor micro-cell environment. It follows, that if the same signal is transmitted in both indoor and outdoor environments, there are far more unresolved multipath components received by the multibeam smart antenna in the indoor case.

5.3.4 Discussions

In the above, we have shown the correlation between the beam power distributions at reception and transmission frequencies. Our experiment and simulation results indicate the number of unresolved multipath components as the key factor underlying the degree of correlation. The number of unresolved multipath components is a result

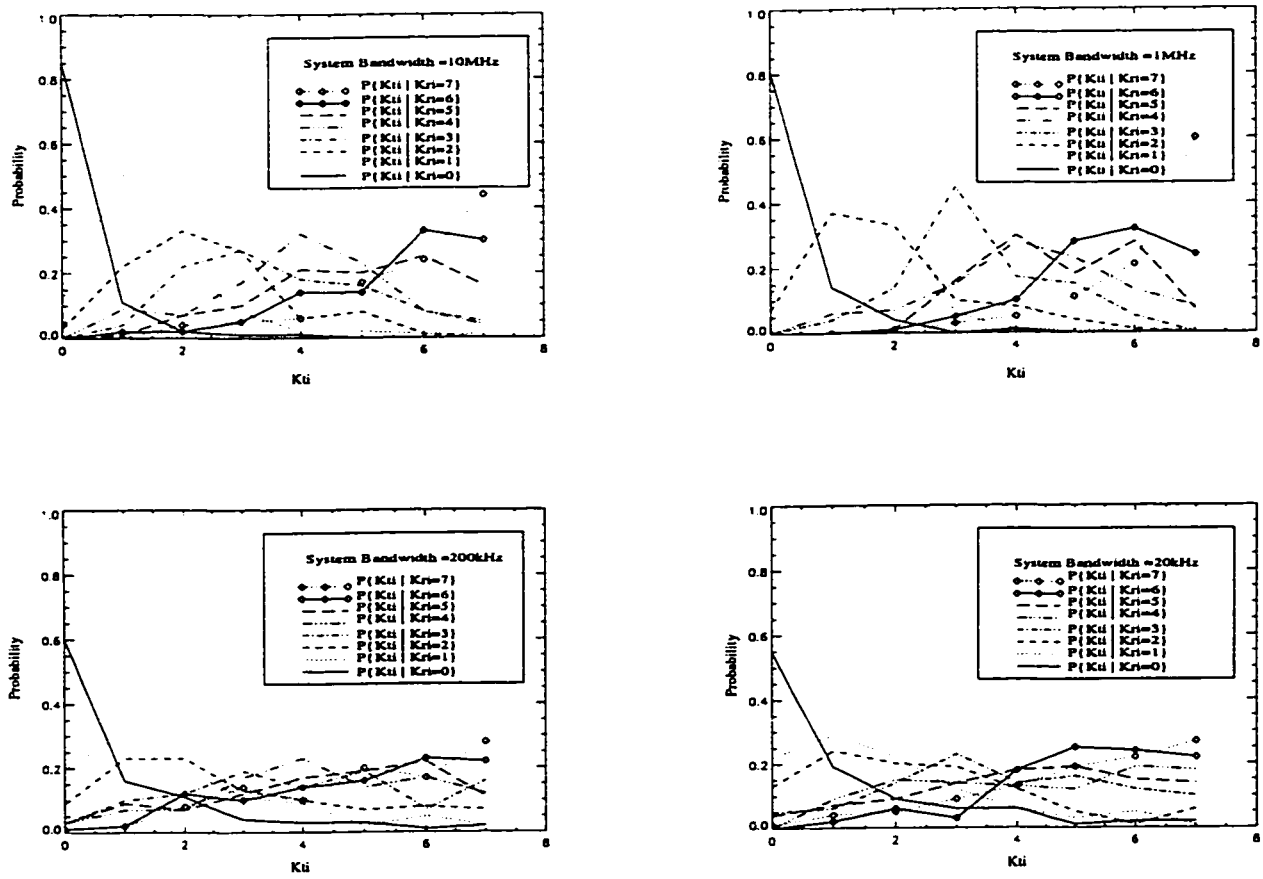

Figure 5.10: The effect of bandwidth on the power distribution relationship at two frequencies : simulation results

of the influence of many factors, most important among them are

- total number of multipath components.
- multipath delay spread.
- multipath angle spread.
- main beamwidth of the multibeam smart antenna.
- signal bandwidth.

While the first three factors are dependent upon the propagation environment the last two are dependent on the characteristics of the smart antenna system.

5.4 A Novel Multibeam Smart Antenna Transmission Algorithm

Our analysis in Section. 5.3 indicates that, for situations where there are still a number of unresolved multipath components, which is usually true in actual wireless environments, using the strongest uplink beam for downlink transmission is inadequate. In this section, we propose a novel transmission algorithm that will bring further improvements in performance. One related topic, which relates to the correlation between signals received from different beams in a multibeam antenna, is examined before presenting this algorithm. The performance and analysis of this algorithm is left to the next section.

5.4.1 Power Correlation Among Different Beams in the Same Multibeam Antenna

Table 5.2: Correlation coefficients between the powers at different beams (Beams are ranked in power descending order, i.e., Beam 0 represents the beam with the strongest signal power)

LOCATION	CONDITION	Beam 0 and 1		Beam 0 and 2	
		1.86GHz	1.94GHz	1.86GHz	1.94GHz
Outdoor 1	NLOS	0.354	0.333	0.291	0.288
Outdoor 1	LOS	0.306	0.289	0.382	0.425
Outdoor 1	Average	0.316	0.315	0.320	0.338
Outdoor 2	NLOS	0.169	0.215	0.189	0.172
Outdoor 2	LOS	0.223	0.240	0.211	0.200
Outdoor 2	Average	0.230	0.210	0.206	0.173
Indoor	Average	0.240	0.203	0.243	0.202

The problem associated with transmitting on the beam which corresponds to maximum received signal power is that this may result in the mobile station being in a deep fade for the transmit frequency although the base station may receive a very strong signal at the receive frequency. The probability of this happening depends on the number of unresolved multipath components, as stated in the last section. The use of a multibeam antenna at the base station gives us extra degrees of freedom in dealing with this problem.

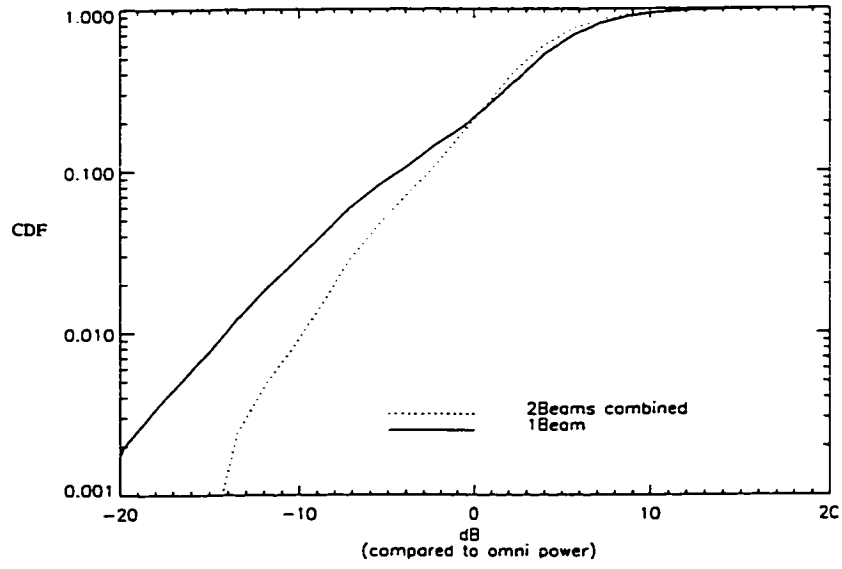

Figure 5.11: Signal power improvement by transmitting on two beams

Table. 5.2 gives the average signal power correlations between beams at several locations where we have conducted propagation measurements. As we can see there is very low correlation, around $0.2 \sim 0.4$, between the power levels of the strongest and second strongest beams as well as that of the strongest and third strongest beams. A number of studies showed that very little performance degradation occurs so long as the correlation between the diversity channels is less than 0.3 to 0.5 [42, 56]. This low degree of correlation suggests it is possible to use diversity to further reduce the probability of mobile station being in a deep fade at the transmit frequency.

To show that this indeed improves system performance, we calculated the cumulative distribution function (CDF) of signal power resulting from two methods using data collected with the 8-element vector channel sounder system. The first simply transmits using the beam which corresponds to the maximum received power, the second splits the power between the two beams with the strongest received powers. Figure. 5.11 shows the improvement obtained at one outdoor site. Figure 5.11 shows that the results for the two methods lie very close to each other for signal power levels of 0dB or higher (compared to omni-directional antenna). The probability of signal power being higher than that for an omni-directional antenna is 90% for both methods. However, the CDF curve for the second method decrease much faster in region where signal power is lower than 0dB. For example, the probability of the signal power level dropping below -10dB is 1% of the time for the second method in contrast to it being 3% for the first method. Since most transmission errors occur

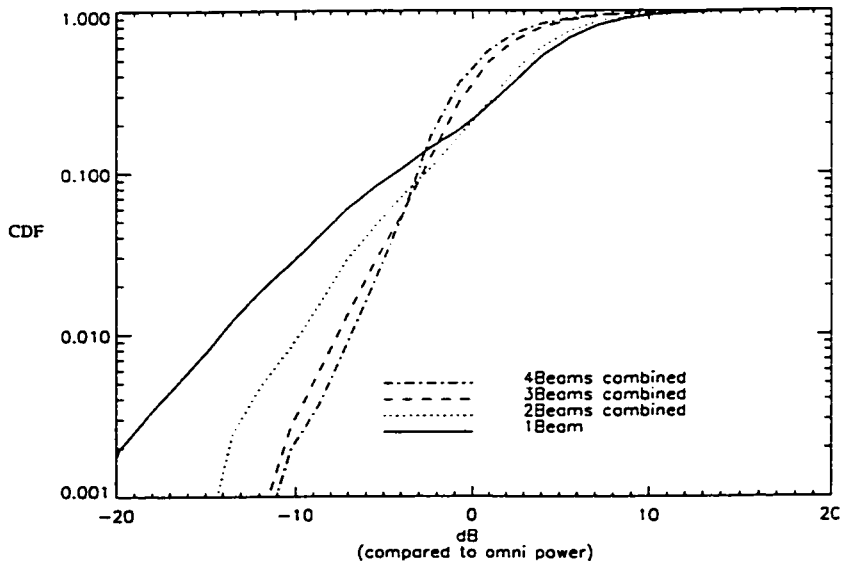

Figure 5.12: Signal power improvement by transmitting on n beams

in the region where the SNR is low, the second method is expected to perform much better than the first method. Figure. 5.12 shows the improvement in average signal power with the transmitter using up to 4 beams. The improvement, that comes about when combining more than 4 beams, is negligible in this case due to the large power difference between beams.

The most important parameter in the design of a digital communication system is the probability of error as a function of the energy per transmitted message input [36]. If we use n beams for downlink transmission and divide the total energy among the n beams, an optimum value of n must exist. This is because on the one hand, the average signal-to-noise ratio decreases at each beam as n increases if the total energy is fixed, on the other hand, increasing n provides additional diversity. This optimum value of n can be expected to be highly dependent upon the environment in which the wireless system operates. As we can see from Figure 5.12 little improvement can be expected by transmitting on more than three beams. Also, one thing worth pointing out is that, if the base station transmits on more than one beam in a cellular environment, the level of co-channel interference will increase, which, in turn, will increase the level of interference at each user.

5.4.2 The Algorithm

In the previous sub-section, the transmitted power is split equally between the two beams. In actual fact, better performance usually can be achieved if we divide

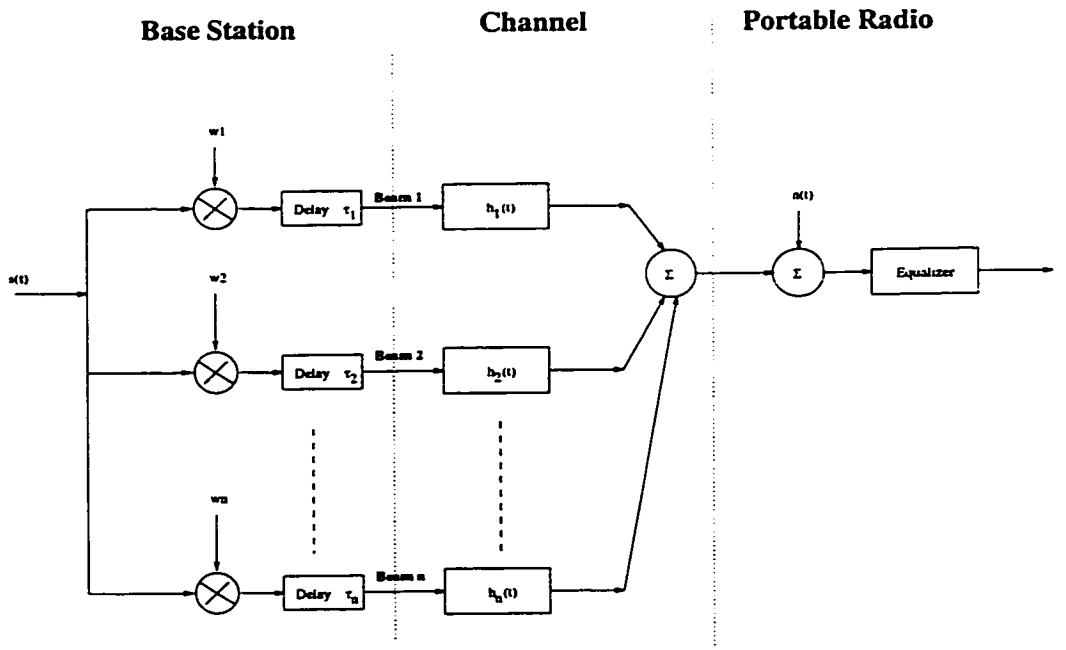

Figure 5.13: The proposed downlink algorithm

the signal power equally among more than two beams. In this subsection we propose an algorithm that expands on the idea introduced in last subsection. The general structure of the algorithm is shown in Figure. 5.13.

In Figure. 5.13 the multibeam smart antenna selects n beams (n is smaller than the total number of beams in the multibeam antenna) for transmission. The signal transmitted by the ith beam is multiplied by a complex weight w_i and delayed by τ_i. The two sets of parameters $\{w_1, \ldots, w_n\}$ and $\{\tau_1, \ldots, \tau_n\}$ are determined by some optimum criterion, for example, minimum probability of error, under the channel conditions of $h_1(t), \ldots, h_n(t)$.

Conceivably, more complicated combining scheme, such as a transversal linear filter, could be used in this algorithm. We find this added level of complexity does not pay off in a real situation. The reason is that limited information on $h_1(t), \ldots, h_n(t)$ at the transmit frequency can be estimated from the signals at the receive frequency.

This transmission algorithm will improve the system performance in both flat fading and frequency selective fading channels. For flat fading channel, the time diversity can be explored by weighting and staggering the transmission delay among different beams in effect to combat the flat fading. For frequency selective fading, the channel delay spread can be adjusted by the relative transmission delay among different beams, thus reducing the burden of equalization. For systems using training sequence for equalization, this means reducing training sequence length and improving system spectrum efficiency.

In the next section, we will analyze the performance of this algorithm under

Rayleigh fading. We will show how one goes about selecting the parameters and the improvement in performance that can be achieved. The analysis is based on a dual transmission scheme, i.e., combining two beams for transmission; however, the results presented should be general enough to be applicable to more than two beams. As a caution, transmission on more than 2 beams may or may not improve system performance depending on the practical situation. The reason is that in using more beams one will introduce more co-channel interference which in turn will affect the SIR achievable at *each* mobile station.

5.5 Performance Analysis

In this section, the proposed multibeam smart antenna transmission algorithm is applied to a QPSK system. We begin with the system model and then proceed to give the analysis and simulation results for a flat Rayleigh fading scenario. The numerical results obtained through simulations indicate that for a SNR = 17dB there is a 4 times reduction in probability of error over simply transmitting on the beam that receives the maximum power. It increases to over 10 times at a value of SNR= 25dB.

5.5.1 System Model

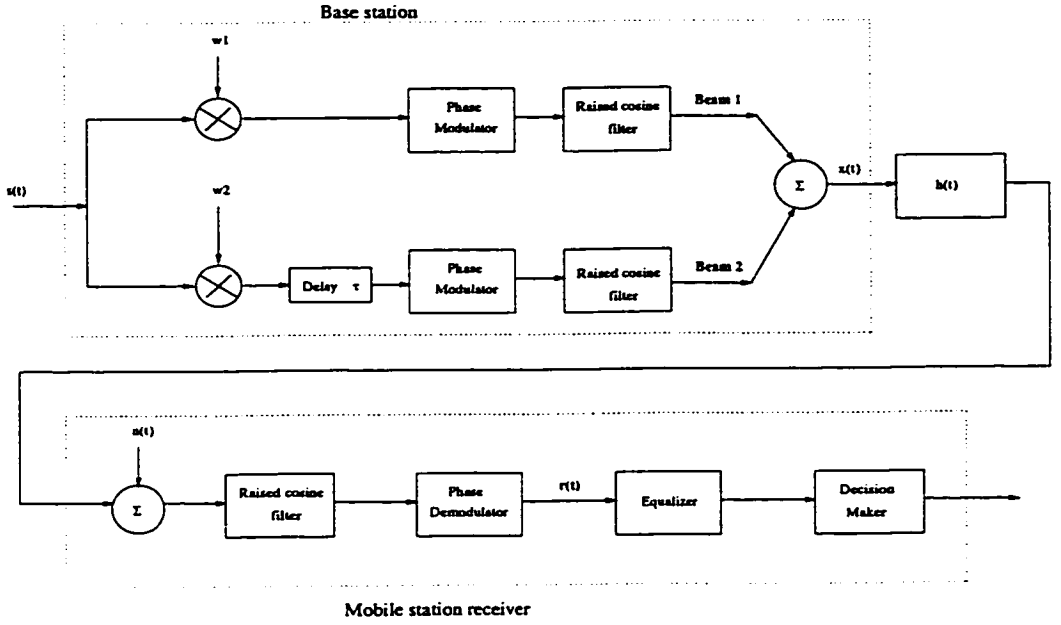

Figure 5.14: Block diagram of the QPSK system in simulation

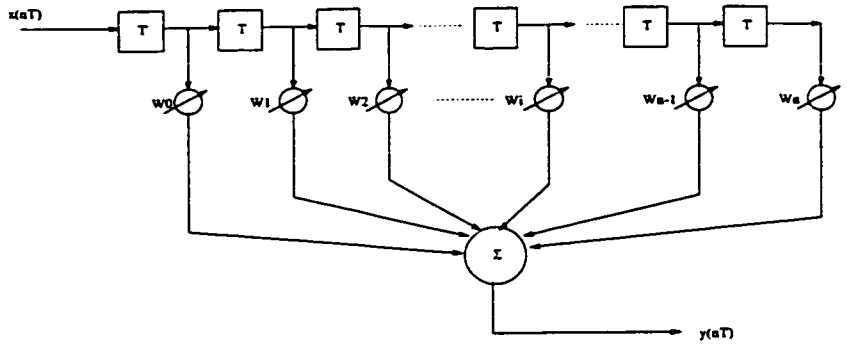

Figure 5.15: Optimum linear equalizer

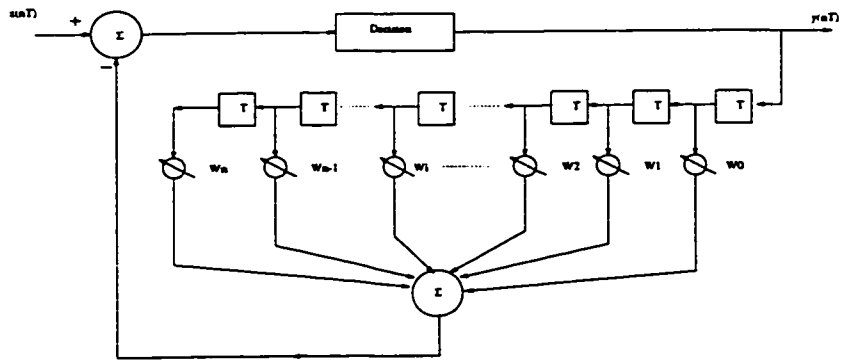

Figure 5.16: Decision feedback equalizer

A QPSK system using the proposed multibeam smart antenna downlink transmission algorithm can be modeled as in Fig. 5.14. Assume dual transmission where two beams are combined for transmission. If bandpass signals and channels are represented and simulated using the corresponding baseband in-phase and quadrature forms, the baseband signal $s(t)$, which the base station transmits, can be express as

$$s(t) = \sum_n x_n \delta(t - nT) \tag{5.2}$$

where $\{x_n\}$ is the complex sequence of data symbols with in-phase and quadrature components.

$s(t)$ is fed into two paths, which correspond to the two beams used for transmission. The gains of the two paths are w_1 and w_2, and the second path is delayed by τ. Each path is phase modulated and passed through a square-root raised cosine filter. The two paths are passed through a channel, which has an impulse response of $h(t)$, and then summed. Receiver noise $n(t)$ is also added. At the receiver side, there is another square-root raised cosine filter. The received signal $r(t)$ can be expressed

as

$$r(t) = (w_1 s(t) * h(t) + w_2 s(t-\tau) * h(t)) * g(t) + n(t) \tag{5.3}$$

where "*" represents convolution. $g(t)$ represents the combined effects of the two square-root raised cosine filters, one located at the base station, the other located in the mobile station. The spectrum of $g(t)$ corresponds to a raised cosine filter which is defined as [62]

$$G(f) = \begin{cases} T, & 0 \le |f| \le (1-\alpha)/2T \\ \frac{T}{2}[1 + \cos\frac{\pi T}{2}(|f| - \frac{1-\alpha}{2T})], & (1-\alpha)/2T \le |f| \le (1+\alpha)/2T \\ 0, & |f| > (1+\alpha)/2T \end{cases} \tag{5.4}$$

where α is called the *rolloff factor*, which takes a value in the range $0 \le \alpha \le 1$. Eqn. (5.3) can be simplified as

$$r(t) = s(t) * h_e(t) + n(t) \tag{5.5}$$

where $h_e(t)$ is the equivalent total system impulse response

$$h_e(t) = (w_1 h(t) + w_2 h(t-\tau)) * g(t) \tag{5.6}$$

Given $r(t)$ in Eqn. (5.5), time equalizer is used to reduce the intersymbol interference (ISI). The equalizer strives to achieve minimum probability of error. We now carry out simulations using two of the most popular adaptive equalizers. One is optimum linear equalizer, the other is decision feedback equalizer. Figures. 5.15 and 5.16 gives the structures of an optimum linear equalizer and a decision feedback equalizer, respectively.

When transmitting, the multibeam smart antenna chooses the two beams on which it receives the highest signal powers. It can adjust three parameters, namely, w_1,w_2 and τ, to optimize its performance. As can be expected, the optimal values of these parameters will depend on the channel, the characteristics of the transmitted signal as well as the receiver structure.

5.5.2 Probability of Error

In this subsection, we derive the probability of error for the minimum mean square-error (MMSE) linear equalized receiver and the decision feedback equalized (DFE) receiver which we will use to analyze system performance.

A. Linear Equalizer Receiver

If we denote $H_e(f)$ as the Fourier transform of $h_e(t)$ defined as in Eqn. (5.6), the minimum mean square error (MMSE) that can be realized by the linear equalized receiver, which operates using QAM modulation (QPSK is a special case of QAM), can shown to be [63]

$$\epsilon_{min}(linear) = T \int_0^{1/T} N_0/[N_0 + S_{hh}(f)]df \tag{5.7}$$

where N_0 is the common noise spectral densities when the noises are assumed to be white; $S_{hh}(f)$ is the aliased signal power spectrum of $\sigma_c^2|H_e(f)|^2$ defined as

$$S_{hh}(f) = \sum_n \sigma_c^2|H_e(f - n/T)|^2, \quad -1/2T \leq f \leq 1/2T \tag{5.8}$$

where $\sigma_c^2 = 2$ for QPSK. In [64], Babylon and Sale derived the probability of error bound as

$$P_e \leq \exp\{-\frac{1 - \epsilon_{min}(Linear)/\sigma_c^2}{\epsilon_{min}(Linear)})\} \tag{5.9}$$

B. Decision feedback Equalizer Receiver

Decision feedback equalizer (DFE) [63] is a nonlinear equalizer which uses previously detected symbols to eliminate the inter-symbol interference caused by previously detected symbols on the current symbol to be detected. It generally provides better performance than the linear equalizer. If we use $H_e(f)$ to denote the Fourier transform of $h_e(t)$, it can be shown in [63] that the minimum mean square error (MMSE) that can be realized using the decision feedback equalizer receiver for QAM modulation is

$$\epsilon_{min}(DFE) = \exp\{-T \int_0^{1/T} ln(1 + S_{hh}(f)/N_0)df\} \tag{5.10}$$

where $S_{hh}(f)$ is the aliased signal power spectrum as in Eqn. (5.8).

Again, in [64], Babylon and Sale derived the probability of error bound for QAM modulation to be

$$P_e \leq \exp\{-\frac{1 - \epsilon_{min}(DFE)/\sigma_c^2}{\epsilon_{min}(DFE)})\} \tag{5.11}$$

5.5.3 Optimum Parameters and Performance Analysis in Flat Fading Channels

A. The System Model

Assuming that the channels from each beam at receive and transmit frequencies are both described by the same Rayleigh fading distribution, the channel impulse response $h(t)$ given in Eqn. (5.3) can be expressed as

$$h(t) = ae^{j\phi}\delta(t) \tag{5.12}$$

where ϕ is a random phase parameters that is uniformly distributed over $[0, 2\pi]$ and a is random variable with a Rayleigh distribution, i.e.

$$P(a) = \begin{cases} \frac{a}{b}e^{-\frac{r^2}{2b}}, & r \geq 0, b > 0 \\ 0, & r < 0 \end{cases} \tag{5.13}$$

If we denote $h_u^{(i)}(t)$ and $h_d^{(i)}(t)$ as the impulse response of the ith beam at receive (uplink) and transmit (downlink) frequencies and use Eqn. (5.12), we have

$$h_u^{(i)}(t) = A_u^{(i)}e^{j\phi_u^{(i)}}\delta(t) \tag{5.14}$$

$$h_d^{(i)}(t) = A_d^{(i)}e^{j\phi_d^{(i)}}\delta(t) \tag{5.15}$$

and $A_u^{(i)}$,$\phi_u^{(i)}$,$A_d^{(i)}$,$\phi_d^{(i)}$ are independent. Assuming the channel changes slowly with time, it can be expected that $E|A_u^{(i)}|^2 = E|A_d^{(i)}|^2$ and we can estimate $E|A_d^{(i)}|^2$ using $A_u^{(i)}$.

Substituting Eqn. (5.15) into Eqn. (5.6), we have the equivalent total system impulse response as

$$\begin{aligned} h_e(t) &= [A_d^{(1)}e^{j\phi_d^{(1)}}w_1\delta(t) + (A_d^{(2)}e^{j\phi_d^{(2)}}w_2\delta(t-\tau)] * g(t) \\ &= A_d^{(1)}e^{j\phi_d^{(1)}}w_1 g(t) + A_d^{(2)}e^{j\phi_d^{(2)}}w_2 g(t-\tau) \end{aligned} \tag{5.16}$$

Generally, w_1 and w_2 are complex weights, however, in the flat Rayleigh fading case, we can choose them to be real values. As we can see from Eqn. (5.16), the two phase terms $\phi_d^{(1)}$ and $\phi_d^{(2)}$ are random and uniformly distributed over $[0, 2\pi]$. Since they are independent of $\phi_u^{(1)}$ and $\phi_u^{(2)}$, the smart antenna can not estimate $\phi_d^{(1)}$ and $\phi_d^{(2)}$ using $\phi_u^{(1)}$ and $\phi_u^{(2)}$. Without any loss of generality, we assume the total transmitted power is unity. That is

$$|w_1|^2 + |w_2|^2 = 1 \tag{5.17}$$

Our goal is to find values for w_1,w_2,and τ that optimize system performance. The received signal at the mobile station becomes

$$\begin{aligned} r(t) &= h_e(t) * s(t) && (5.18) \\ &= (A_d^{(1)} e^{j\phi_d^{(1)}} w_1 g(t) + A_d^{(2)} e^{j\phi_d^{(2)}} w_2 g(t-\tau)) * s(t) && (5.19) \end{aligned}$$

where "*" denotes convolution. Since

$$s(t) = \sum_n x_n \delta(t - nT) \tag{5.20}$$

assuming $\{x_n\}$, the complex sequence of data symbols with in-phase and quadrature components, is uncorrelated, i.e.,

$$E(x_n x_m^*) = \begin{cases} \sigma_c^2, & n = m \\ 0, & n \neq m \end{cases} \tag{5.21}$$

For QPSK, $\sigma_c^2 = 2$. The average power of $r(t)$ is

$$E(|r(t)|^2) = \frac{\sigma_c^2}{T} \int_{-\infty}^{\infty} |G(f)|^2 |A_d^{(1)} e^{j\phi_d^{(1)}} w_1 + A_d^{(2)} e^{j\phi_d^{(2)}} w_2 e^{j2\pi f\tau}|^2 df \tag{5.22}$$

In contrast, if we transmit all the signal power using Beam 1, the received signal is (we denote it as $r_1(t)$ to differentiate it from $r(t)$)

$$\begin{aligned} r_1(t) &= h_1(t) * s(t) && (5.23) \\ &= [A_d^{(1)} e^{j\phi_d^{(1)}} g(t)] * s(t) && (5.24) \end{aligned}$$

the average received signal power would be

$$E(|r_1(t)|^2) = \frac{\sigma_c^2}{T} \int_{-\infty}^{\infty} |G(f)|^2 |A_d^{(1)}|^2 df \tag{5.25}$$

We now define the average signal-to-noise ratio SNR as

$$\begin{aligned} \rho &= \frac{E(|r_1(t)|^2)}{W N_0} && (5.26) \\ &= \frac{\sigma_c^2}{N_0} \int_{-\infty}^{\infty} |G(f)|^2 |A_d^{(1)}|^2 df && (5.27) \\ &= \frac{\sigma_c^2 |A_d^{(1)}|^2}{N_0} && (5.28) \end{aligned}$$

N_0 the single-sided noise spectrum. In deriving Eqn. (5.27), we used $WN_0 = N_0/T$, where W is the noise power measured in the Nyquist band. $W = 1/T$ and also

$$\int_{-\infty}^{\infty} |G(f)|^2 |A_d^{(1)}|^2 df = 1 \tag{5.29}$$

The Fourier transform of $h_e(t)$ in Eqn. (5.16) is

$$H_e(f) = (A_d^{(1)} e^{j\phi_d^{(1)}} w_1 + A_d^{(2)} e^{j\phi_d^{(2)}} w_2 e^{j2\pi f\tau}) G(f) \tag{5.30}$$

Combining Eqns.(5.30) and (5.8) yields

$$S_{hh}(f) = \sum_n \sigma_c^2 |(A_d^{(1)} e^{j\phi_d^{(1)}} w_1 + A_d^{(2)} e^{j\phi_d^{(2)}} w_2 e^{j2\pi(f-n/T)\tau}) G(f)|^2, \quad -1/2T \leq f \leq 1/2T \tag{5.31}$$

If we substitute Eqn. (5.31) into Eqn. (5.7), we obtain

$$\begin{aligned} &\epsilon_{min}(linear) \\ &= T \int_{-1/2T}^{1/2T} N_0/[N_0 + \textstyle\sum_n |(A_d^{(1)} e^{j\phi_d^{(1)}} w_1 + A_d^{(2)} e^{j\phi_d^{(2)}} w_2 e^{j2\pi(f-n/T)\tau}) G(f)|^2] df \\ &= \int_{-1/2}^{1/2} 1/[1 + \rho \textstyle\sum_n |(A_d^{'(1)} e^{j\phi_d^{(1)}} w_1 + A_d^{'(2)} e^{j\phi_d^{(2)}} w_2 e^{j2\pi/T(x-n)\tau}) G'[2\pi(x-n)/T]|^2] dx \end{aligned} \tag{5.32}$$

where ρ is the average signal-to-noise ratio, $G'(.) = G(.)/\sqrt{T}$, $A_d^{'(1)}$ and $A_d^{'(2)}$ are independent Rayleigh variables with variance $E|A_d^{'(1)}|^2 = 1$ and $E|A_d^{'(2)}|^2 = E|A_d^{(2)}|^2/E|A_d^{(1)}|^2$, respectively. The parameter $E|A_d^{'(2)}|^2$ gives the ratio of the powers transmitted on Beam 1 and Beam 2. We denote it by η.

In a similar manner, by substituting Eqn. (5.31) into Eqn. (5.10) we derive MMSE for a decision feedback equalized receiver to be

$$\begin{aligned} &\epsilon_{min}(DFE) \\ &= \exp\{\int_{-1/2}^{1/2} -ln[1 + \rho \textstyle\sum_n |(A_d^{'(1)} e^{j\phi_d^{(1)}} w_1 + A_d^{'(2)} e^{j\phi_d^{(2)}} w_2 e^{j\frac{2\pi}{T}(x-n)\tau}) G'[\frac{2\pi}{T}(x-n)]|^2] dx\} \end{aligned} \tag{5.33}$$

If we substitute either Eqn. (5.32) or Eqn. (5.33) into Eqn. (5.9) we get an expression for the probability of symbol error bound on the linear receiver or decision feedback equalized receiver. It is not possible to evaluate the integral. Consequently, it is not possible to obtain a closed form for the probability of error. We therefore resort to Monte-Carlo techniques.

Before presenting the numerical results, the symbols and parameters used in simulation are defined and summarized as follows:

1. SNR: defined as the average signal-to-noise ratio at the mobile station when all the signal power is transmitted over the beam with the maximum received power.

2. η: the ratio of average power in the strongest beam to that of the second strongest beam. When the channel changes slowly, η is expected to be the same at both the receive and transmit frequencies, it can be estimated from the signal received by the multibeam smart antenna.

3. γ: $\gamma = |w_1|^2/|w_2|^2$, the ratio of the power transmitted on Beam 1 to that on Beam 2 in Figure. 5.14. The value for γ is derived by the transmission algorithm.

4. τ/T: the relative time delay normalized to the symbol period as in Figure. 5.14. τ/T is also selected by the transmission algorithm.

5. P_e: probability of symbol error.

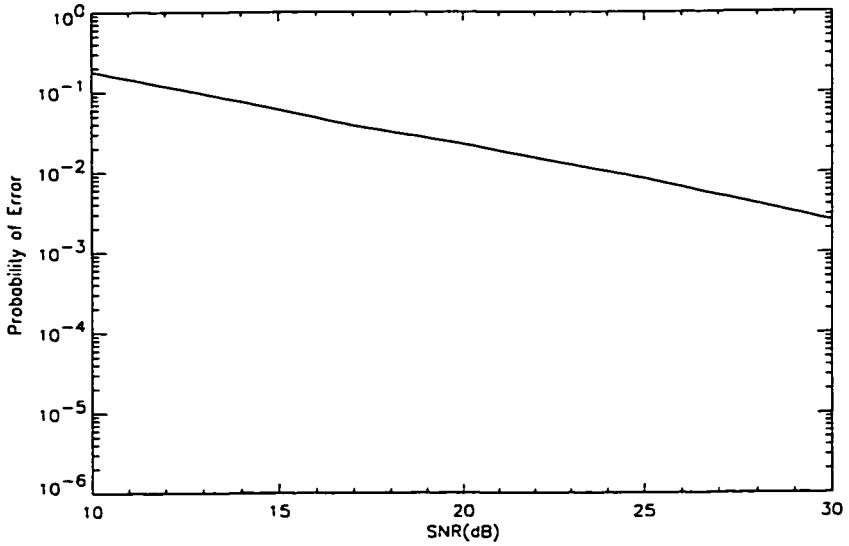

Figure 5.17: Average probability of symbol error when transmitting on the beam with the maximum received signal power under Rayleigh flat fading channel assumption

B. The Effect of Relative Time Delay τ/T

We first analyze how the proposed algorithm makes use of the multipath time delay to reduce P_e.

Setting $w_1 = 1$, $w_2 = 0$ and $\tau = 0$ in Eqns. (5.32) and (5.33) gives us the MMSE and probability of symbol error for the first method, where transmission occurs on the beam with the maximum received power. Figure. 5.17 shows the probability of error under various SNRs. We will refer to Figure. 5.17 from time to time and use it as a benchmark for comparing system performance.

Next, we evaluate probability of error under various γ and τ. As the relative delay τ/T is increased from 0 to 1.5, Fig.5.18 depicts the average probability of error for three different values of SNR and filter roll-off factor $= 0.35$, $\eta = 5$dB, and

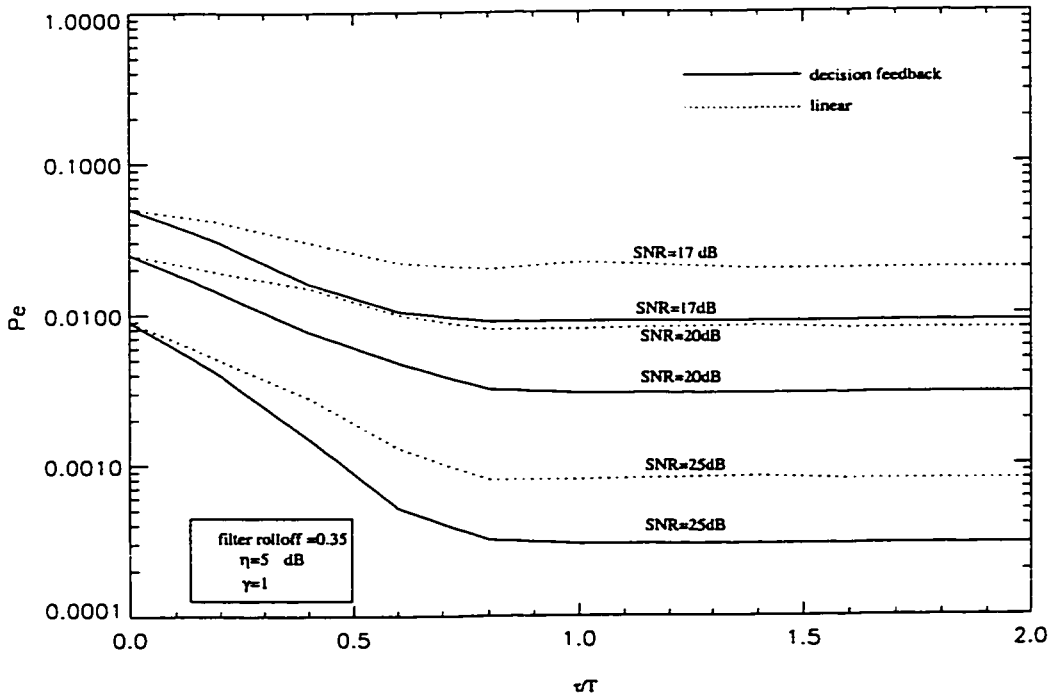

Figure 5.18: Average probability of symbol error when dividing transmitted signal power equally among the two beams with the strongest received signal power at Rayleigh flat fading channel

$\gamma = 1$, i.e., $|w_1|^2 = |w_2|^2 = 1/2$. The curves associated with linear and decision feedback equalized receivers are both seen to decrease as the relative delay increases. This indicates the algorithm is able to take advantage of the multipath time delay. The slopes of the linear receiver cases are shallower than for the feedback equalized receiver cases. This suggests that those receivers are less able to take advantage of the multipath delays. This difference is more prominent for the high SNR cases. The numerical results also show average probability of error approaches its minimum at about $\tau/T = 0.7 \sim 0.8$, beyond this value, further increase in the relative time delay will not reduce the probability of error. Since larger τ/T values require more complex equalization structure at the mobile station receiver, the value $\tau/T = 0.7 \sim 0.8$ serves as the desirable value for achieving low probability of error while keeping the receiver structure simple.

C. The effect of η and γ

As have been shown, P_e reaches its minimum when $\tau/T \geq 0.8$ if the values

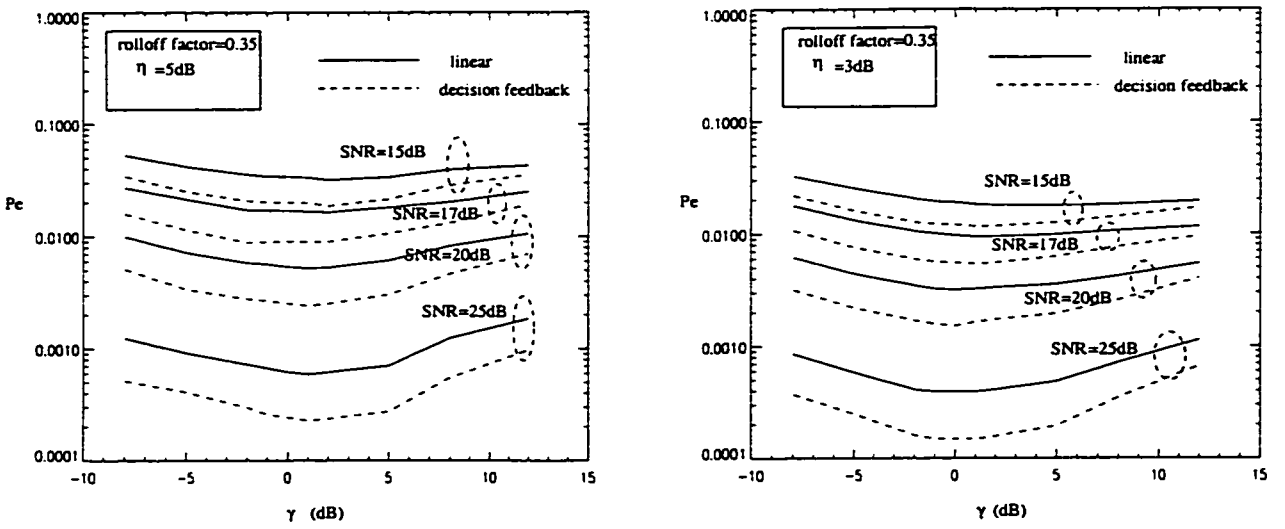

Figure 5.19: Average probability of symbol error when transmitting on the two beams with the strongest received signal power at Rayleigh flat fading channel: the effects of varying $\gamma = |w_1|^2/|w_2|^2$

of SNR, η, and γ are kept fixed. However, simulation results show that P_e generally varies with SNR, η, and γ. In order to determine the optimum γ, we set $\tau/T = 0.8$ and calculate P_e under varying values of SNR and η. Fig. 5.19 shows how P_e varies with γ under different values of SNR and η. As expected, the optimum value of γ is a function of both SNR and η. However as shown in Fig. 5.19. The bottoms of the curves are quite flat, indicating there is a fairly wide range of values for γ in which one can achieve close to the minimum probability of error. The value, γ = 0dB , where we divide the transmitted power equally between two beams seems to work well for many values of SNRs and η's.

D. Minimum P_e

The minimum probability of symbol error for various SNRs is plotted in Fig. 5.20. In moving from a SNR value of 15dB to 17dB, the P_e is reduced 4 times using the proposed algorithm. If the SNR is increased to 25dB, rather than 17dB, P_e is reduced by a factor of 10 times. As we can see, the improvement achievable is highly dependent upon the value of η. When the SNR is kept fixed, P_e increases with η. However, the increase is not all that significant for $\eta \leq$ 5dB. This can be concluded from the fact that the P_e curves for η = 0dB and η = 5dB are quite close

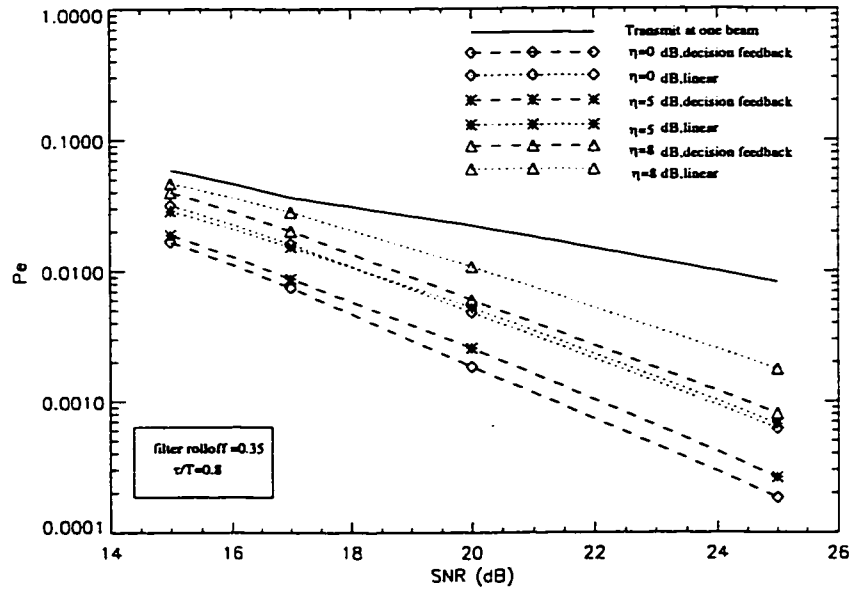

Figure 5.20: Average probability of error of the proposed algorithm using dual beams under Rayleigh flat fading channel assumption

to each other. P_e increases rapidly as η approaches 8dB. The numerical results show that there is little improvement when η exceeds 10dB. This indicates the algorithm is unable to make use of the multipath delay when the difference of the signal power between the beams is too large.

Chapter 6

Multibeam Smart Antennas for Multiuser Detection

6.1 Introduction

There has been substantial interest in code-division multiple-access (CDMA) technology in recent years due to its many attractive properties for the wireless communications [65, 66]. Several air interface standards based on direct sequence code-division multiple-access (DS-CDMA) have been proposed including the well-known IS-95 standard. Currently, there is also a strong effort underway to develop wideband CDMA for the next generation wireless communications systems [67]. However, despite the many desirable features, DS-CDMA systems are interference-limited and suffer from the near-far problem.[1] The current CDMA detection method uses a bank of matched filters followed by quantizers. Each user is treated as signal at its detection time while all the others are treated as if they are noise for that user. Fig. 6.1 shows the structure of this DS-CDMA detection scheme. It is reliable only if the signature waveforms of all the users have low cross-correlations for all possible delays, and the powers of the users are not very different. Unfortunately, these two conditions are rarely met in the real world. This places a bottle-neck on the capacity of the current CDMA systems.

Recent advances in CDMA detection theory show that the shortcomings of the current CDMA system are not inherent to the system itself. As will be explained in the next section, a base station has information on all the mobiles in its own cell. The information about all the users can be used for their mutual benefit through multiuser detection (joint detection), by considering all users as signals for each other

[1] In a DS-CDMA system, strong users usually have better quality than weak users. This is known as the near-far problem. The near-far problem is due to the existence of multiple access interference at the output of matched filters. Weak users experience relatively higher multiple access interference and are subject to the interference of stronger users. In addition to the physical distance between the mobiles and their base station, fading is also another major cause of near-far problem.

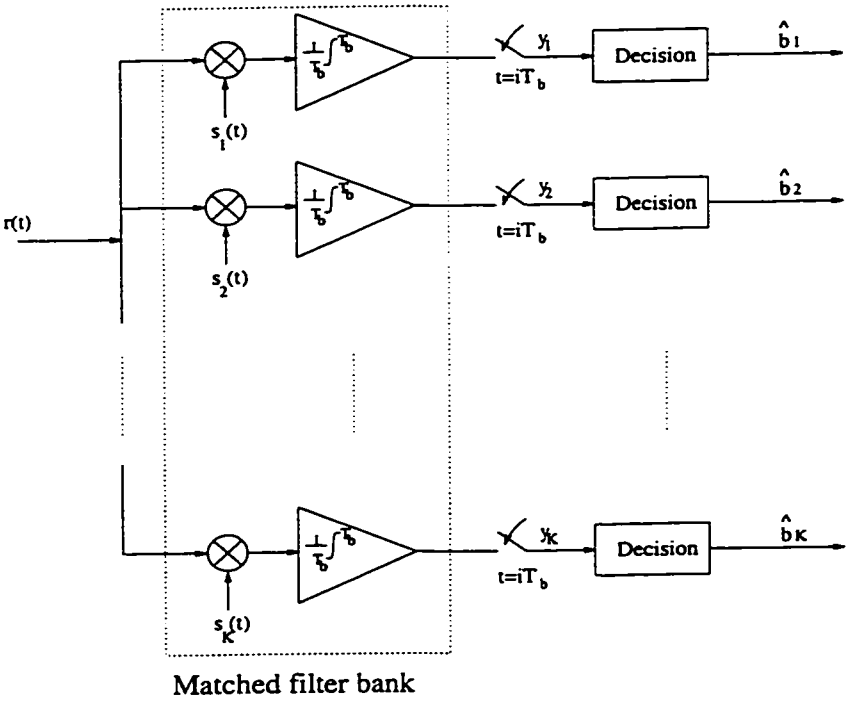

Figure 6.1: The conventional DS-CDMA detection architecture

instead of interference for each other [68, 69, 70].

At the present, major obstacles to the application of multiuser detection in practical wireless systems are processing complexity and delay [68]. Optimum multiuser detection is too complex for applications in a system with large user population, even the suboptimal structures can lead to unacceptable levels of complexity. Many suboptimal detectors, such as decorrelating detectors and decision-feedback detectors, require inversion and/or factorization of matrices proportional in size to the number of users, which is difficult to perform in real time when the number of users is large. For example, for a system with K users and N bits per user, the decorrelating detector in an asynchronous case results in the inversion of a $NK \times NK$ cross-correlation matrix. Others such as the successive interference cancellor (SIC) require processing delay proportional to the number of users. This may lead to unacceptable processing delays when there is a large user population.

The spatial filtering properties of directional array antennas in wireless communications makes it possible to confine the radio energy associated with a given user to a particular direction. One such example is a multibeam smart antenna in which multiple narrow beams illuminate the entire coverage area of a base station. Each beam usually consists of a main beam that covers a certain angular extent. Although the use of multibeam smart antenna systems in wireless communications is

a relatively new concept, multibeam smart antenna systems have already been used in radar systems and have proven to be very effective [71].

In this chapter we propose employing multibeam smart antennas together with multiuser detection at the base station. We call this approach the multibeam smart antenna multiuser detection (MSAMD) technique. By using the spatial filtering property of multibeam smart antenna, existing optimum as well as suboptimal multiuser detectors can be implemented with much lower computational complexity; in addition, substantial performance improvements can also be achieved as a result of the capability of multibeam smart antennas to spatially suppress multiple access interference (MAI). MSAMD can thus reduce the computational complexity of various existing multiuser detectors as well as improve their performance. Attention is focused on the analysis of symbol-synchronous systems, however, the analysis conducted in this chapter applies to asynchronous CDMA systems. This comes about because synchronous CDMA systems are a special case of its asynchronous CDMA systems. The performance would also be indicative of its asynchronous counterpart.

The chapter is organized as follows. The multiuser detection concept is explained first in Section. 6.2. In section 6.3, we present the concept and system model of the proposed MSAMD approach. In Section 6.4, we analyze the use of a decorrelating detector for MSAMD and introduce the concept of partial decorrelation. A partial decorrelator-based MSAMD algorithm is then developed. In Section 6.5, its performance is analyzed and examples are given. The lower bound of probability of error for MSAMD is established and the sidelobe effect is also analyzed in this section. Section 6.6 is the summary and outline for future work.

6.2 Multiuser Detection

A conventional DS-CDMA system treats each user separately as signal while considering all other users as interference or noise. Referring back to Fig. 6.1, we see that the structure of conventional DS-CDMA detection scheme has a bank of correlators. The correlators are sampled and decisions are made based on the sampled signals y_k. It is clear that the conventional detector has no sharing of multiple user information. Assume K users communicate with the base station in symbol-synchronous fashion over a shared channel. Each user is assigned a finite energy signature waveform $s_k(t), t \in [0,T], k = 1, \cdots, K$. Without loss of generality, assume that $S_k(t)$ satisfies the following

$$\int_0^T s_k^2(t)dt = 1 \tag{6.1}$$

Each user transmits information by modulating that waveform antipodally. The received signal at the base station, $r(t)$, can be modeled as a superposition of the K simultaneously transmitted waveforms combined with an additive noise. Assuming

real channel attenuations, [2] $r(t)$ is represented by

$$r(t) = \sum_{k=1}^{K} b_k(j)\sqrt{w_k(j)}s_k(t - jT) + n(t)$$
$$t \in [jT, jT + T] \tag{6.2}$$

where $n(t)$ is white Gaussian noise with power spectral density σ^2. $b_k(j)$ ($b_k(j) \in \{-1, 1\}$) is the kth user's jth information bit and $w_k(j)$ is the energy received from user k in the jth time slot.

Assuming all possible information sequences are equally likely, we drop the time subscript and restrict attention to only $j = 0$. If we denote $\mathbf{b}(t) = [b_1(t), b_2(t), ..., b_K(t)]^T$, $\mathbf{S}(t) = [s_1(t), s_2(t), ..., s_K(t)]^T$, $W = diag(\sqrt{w_1}, \sqrt{w_2}, \ldots, \sqrt{w_K})$, we have

$$r(t) = \mathbf{S}^T(t)\mathbf{W}\mathbf{b}(t) + n(t), t \in [0, T] \tag{6.3}$$

When a bank of filters, which is matched to the set of signature waveforms $\mathbf{S}(t)$, is followed by samplers at time T, the sampled output vector $\mathbf{y}$ ($\mathbf{y} = [y_1, y_2, \ldots, y_K]^T$) is

$$\mathbf{y} = \mathbf{H}\mathbf{W}\mathbf{b} + \mathbf{z} \tag{6.4}$$

where $\mathbf{z}$ is a colored zero-mean Gaussian noise vector with a covariance matrix $\sigma^2\mathbf{H}$. $\mathbf{H}$ is the cross-correlations matrix where the $(k, l)th$ element is

$$h_{kl} = \int_0^T s_k(t)s_l(t)dt \tag{6.5}$$

The conventional detector uses eqn. (6.4) to estimate input signals, i.e., the estimated signal vector $\hat{\mathbf{b}}$ is

$$\hat{\mathbf{b}} = sgn[\mathbf{y}] \tag{6.6}$$

Let us take a closer look at the individual elements in $\mathbf{y}$ in the above equation to gain some further insights. The output of the kth correlator, y_k, is

$$y_k = \sqrt{w_k}b_k + \sum_{l=1, l\neq k}^{K} h_{kl}\sqrt{w_l}b_l + z_k \tag{6.7}$$

Only the first term on the right hand side of the above equation is the recovered data term while the second and the third terms are due to multiple access interference (MAI) and the noise, respectively. Since the detection of b_k is dependent upon the

[2]The real attenuation model is convenient for analyzing coherent methods, and can easily be generalized to the complex case. For a complete treatment of the complex attenuation case, please refer to [68].

sign of y_k, the presence of MAI and noise as evident in Eqn. (6.7) has a significant impact on the performance of the conventional detector. As the number of interfering users increases, the amount of MAI increases. In addition, the presence of strong users introduce higher MAI, thereby obscuring the weaker users as can be seen from Eqn. (6.7). Weaker users may be overwhelmed by stronger users and cause the well known near-far problem.

A better strategy is to jointly detect $y_1, \ldots, y_k$. Information about multiple users can be used jointly to better detect each individual user. This is known as *multiuser detection*. For example, instead of using Eqn. (6.6) , we apply the inverse of the cross-correlation matrix $\mathbf{H}^{-1}$ to the conventional detector in order to reduce the MAI, i.e., the estimated signals are

$$\hat{\mathbf{b}} = sgn[\mathbf{H}^{-1}\mathbf{y}] \tag{6.8}$$

This kind of multiuser detector is called *decorrelating detector*, or simply *decorrelator*. It can be shown that this approach provides significant improvement in performance over the conventional single user detection approach.

The major improvements of using multiuser detection include [68] [69]:

- Significant capacity improvement: more users can be accommodated as a direct result of MAI reduction.
- More efficient use of spectrum: the reduction of MAI allows mobiles to operate at a lower processing gain. This leads to lower chip rate which requires less bandwidth.
- Reduced requirements for power control: since the near-far problem is alleviated, the accuracy of power control needed at the mobiles can be relaxed.
- More efficient power utilization: the reduction of interference can allow mobiles to transmit less power.

Multiuser detection methods can be divided into two groups: optimum multiuser detector and sub-optimum multiuser detectors. The optimum multiuser detector is a maximum likelihood sequence detector. It yields the most likely transmitted sequence $\mathbf{b}$ by choosing $\mathbf{b}$ to be the sequence that maximizes the probability of $\mathbf{b}$ being transmitted for a certain received $\mathbf{r}(t)$. The optimum detector requires a search over the 2^K possible combinations of the components of vector $\mathbf{b}$, where K is the number of users. It has a complexity that is exponential in the number of users. The optimum detector offers huge performance and capacity improvement over the conventional detector, however, its implementation is impractical. A realistic DS-CDMA systems has a relatively large number of active users which makes the cost of this detector too high. Sub-optimum detectors are less complicated, and offer performance close to the optimum detector.

The sub-optimum detectors can be further divided into two sub-groups: linear multiuser detector and non-linear multiuser detector. The linear detectors apply a linear transformation to the output of the bank of correlators to reduce the MAI seen by each user. Important linear multiuser detectors include decorrelating, minimum mean-squared error (MMSE), and polynomial expansion (PE) detectors. Non-linear suboptimum detectors use non-linear methods to cancel MAI. Multistage detectors, decision-feedback detectors, and successive interference cancellers are some of the well-known non-linear multiuser detectors [68] [69].

Major obstacles to the application of the multiuser detectors in practical wireless systems include the processing complexity and possible processing delays [68]. The optimum multiuser detector is clearly too complex for application to a system with a large number of users. Even the suboptimal multiuser detectors can lead to unacceptable levels of complexity. In the rest of the chapter, we will focus on using the multibeam smart antenna to reduce the complexity and processing delays of various multiuser detectors.

6.3 Applying Multibeam Smart Antenna to Multiuser Detection

In this section, we present the concept and system model of multiuser detection with a multibeam smart antenna used at the base station. We call this approach multibeam smart antenna multiuser detection (MSAMD). We denote the number of beams as M, and also assume we have M receivers.

6.3.1 The Benefits of Multibeam Smart Antenna Multiuser Detection

The concept of MSAMD can be best explained using an ideal multibeam antenna. By an ideal multibeam smart antenna, we refer to a multibeam smart antenna whose beam pattern has zero gain in all directions except its main beam. The beam pattern of its mth beam, $g_m(\theta)$ satisfies the following

$$\begin{cases} \|g_m(\theta)\|^2 = 1, \text{ for } & \theta_{m,1} < \theta < \theta_{m,2} \\ \|g_m(\theta)\|^2 = 0, & otherwise \end{cases}$$

where $m = 1, 2, \ldots, M$. $[\theta_{m,1}, \theta_{m,2}]$ is the main lobe (main beam) area of the mth beam. The set of $\{[\theta_{1,1}, \theta_{1,2}], [\theta_{2,1}, \theta_{2,2}], \ldots, [\theta_{M,1}, \theta_{M,2}]\}$ covers the whole coverage area of the base station. Of course, such a multibeam antenna can not be realized in the real world, nevertheless, it is useful in analyzing the characteristics of various multibeam antennas as we will see later in this chapter.

If the base station is equipped with such an ideal multibeam smart antenna, Eqn. (6.2) can still be used to describe $r_m(t)$, which is the signal received by the mth beam. More specifically, the output at mth beam can be expressed as

$$r_m(t) = \sum_{k=m_1}^{m_L} b_k(j)\sqrt{w_k(j)}s_k(t - jT) + n_m(t), \quad t \in [jT, jT + T] \tag{6.9}$$

In the above equation, we have assumed $m_1, m_2, \ldots, m_L$ $(L < K)$ to be the indices of the L users covered by the mth beam. $n_m(t)$ is white Gaussian noise with power spectral density σ_m^2. $b_k(j)$ is the kth user's jth information bit and $b_k(j) \in \{-1, 1\}$. $w_k(j)$ is the received energy for user k in the jth time slot.

With the time subscripts dropped and setting j to 0, Eqn. (6.9) can be written in vector form as the following

$$r_m(t) = \mathbf{S}_m^T(t)\mathbf{W}_m\mathbf{b}_m(t) + n_m(t), t \in [0, T] \tag{6.10}$$

where

$$\begin{aligned} \mathbf{b}_m(t) &= [b_{m_1}(t), b_{m_2}(t), ..., b_{m_L}(t)]^T \\ \mathbf{S}_m(t) &= [s_{m_1}(t), s_{m_2}(t), ..., s_{m_L}(t)]^T \\ \mathbf{W}_m &= diag(\sqrt{w_{m_1}}, \sqrt{w_{m_2}}, \ldots, \sqrt{w_{m_L}}) \end{aligned}$$

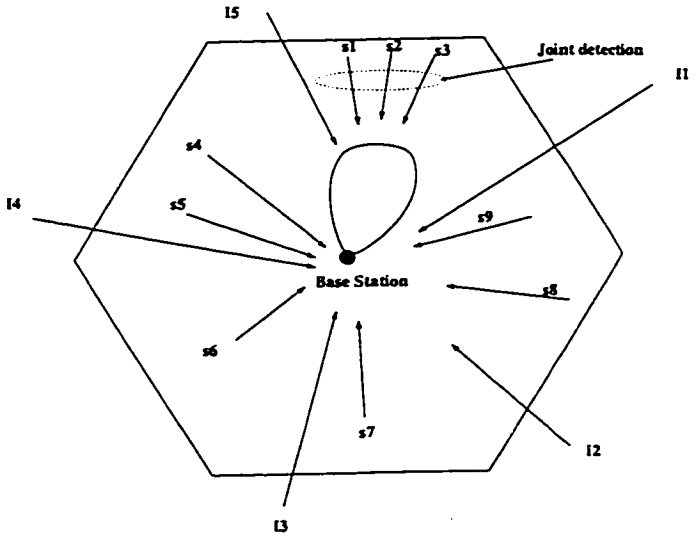

Figure 6.2: An illustration of multibeam smart antenna multiuser detection.

Comparing Eqns. (6.10) and (6.3), we can see that $r_m(t)$ contains L users, with all the other $K - L$ user signals being eliminated by the multibeam smart antenna. Since all users are located randomly, L would be much smaller than K when M is large. If multiuser detectors can be used at each beam output to jointly detect only those L users, the computational complexity can be reduced. If all users are equally spread in angle, L equals K/M. In this situation, only M inversions of matrices of the size $(KN/M) \times (KN/M)$ are needed, instead of inverting a $NK \times NK$ matrix if we want to decorrelate the asynchronous DS-CDMA system with K users and N bit/user. This corresponds to a factor of M^2 reduction in computational complexity. [3] More importantly, each user will be detected with less probability of error since the MAI seen at the output is greatly reduced by the multibeam smart antenna. A point that is worth making here is that multibeam smart antenna not only reduces the MAI from other users in the same cell, but also reduces the MAI from users in other cells. Users in other cells are not included in the current multiuser detection schemes due to either the lack of information about them or the complexity of including them in multiuser detection. Taking this into consideration, the benefit of multibeam smart antenna multiuser detection over conventional multiuser detection scheme would become even greater.

Fig. 6.2 illustrates the performance of multiuser detection implemented with a multibeam smart antenna. With the ability of a multibeam smart antenna to spatially filter out other users and interferences, Users $s1$, $s2$ and $s3$ can be jointly detected with only one interference $I5$ which originates from another cell. As is evident in this illustration, MAI from Users $s4$ to $s9$ which originated from within the same cell as well as $I1$ to $I4$, which are from other cells, are all eliminated through spatial filtering by the antenna.

The practical situation is less ideal. In particular, antennas with very low side lobes are difficult and expensive to build, which means the ideal case we just mentioned above usually does not hold – the user signals are received from the side lobes as well as the main beam. In a system with a large number of users and moderate side lobes (-15dB to -20dB), the MAI from the side lobes cannot be ignored. To make the situation more complicated, users are often not equally distributed in angle, and are likely to may move with time, which results in the addition/removal of users in each beam. Despite of all these issues, the ideal multibeam antenna is an important abstraction for the analysis of MSAMD. For example, the probability of error obtained from an ideal multibeam antenna serves as the lower bound of the achievable performance for various MSAMD structures as will become evident later in this chapter.

[3] Since inversion of an $X \times X$ cross-correlation matrix requires computation complexity of $O(X^3)$ [72, 73].

6.3.2 System Model

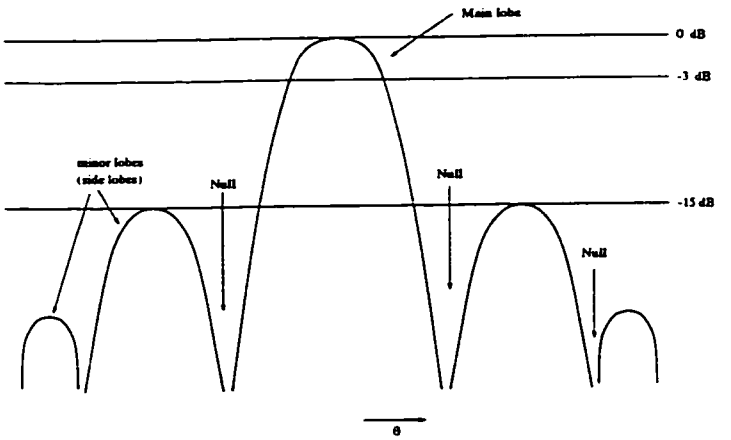

Figure 6.3: The beam pattern of a practical multibeam antenna

In deriving the system model of MSAMD, we use a practical multibeam antenna. Fig. 6.3 shows the pattern of one beam in a practical multibeam antenna. It has a main-lobe which points in a particular direction, the beam direction, and minor lobes (side lobes) which point in other directions. Between the lobes are located the nulls in the antenna pattern, i.e., directions along which the radiation assumes a local minimum.

Eqn. (6.9) can be revised to include the effects of multibeam smart antennas that are less than ideal. Suppose the radiation pattern of *mth* beam is denoted by $g_m(\theta)$, where $m = 1, ..., M$. $r_m(t)$, the output at the *mth* beam can be re-written as

$$r_m(t) = \sum_{k=1}^{K} b_k(j)\sqrt{w_k(j)}s_k(t - jT)g_m(\theta_k) + n_m(t), \quad t \in [jT, jT + T] \tag{6.11}$$

If we write Eqn. (6.11) in vector form we have

$$r_m(t) = \mathbf{S}^T(t)\mathbf{W}g_m(\Theta)\mathbf{b}(t) + n_m(t), t \in [0, T] \tag{6.12}$$

Where

$$\begin{aligned} g_m(\Theta) &= diag(g_m(\theta_1), g_m(\theta_2), ..., g_m(\theta_K)) \\ \mathbf{b}(t) &= [b_1(t), b_2(t), ..., b_K(t)]^T \\ \mathbf{S}(t) &= [s_1(t), s_2(t), ..., s_K(t)]^T \\ \mathbf{W} &= diag(\sqrt{w_1}, \sqrt{w_2}, \ldots, \sqrt{w_K}) \end{aligned}$$

When a bank of filters, which is matched to the set of signature waveforms $\mathbf{S}(t)$, is followed by A/D converter that takes samples at time T, the sampled output vector $\mathbf{y}$ ($\mathbf{y} = [y_1, y_2, \ldots, y_K]^T$) can be expressed as

$$\mathbf{y} = \mathbf{H}\mathbf{W}g_m(\Theta)\mathbf{b}(t) + \mathbf{z} \tag{6.13}$$

where $\mathbf{z}$ is a colored zero-mean Gaussian noise vector with covariance matrix $\sigma^2\mathbf{H}$. $\mathbf{H}$ is the cross-correlations matrix with the $(k,l)th$ element as

$$h_{kl} = \int_0^T s_k(t)s_l(t)dt \tag{6.14}$$

Without any loss of generality, we assume that the gain of the main beam gain to be unity, [4] Eqn. (6.11) can be rewritten as

$$\begin{aligned} r_m(t) &= \sum_{k=1}^{L} b_k(j)s_k(t - jT)\sqrt{w_k(j)} \\ &+ \sum_{q\neq 1,\cdots,L} b_q(j)s_q(t - jT)\sqrt{w_q(j)}g_m(\theta_q) + n_m(t), \\ &\quad t \in [jT, jT + T] \end{aligned} \tag{6.15}$$

Compared to Eqn. (6.10), the second term in Eqn. (6.15) is caused by the effects of the non-ideal multibeam smart antenna.

6.4 Decorrelator-Based Multibeam Smart Antenna Multiuser Detection Algorithms

In this section, we propose an MSAMD algorithm that is based on the widely used decorrelating detectors.

The decorrelating detector has been shown to be independent of the energy of the interfering users and exhibits the same degree of near-far resistance as the optimum multiuser detector [74, 75]. Because of its many advantages, the decorrelating detector has probably received the most attention in the literature. However, as we have pointed out before, the inversion of the cross-correlation matrix which is associated with the decorrelating detector requires considerable computation time when the matrix is large.

Multibeam smart antennas give us the capability to reduce the size of this correlation matrix. Decorrelation can be carried out among a smaller number of users.

[4] For an ideal multibeam smart antenna, matrix $\mathbf{g}_m(\Theta)$ then contains only L 1's with all the other elements being 0.

We call this approach *partial decorrelation* to differentiate it from the commonly used decorrelation process. [5]

6.4.1 Partial Decorrelation

Without loss of generality, assume $1, 2, ...L$ are users that have higher powers and the total number of users is K. We divide all the users in Eqn. (6.13) into two groups: those L users who have relative high powers and the rest $K - L$ users who have low powers, [6] and partition the cross-correlation matrix $\mathbf{H}$ accordingly

$$\mathbf{H} = \left[\begin{array}{c|c} \mathbf{H}_{11} & \mathbf{H}_{12} \\ \hline \mathbf{H}_{21} & \mathbf{H}_{22} \end{array}\right] \tag{6.16}$$

$$= \left[\begin{array}{cc|cc} h_{11} \cdots & h_{1L} & h_{1(L+1)} \cdots & h_{1K} \\ \vdots \ddots & \vdots & \vdots \ddots & \vdots \\ h_{L1} \cdots & h_{LL} & h_{L(L+1)} \cdots & h_{LK} \\ \hline h_{(L+1)1} \cdots & h_{(L+1)L} & h_{(L+1)(L+1)} \cdots & h_{(L+1)K} \\ \vdots \ddots & \vdots & \vdots \ddots & \vdots \\ h_{K1} \cdots & h_{KL} & h_{K(L+1)} \cdots & h_{KK} \end{array}\right] \tag{6.17}$$

We propose a multiuser detection method, which we call partial decorrelation, for detecting L strong users at the mth beam output as the following

$$\hat{\mathbf{b}}_m = sgn[\mathbf{H}_{11}^{-1}\mathbf{y}_m] \tag{6.18}$$

where $\hat{\mathbf{b}}_m = [b_1(t), b_2(t), ..., b_L(t)]^T$. $\mathbf{y}_m$ ($\mathbf{y}_m = [y_1, y_2, \ldots, y_L]^T$) is the output of matched filter bank which is sampled at $t = nT$ (T is the symbol period). $\mathbf{y}_m$ thus satisfies the following equation:

$$\mathbf{y}_m = [\mathbf{H}_{11} \;\; \mathbf{H}_{12}]\mathbf{W}g_m(\Theta)\mathbf{b} + \mathbf{z_m} \tag{6.19}$$

where $\mathbf{z_m}$ is a colored Gaussian noise term with power spectral density $\sigma^2\mathbf{H}_{11}$.

In Eqn. (6.18), only the cross-correlation matrix involving those users having higher powers is inverted. At the output of each beam, multiuser detection is carried

[5] In the rest of the chapter, the term decorrelation refers specifically to the conventional decorrelation scheme in which all user signals are decorrelated at the same time.

[6] For the present, assume the threshold for dividing these two groups are known. In the sections to follow, we will show how to choose this threshold depending on factors such as bit-error rate requirements, sidelobe levels, etc.

out by using mainly those signals received by the main lobe of that beam, while regarding the other users as noise. Since only $\mathbf{H}_{11}^{-1}$ needs to be computed instead of $\mathbf{H}^{-1}$, computational complexity is greatly reduced.

6.4.2 The Algorithm and Structure of Partial Decorrelation Using Multibeam Smart Antennas

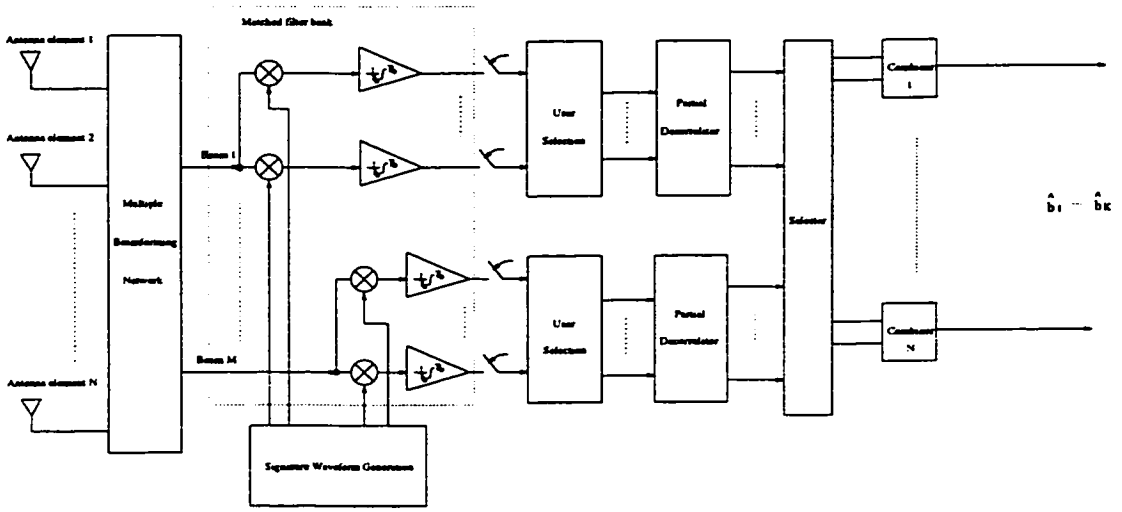

Figure 6.4: Partial decorrelation using a multibeam smart antenna

Fig. 6.4 shows a possible structure of applying multibeam smart antennas to partial decorrelation. In this figure, there is one corresponding partial decorrelator for each beam, and one corresponding combiner for each user. The output of each beam is first fed into a bank of K matched filters, where K is the total number of users that a base station can support on one CDMA carrier frequency. Strong outputs from the matched filters are then selected for partial decorrelation. Since it is sometimes necessary to include a user in more than one partial decorrelator,[7] a selector routes the outputs of partial decorrelation pertaining to each user to the corresponding combiner upon the completion of the partial decorrelation operation. Various combining algorithms, such as selection combining, maximal ratio combining, or equal gain combining as described in Chapter 4, can be used for the combiners.

The system shown in Fig. 6.4 has one obvious drawback – there are too many matched filters. Since a user signal does not need to be used in all partial

[7]Multipath propagation can cause a user signal to be received by multiple beams. If a user signal is very strong, it is also possible to be received by the sidelobes of other beams. In either case, the user signal may have to be included in partial decorrelation in the beams that receive it in order to reduce the multiple access interference it may cause to other users.

decorrelators, we only need as many matched filters that the partial decorrelator needs in each beam. But, two problems need to be solved before we can do this:

1. We need to determine which users should be retained for partial decorrelation in each beam without dedicating a matched filter to each user.

2. Since users move from time to time in a wireless network, we need to determine how to keep updating this decision in order to reflect changes in user location.

Research results obtained by other workers on the characteristics of AOAs, including our measurements, show a slow rate of change in mobile AOAs in practical propagation environments [76, 57]. This suggests the suitability of using block adaptation to solve the above problems. [8]

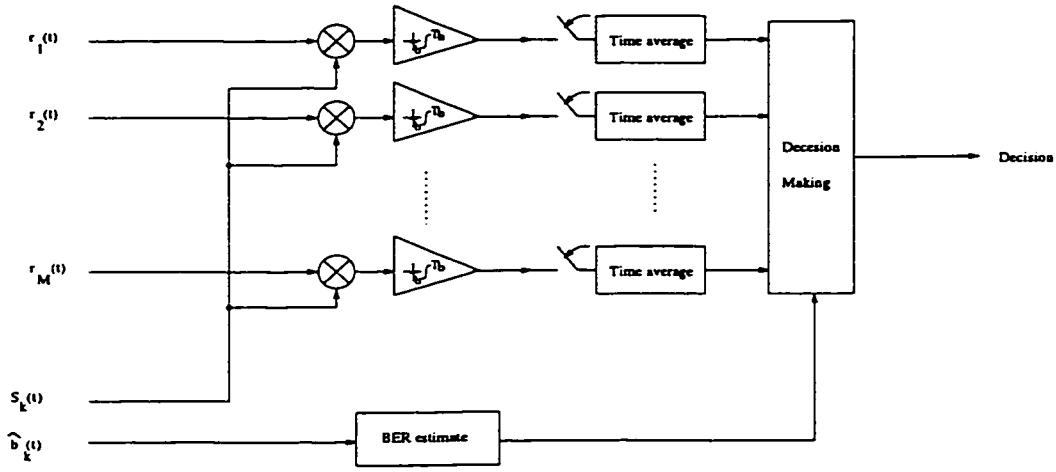

Figure 6.5: A user selection method

We reserve a few matched filters in each beam and transform them into a "matched filter pool". When a user first appears in a cell, a matched filter is selected in each beam and "tuned to" that user to measure its signal strength. Time averaging is used in order to filter out the possible fading/fluctuation in each user signal. Once the user signal strength is measured in each beam, these matched filters are released to the "matched filter pool", and can be used for other users. For each user, the user selection and signature waveform generation processor makes the decision of which decorrelator(s) need to include this user based on the results of its signal strength measurement. This decision is then updated using block adaptation. When

[8]There are usually two approaches to the problem of adaptation: (1) block estimation; (2) Adaptive estimation. In block estimation, the available data is divided into individual blocks, each of length N. The block length N is usually chosen short enough to ensure pseudostationarity of the input data over the length N [77, 78].

updating the decision, the same process is used again. The adaptive rate depends on parameters such as beamwidth, signal bandwidth, and the environment. In addition to block adaptation, the BER of each user is constantly estimated and monitored. When the BER rises above a certain pre-defined threshold it triggers the processor to update its decision. [9] Fig. 6.5 shows a diagram of this decision making scheme.

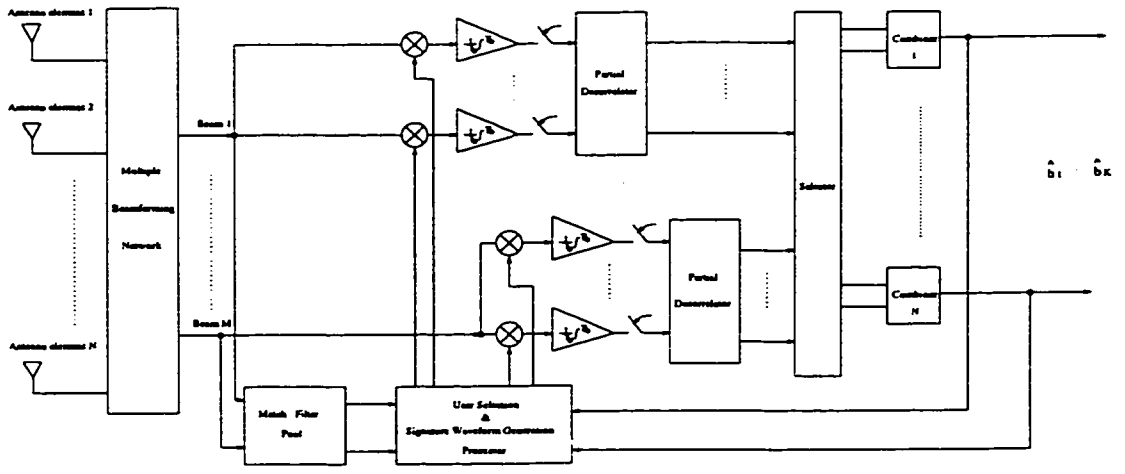

Figure 6.6: An improved method of partial decorrelation using a multibeam smart antenna

An improved structure of applying multibeam smart antenna to partial decorrelation is shown in Fig. 6.6.

6.5 Performance Analysis and Simulation Results

In this section, we compare the performance of the proposed partial decorrelator based MSAMD algorithm with those of conventional detectors and decorrelators using a single antenna. we will show that

- The proposed MSAMD algorithm always achieves better performance than a conventional detector.
- The proposed MSAMD method can achieve performance similar to or better than that of a decorrelator by carefully choosing the sidelobe levels or employing some power control.

[9]The threshold is determined depending on the practical situation. For voice communication, BER from 10^{-2} to 10^{-3} may suffice.

The metric used for comparison is probability of error. In making the comparison, we assume that the selection combining algorithm is used in the combiners. Selection combining is selected not only for the simplicity in analyzing its performance, but also, in many cases, it can yield performance close to equal gain combining or maximal ratio combining.

6.5.1 Error Probability Formula

Since it is assumed that selection combining is used in the combiners, Eqns. (6.19) and Eqn. (6.18) can be used to derive the error probability formula. For a specific user in the mth beam, we only need to substitute m in Eqns. (6.19) and Eqn. (6.18) with the beam that has its partial decorrelator output is selected at the selection combiner.

Substituting Eqn. (6.19) into Eqn. (6.18) yields

$$\hat{\mathbf{b}}_m = sgn\{[\mathbf{I}\ \ \mathbf{H}_{11}^{-1}\mathbf{H}_{12}]\mathbf{W}g_m(\Theta)\mathbf{b}(t) + \mathbf{H}_{11}^{-1}\mathbf{z}_m\} \tag{6.20}$$

where $\mathbf{I}$ is the $L \times L$ identity matrix, and L is the number of users included in partial decorrelation. If we divide $\mathbf{b}$,$\mathbf{W}$ and Θ into two parts as the following

$$\mathbf{b} = [\mathbf{b}_m\ \mathbf{b}_{m\cdot}]^T \tag{6.21}$$

$$\mathbf{W} = \begin{bmatrix} \mathbf{W}_1 & \mathbf{0} \\ \mathbf{0} & \mathbf{W}_2 \end{bmatrix} \tag{6.22}$$

$$\Theta = [\Theta_1\ \Theta_2]^T \tag{6.23}$$

where

$$\begin{aligned} \mathbf{b}_m &= [b_1, \cdots, b_L]^T \\ \mathbf{b}_{m\cdot} &= [b_{L+1}, \cdots, b_K]^T \\ \mathbf{W}_1 &= diag[\sqrt{w_1}, \cdots, \sqrt{w_L}] \\ \mathbf{W}_2 &= diag[\sqrt{w_{L+1}}, \cdots, \sqrt{w_K}] \\ \Theta_1 &= [\theta_1, \cdots, \theta_L] \\ \Theta_2 &= [\theta_{L+1}, \cdots, \theta_K] \\ K &= \text{The total number of users} \end{aligned}$$

And denote

$$\mathbf{F} = \mathbf{H}_{11}^{-1}\mathbf{H}_{12} \tag{6.24}$$

Eqn. (6.20) then becomes

$$\hat{\mathbf{b}}_m = sgn[\mathbf{W}_1 g_m(\Theta_1)\mathbf{b}_m(t) + \mathbf{F}\mathbf{W}_2 g_m(\Theta_2)\mathbf{b}_{m\cdot}(t) + \mathbf{\Gamma}] \tag{6.25}$$

where $\mathbf{\Gamma} = \mathbf{H}_{11}^{-1}\mathbf{z}_m$ is the colored Gaussian noise term with covariance $\sigma^2\mathbf{E}$, and

$$\begin{aligned} \mathbf{E} &= \mathbf{H}_{11}^{-1}\mathbf{H}_{11}(\mathbf{H}_{11}^{-1})^T \\ &= (\mathbf{H}_{11}^{-1})^T \end{aligned} \tag{6.26}$$

Denoting the expectation over the ensemble of independent, uniformly distributed $\mathbf{b}_2$ as $\mathbf{E}\langle\rangle$, and the probability of error as $P[\ ]$, the probability of error for User 1 can be expressed as [10]

$$\begin{aligned} P_{err\_p} = & \quad P[\hat{b}_1 = 1 | b_1 = -1] \\ = & \quad P[\sqrt{w_1} + (\mathbf{F}\mathbf{W}_2 g_m(\Theta_2)^T \mathbf{b}_{m\cdot}(t) + \mathbf{\Gamma})_1 > 0 | b_1 = -1] \\ = & \quad \mathbf{E}\langle P(\gamma_1 > \sqrt{w_1} - \textstyle\sum_{i=L+1}^{K} f_{1(j-L)} b_j \sqrt{w_j} g_m(\theta_j)) \rangle \\ = & \quad \mathbf{E}\langle \tfrac{1}{2^{K-L}} \textstyle\sum_{\mathbf{b}_{m\cdot}} Q(\frac{\sqrt{w_1} - \sum_{j=L+1}^{K} f_{1(j-L)} b_j \sqrt{w_j} g_m(\theta_j)}{\sqrt{\sigma^2 e_{11}}}) \rangle \\ = & \quad \tfrac{1}{2^{K-L}} \textstyle\sum_{\forall \mathbf{b}_{m\cdot}} Q(\frac{\sqrt{w_1} - \sum_{j=L+1}^{K} f_{1(j-L)} b_j \sqrt{w_j} g_m(\theta_j)}{\sqrt{\sigma^2 e_{11}}}) \end{aligned} \tag{6.27}$$

where $f_{1(j-L)}$ and e_{11} are the $(1,(j-L))th$ and $(1,1)th$ elements of $\mathbf{F}$ and $\mathbf{E}$ respectively; $\forall \mathbf{b}_{m\cdot}$ means "for all possible values of $\mathbf{b}_{m\cdot}$". The Q-function is as follows

$$Q(x) = \frac{1}{\sqrt{2\pi}} \int_x^{\infty} \exp(\frac{-y^2}{2}) dy \tag{6.28}$$

The error probability of a decorrelator is [74]

$$P_{err\_d} = Q(\frac{\sqrt{w_1}}{\sqrt{\sigma^2 g_{11}}}) \tag{6.29}$$

Where g_{11} is the $(1,1)$th element of $\mathbf{G}$, and $\mathbf{G} = \mathbf{H}^{-1}$.

The error probability of a conventional detector is obtained by setting L to 1 and $g_m(\theta_j)$ to 1 in Eqn. (6.27)

$$P_{err\_c} = \tfrac{1}{2^{K-1}} \textstyle\sum_{\forall \mathbf{b}_2} Q(\frac{\sqrt{w_1} - \sum_{j=2}^{K} f_{1(j-1)} b_j \sqrt{w_j}}{\sqrt{\sigma^2 e_{11}}}) \tag{6.30}$$

In order to facilitate comparison, the single user bound are also given here.[11]

$$P_{err\_s} = Q(\frac{\sqrt{w}}{\sigma}) \tag{6.31}$$

[10] assume $g_m(\theta_1) = 1$ as before.

[11] The single user bound is the probability of error when there is no multiple access interference in the systems, i.e., the errors are caused by noise only. The single user bound serves as the lower bound on the performance of any detectors including the proposed MSAMD method.

where w is the power of the associated user.

Eqns. (6.27), (6.29), (6.30), and (6.31) are used to compute the error probabilities. Since the probability of error for the proposed MSAMD method as shown in Eqn. (6.27) is dependent on the beam pattern $g_m(\theta_j)$, let us first derive its lower bound of probability of error for the proposed algorithm before we start to compare the performances.

6.5.2 The Lower Bound of Probability of Error

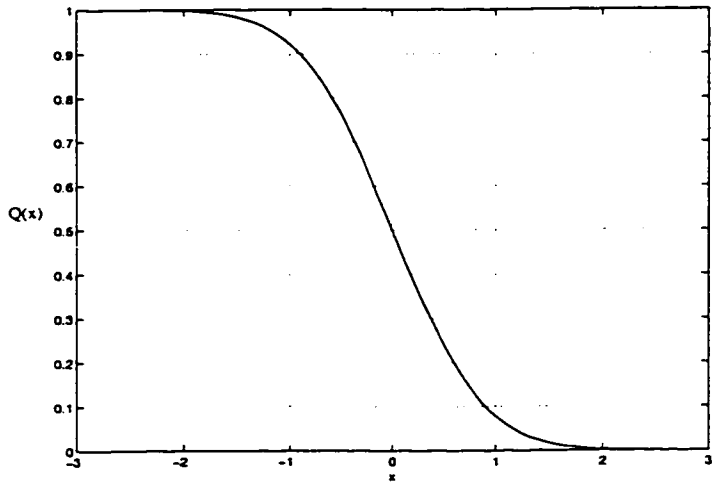

Figure 6.7: The Q-function

Eqn. (6.27) is the equation for calculating the probability of error with arbitrary antenna patterns $g_m(\theta_j)$. Apparently, different $g_m(\theta_j)$ gives different values for the probability of error. What is the antenna pattern that gives us the smallest probability of error given that all other conditions remain unchanged? In another word, what is the lower bound of probability of error for the proposed MSAMD method in relation to the multibeam smart antenna patterns?

To answer this question, we show a plot of Q-function in Fig. 6.7. Q-function satisfies the following equation:

$$Q(x) = \frac{1}{\sqrt{2\pi}} \int_x^{\infty} \exp(\frac{-y^2}{2}) dy \tag{6.32}$$

It is obvious from Fig. 6.7 that [12]

[12] As can be seen from Fig. 6.7, Q-function decreases with x in general. But the rate of decrease increases with x for $x \leq 0$ while that rate decreases with x for $x \geq 0$.

$$\begin{cases} \frac{Q(x-a)+Q(x+a)}{2} > Q(x) & for\ x > 0, a \neq 0 \\ \frac{Q(x-a)+Q(x+a)}{2} = Q(x) & for\ x > 0, a = 0 \end{cases} \tag{6.33}$$

There are 2^{K-L} terms of $Q(\frac{\sqrt{w_1}-\sum_{j=2}^{K} f_{1(j-1)} b_j \sqrt{w_j} g_m(\theta_j)}{\sqrt{\sigma^2 e_{11}}})$ in Eqn. (6.27). For each $Q(\frac{\sqrt{w_1}-\sum_{j=2}^{K} f_{1(j-1)} b_j \sqrt{w_j} g_m(\theta_j)}{\sqrt{\sigma^2 e_{11}}})$, there is a corresponding term of $Q(\frac{\sqrt{w_1}+\sum_{j=2}^{K} f_{1(j-1)} b_j \sqrt{w_j} g_m(\theta_j)}{\sqrt{\sigma^2 e_{11}}})$. Use Inequality (6.33), we have the probability of error for multibeam partial detection as

$$\begin{cases} P_{err\_p} > Q(\frac{\sqrt{w_1}}{\sqrt{\sigma^2 e_{11}}}) & for\ g_m(\theta_j) \neq 0, j \neq 1 \\ P_{err\_p} = Q(\frac{\sqrt{w_1}}{\sqrt{\sigma^2 e_{11}}}) & for\ g_m(\theta_j) = 0, j \neq 1 \end{cases} \tag{6.34}$$

In other words, the ideal multibeam antenna patterns give the lowest probability of error.

Having established the lower bound of probability of error, we wish to investigate its relation with that of decorrelation. In particular, we want to know how the proposed MSAMD algorithm using an ideal multibeam smart antenna compares to decorrelation with respect to the probability of error.

If $\mathbf{G}$ is defined as the inverse of matrix $\mathbf{H}$, we can express $\mathbf{G}$ in terms of partitioned matrix of $\mathbf{H}$. Using Eqn. (6.24), and $\mathbf{H}_{12} = \mathbf{H}_{21}$, we have [13]

$$\begin{aligned} \mathbf{G} &= \mathbf{H}^{-1} \\ &= \left[\begin{array}{c|c} \mathbf{H}_{11} & \mathbf{H}_{12} \\ \hline \mathbf{H}_{21} & \mathbf{H}_{22} \end{array}\right]^{-1} \\ &= \left[\begin{array}{c|c} \mathbf{H}_{11}^{-1} + \mathbf{F}\mathbf{C}^{-1}\mathbf{F}^T & -\mathbf{F}\mathbf{C}^{-1} \\ \hline (-\mathbf{F}\mathbf{C}^{-1})^T & \mathbf{C}^{-1} \end{array}\right] \end{aligned} \tag{6.35}$$

Where

$$\mathbf{C} = \mathbf{H}_{22} - \mathbf{H}_{21}\mathbf{H}_{11}^{-1}\mathbf{H}_{12} = \mathbf{H}_{22} - \mathbf{H}_{12}^T\mathbf{H}_{11}^{-1}\mathbf{H}_{12} \tag{6.36}$$

[13] For the detailed derivation of the inverse of a partitioned matrix, see [79].

We can use Eqns.(6.29), and (6.34), and (6.35) to compare the performance of the proposed MSAMD algorithm using an ideal multibeam smart antenna with that of conventional decorrelation. The comparison cannot be made straight forward as we can see from Eqn.(6.35) that g_{11} is equal to $e_{11} + m_{11}$, where m_{11} is $(1,1)th$ element of $\mathbf{M} = (\mathbf{F}\mathbf{C}^{-1}\mathbf{F}^{\mathbf{T}})$. But it turns out that we can prove that Eqn. (6.34) always gives lower probability than Eqn.(6.29). The proof is provided in Appendix B.

The proposed MSAMD algorithm using an ideal multibeam smart antenna always yields lower probability of error than the decorrelator, however, the extent of performance improvement depends also on the specific structure of the cross-correlation matrix $\mathbf{H}$ and the number of beams, which determines the number of users that can be jointly detected. This is not a surprising result, as there are fewer user signals in the output of an ideal multibeam smart antenna, the multiple access interference (MAI) each user experiences become less severe and thus yields few errors. What is interesting is using a non-ideal multibeam smart antenna. This is the question to be answered in the next sub-section.

6.5.3 Sidelobe Effects

One important thing to notice is that the proposed MSAMD algorithm using a practical multibeam smart antenna is no longer near-far resistant. That is, the probability of error of each user is also dependent upon the power levels of other users. This is in sharp contrast to the decorrelator for which the error probability of each user is independent of the power levels of others.

Comparing with the Conventional CDMA Detector

Eqns.(6.30) and (6.27) enable us to compare the performance of the proposed MSAMD algorithm using an non-ideal multibeam smart antenna with that of a conventional CDMA detector. In general, Eqn.(6.27) has fewer terms than Eqn.(6.30). This is true even for the worst case when all the users are "crowded" into the coverage area of a single beam. Although, K, the total number of users, is the same for both equation in this case, $L+1$ in Eqn.(6.34) is still larger than 2 since we employ multiuser detection.

It can be proven that the proposed MSAMD algorithm using a multibeam smart antenna always gives lower probability of error than the conventional CDMA detector. The proof is as the following:

$$
\begin{aligned}
P_{err\_p} &= \frac{1}{2^{K-L}} \sum_{\forall \mathbf{b}_m} Q\left(\frac{\sqrt{w_1} - \sum_{j=L+1}^{K} f_{1(j-L)} b_j \sqrt{w_j} g_m(\theta_j)}{\sqrt{\sigma^2 e_{11}}}\right) \\
&< \frac{1}{2^{K-1}} \sum_{\forall \mathbf{b}_m} Q\left(\frac{\sqrt{w_1} - \sum_{j=2}^{K} f_{1(j-L)} b_j \sqrt{w_j} g_m(\theta_j)}{\sqrt{\sigma^2 e_{11}}}\right)
\end{aligned}
$$

$$< \quad \frac{1}{2^{K-1}} \sum_{\forall \mathbf{b}_m} Q\left(\frac{\sqrt{w_1} - \sum_{j=2}^{K} f_{1(j-1)} b_j \sqrt{w_j}}{\sqrt{\sigma^2 e_{11}}}\right)$$

$$= \quad P_{err\_c} \tag{6.37}$$

The second part of the inequality is true because

$$Q(x+a) + Q(x-a) < Q(x+b) + Q(x-b) \text{ for any } x > 0, b > a > 0 \tag{6.38}$$

Comparing with the Decorrelator

MSAMD using a practical multibeam smart antenna has higher probability of error than MSAMD using an ideal multibeam smart antenna. In addition to the specific structure of the cross-correlation matrix **H**, the radiation pattern of the multibeam smart antenna $g_m(\theta_j)$ also plays an important part. To make the situation more complex, unlike the conventional decorrelation detector, the probability of error for each users also depends on the power of other users as well. However, with careful design of $g_m(\theta_j)$, the proposed MSAMD algorithm can achieve better than or close to the probability of error of the conventional decorrelation detector as we will show in the next two examples.

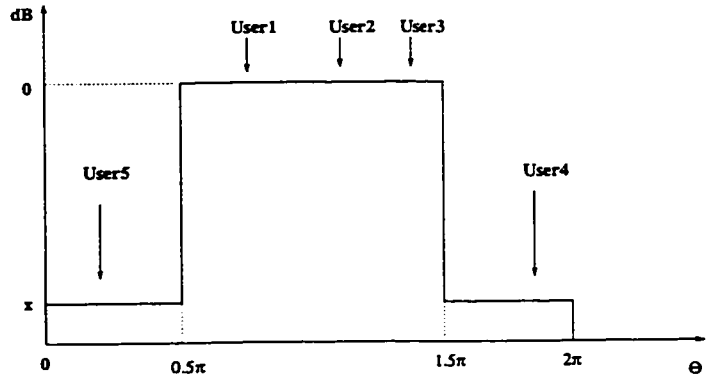

Figure 6.8: First order approximation of a practical multibeam smart antenna

Example 1

Consider a 2-beam multibeam smart antenna. We use a first order approximation of a practical multibeam smart antenna as shown in Fig. 6.8. It has constant main lobe and sidelobes which are at 0dB and xdB respectively. Users 1,2 and 3 are the three users received by the main lobe of beam 1 while Users 4 and 5 are received by the main lobe of beam 2 and the side lobes of beam 1. Users 1, 2 and 3 have their SNRs set at $13dB$, $10dB$ and $6dB$ respectively. The other two users, i.e., Users 4 and 5 have variable SNRs with respect to the SNR of Users 1.

Figs. 6.9, 6.10 and 6.11 show the probability of error for Users 1, 2 and 3, with varying power levels of Users 4 and 5 (relative to User 1). As well, three

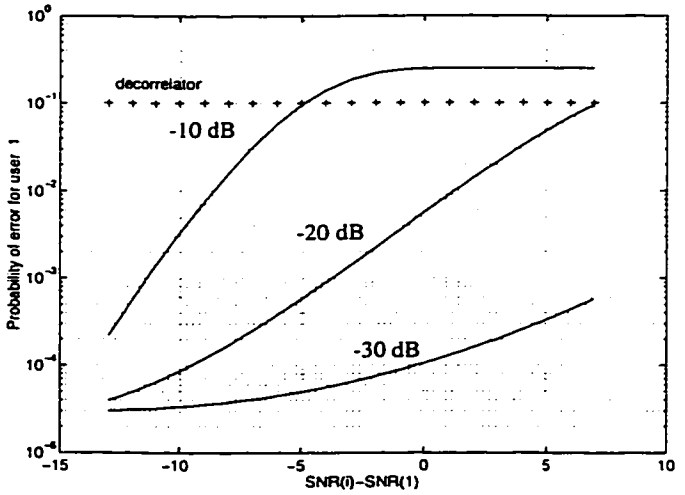

Figure 6.9: Simulation results for the proposed MSAMD algorithm: probability of error for User 1 with SNR(1)=13dB, SNR(2)=10dB, SNR(3)=6dB, and varying SNRs(i), $i = 4, 5$ (sidelobe =-10dB, -20dB, -30dB)

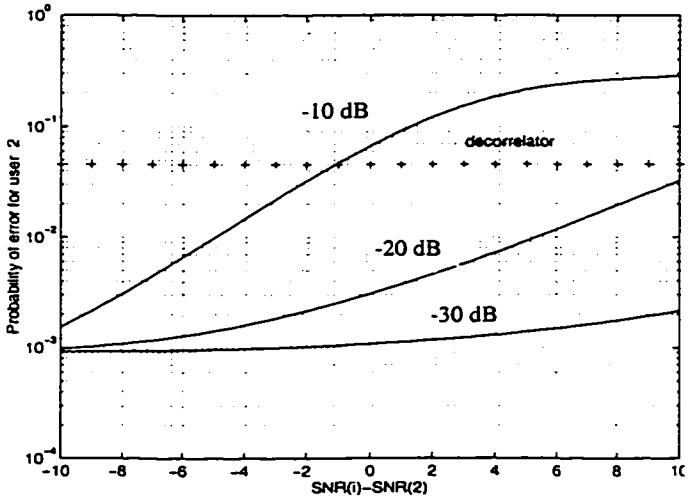

Figure 6.10: Simulation results for the proposed MSAMD algorithm: probability of error for User 2 with varying SNRs(i), $i = 4, 5$, SNR(1)=13dB, SNR(2)=10dB, SNR(3)=6dB (sidelobe =-10dB, -20dB, -30dB)

different sidelobe levels are used, namely, $x = -30dB, -20dB$ and $-10dB$. The probability of error for a decorrelation detector is given in those figures for the purpose of comparison. This example corresponds to a strong MAI case in which the MAI renders the conventional single user detector completely useless.

As we can see in Fig. 6.9 the probability of error for User 1 decreases with a reduction in the levels of sidelobes. This result is to be expected. However, the probability of error increases with increases in the powers of Users 4 and 5, when signals arrive through the side lobes of beam 1, although it is independent of the powers of other users under partial decorrelation, i.e., User 2 and User 3. This behavior is different from that obtained using decorrelation detectors, which have probability of errors independent of the energies of all the other users. In Fig. 6.9, curves corresponding to sidelobes of -20dB and $-30dB$ give much lower probability of error than that of decorrelators. This can be explained by the effect of the high attenuation at the side lobe – signals from Users 4 and 5 are so well attenuated that they contribute much less to the resulting multiple access interference when partial decorrelation is carried out. It is worth pointing out that the reduction in the probability of errors are very significant.

By contrast, the curve that corresponds to the sidelobe level of $-10dB$ yields probability of error lower than or close to that of the decorrelator when the power levels of Users 4 and 5 are comparable to User 1. Its performance is degraded as the power levels of Users 4 and 5 surpass that of User 1. The performance of User 1 would probably not be satisfactory in this case. However, if we exercise a little bit of power control to restrict the power of multiple access interference received from to certain limits, this problem could be remedied.

Figs. 6.10 and 6.11 give results for Users 2 and 3. It is easily seen that similar conclusions can be made for User 2 and User 3 as well, i.e., if the MAI power from the other users is controlled, the performance for Users 2 and 3 goes from unsatisfactory to satisfactory.

When carrying out the simulations in Example 1, we used a first order approximation for the real multibeam smart antenna patterns. By varying the sidelobe level, we identified the importance of sidelobe level control in determining system performance. Next, we carry out an analysis of the proposed MSAMD algorithm using real multibeam smart antenna patterns. Naturally, we do not have a closed form for the probability of error. We overcome this by resorting to Monte-Carlo simulations.

Example 2

The same 5-user DS-CDMA system and 2-beam multibeam smart antenna are used, however, the radiation pattern is different. In Fig. 6.12 the beam patterns are given. These are typical radiation patterns for rectangular microstrip antennas [71]. Again, as in example 1, the SNR values for User 1, 2 and 3 are set at $13dB$, $10dB$ and $6dB$ respectively. The other two users have variable SNR values with respect to users 1, 2 and 3. To reduce the computation involved, the angles of arrival (AOA)

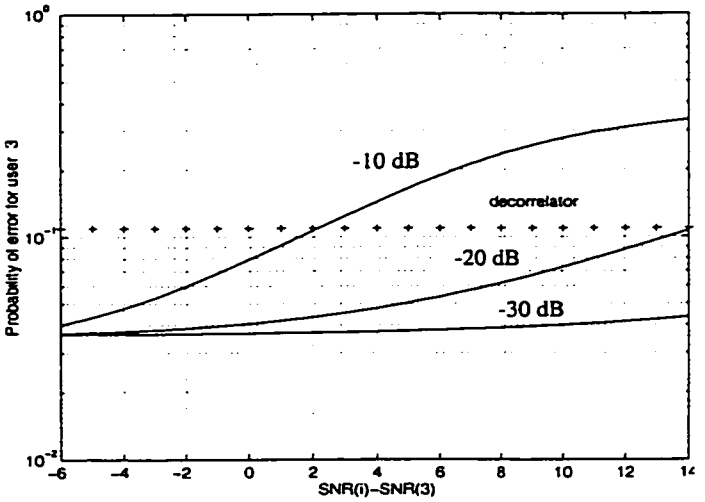

Figure 6.11: Simulation results for the proposed MSAMD algorithm: probability of error for User 3 with varying SNR(i), $i = 4, 5$, SNR(1)=13dB, SNR(2)=10dB, SNR(3)=6dB (sidelobe =-10dB, -20dB, -30dB)

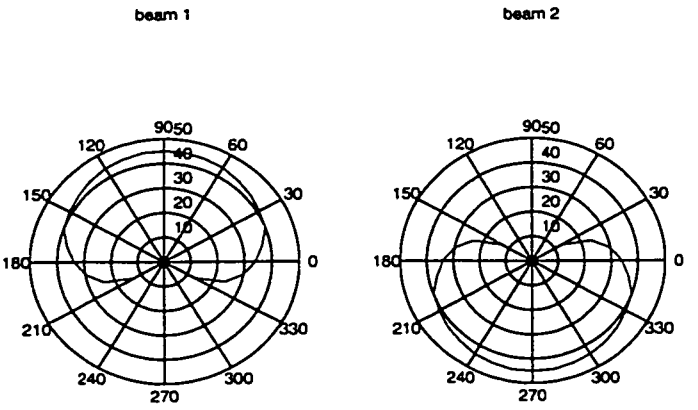

Figure 6.12: Beam patterns used in Example 2

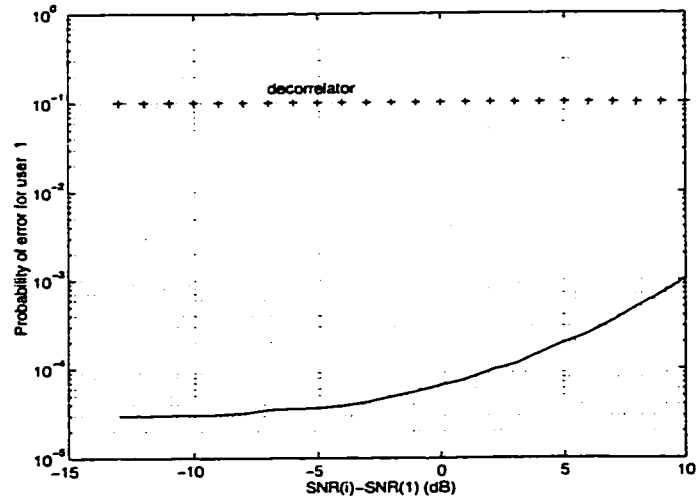

Figure 6.13: Simulation results for the proposed MSAMD algorithm: probability of error for User 1 with varying SNR(i), $i = 4, 5$, SNR(1)=13dB, SNR(2)=10dB, SNR(3)=6dB

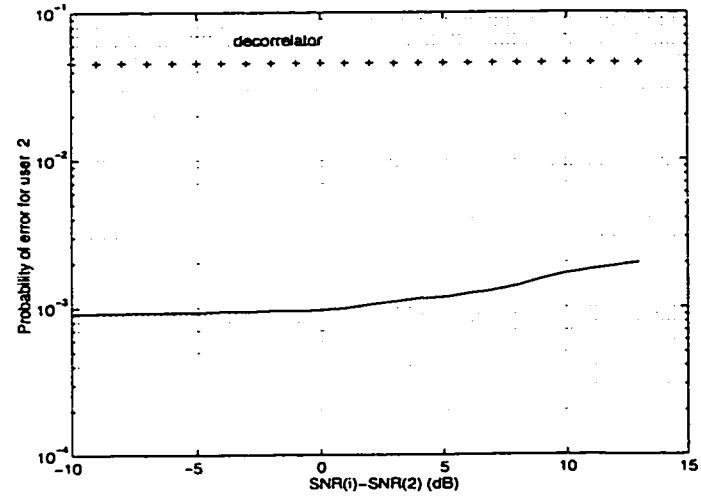

Figure 6.14: Simulation results for the proposed MSAMD algorithm: probability of error for User 2 with varying SNR(i), $i = 4, 5$, SNR(1)=13dB, SNR(2)=10dB, SNR(3)=6dB

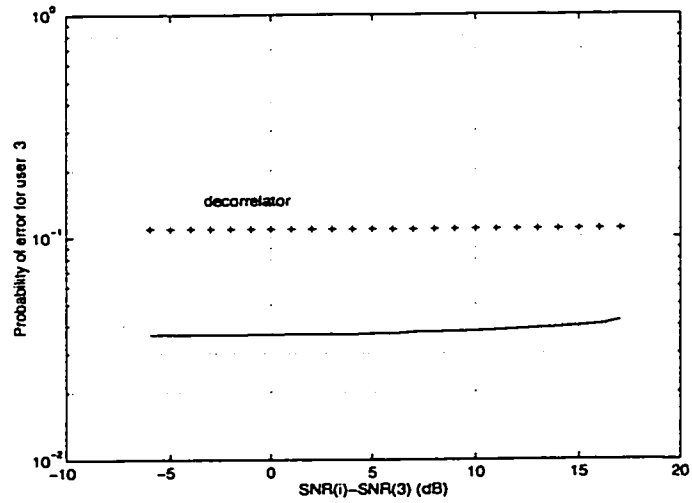

Figure 6.15: Simulation results for the proposed MSAMD algorithm: probability of error for User 3 with varying SNR(i), $i = 4, 5$, SNR(1)=13dB, SNR(2)=10dB, SNR(3)=6dB

for Users 1, 2 and 3 are set to be 90^o, 80^o and 110^o respectively, while the AOAs for Users 4 and 5 are assumed to be random and uniformly distributed in $[180^0, 360^o]$. Figs. 6.13 to 6.15 show the probability of error for Users 1,2 and 3 with varying power levels for Users 4 and 5.

We can see that the results in Figs. 6.9 to 6.11 are similar to the curves corresponding to sidelobe level of $-30dB$ in in Figs. 6.13 to 6.15.

6.6 Conclusions

In this chapter we proposed and analyzed a multiuser detection scheme which differs from those proposed by others in that it employed a multibeam smart antenna at the base station. We have shown both analytically and numerically that this approach results in a significant reduction in computational complexity compared with the conventional multiuser detection methods. We then introduced the concept of partial decorrelation and developed an effective algorithm for partial decorrelation using a multibeam smart antenna. The proposed multibeam multiuser detection approach would be most useful for implementing multiuser detection in CDMA systems in which many users access the system simultaneously. It is a simple and effective way of achieving the performance of multiuser detection without the penalty of computational complexity.

Chapter 7

Conclusions

This thesis is devoted to the development of algorithms and structures that can improve the quality and capacity of the existing and future wireless networks using multibeam smart antennas. The main contributions made by this thesis to the smart antenna technology are in two areas: (1)downlink transmission algorithms in FDD systems; (2)multibeam smart antenna algorithms for CDMA multiuser reception.

Developing effective downlink transmission algorithms for FDD systems is a major challenge facing researchers of smart antenna technology today. One main accomplishment of this thesis is the development of an effective downlink multibeam smart antenna transmission algorithm. The algorithm is based on our measurement data of an 8-element circular array and FDD smart antenna simulations using the Geometrically Based Single Bounce (GBSB) model. The results of the analysis and simulations reveal that the correlation of signal powers at the receive and transmit frequencies are high in beams that receive strong signal powers, while the correlation at the transmit frequency between beams with strong received signal powers is usually very low. Based on this, we have developed an algorithm that selects n beams which have the strongest received signal powers (n should be much smaller than the total number of beams in the multibeam antenna) for transmission. The signal transmitted by each beam is multiplied by a complex weight and then adjusted with different time delays. The weights and time delays can be determined using criteria such as minimizing probability of error. This algorithm improves the system performance in both flat fading and frequency selective fading channels. For flat fading channel, the time diversity can be explored by weighting and staggering the transmission delays among different beams to combat the flat fading. For frequency selective fading, the channel delay spread can be controlled by adjusting the relative transmission delays on different beams. Long delays can be avoided to reduce the burden of equalization. For systems using a training sequence for equalization, this reduces training sequence length and improves system spectrum efficiency. Our simulation results show 4 times reduction in probability of error over the method which simply transmits on the beam with the strongest received signal. It is assumed the system is a QPSK system under

flat Rayleigh fading with SNR= 17dB. It increases to 10 times for SNR= 25dB.

In developing this downlink transmission algorithm for smart antennas, the GBSB model is used for vector channel simulations in FDD systems. The GBSB model was first proposed by Liberti and Rappaport in [43, 44] to simulate wave propagation in multipath environments based on the geometrical properties of the environment. There have not been any reports in the literature on its use in the simulation of FDD systems. As a matter of fact, there has been a dearth of information reported in the literature on FDD smart antenna systems. For the most part this is probably due to the lack of availability of "good" propagation models which can be used for FDD simulations. Since the GBSB model is geometrically based, it is more easily adapted to FDD simulations than other models. Our use of the GBSB model to simulate FDD smart antennas is among the first of its kind. Our simulation results indicate the suitability of the GBSB model in such simulations although some improvements may be needed with regards to capturing the characteristics of wave propagation where the wave has more than one bounce. This could be an interesting research topic.

Another main contribution of this thesis is, for the first time, multibeam smart antennas have been applied to multiuser detection. Currently, there is a strong effort underway to develop wideband CDMA for the next generation wireless communications systems [67]. As a result, CDMA multi-user detection has become a very active research area in recent years. At the present, major obstacles to the application of multiuser detection in practical wireless systems are processing complexity and delays [68]. By applying the multibeam smart antenna to multi-user detection, the computational complexity and delays can be greatly reduced. Our focus is on decorrelator-based algorithms, in particular, we modified the popular decorrelation multi-user detection scheme and developed a new method, which we call partial decorrelation. Instead of decorrelating all users at the same time, which is a complex and time-consuming process, partial decorrelation attempts to decorrelate only those users that have higher powers. Since the strength of different multipath component received by a typical multibeam antenna is very different – there are usually several strong multipath components coupled with many weak ones – partial decorrelation is especially suitable for multibeam smart antenna multi-user detection. The outputs from the partial decorrelators are combined using diversity combining algorithms. Our simulation results show performance close to or better than that of a decorrelator that uses the selection combining algorithm. The proposed multibeam smart antenna multiuser detection approach would be most useful for implementing multiuser detection in CDMA systems with a large number of simultaneous users. Such systems require multiuser detection methods which are less computationally intensive to meet the practical requirements.

When developing the multibeam smart antenna multiuser detection algorithms, our focus has been on using decorrelation-based detectors. The results obtained in this thesis can be expected to be applicable to other methods of multibeam

smart antenna multiuser detection methods, such as those using decision feedback or SIC multiuser detector. However, more research is needed to fully understand the behavior of multibeam smart antnena multiuser detection under these circumstances. This can be an interesting area of future research.

Appendix A

Description of the 8-Element Array Vector Channel Sounder

The 8-element circular array vector channel sounder uses pulse compressing sounding technique as described in Section 2.4.5. It consists of a transmitter and a receiver (including a Sun Sparc workstation). It is designed and developed by the Wireless Technology Group at McMaster University to measure the spatial channel characteristics of the wireless channel at the PCS frequency band (around 2GHz).

A.1 Transmitter

The transmitter of the channel sounding system is capable of transmitting at two frequencies. They can be choosen to be the same as the up-link and downlink frequencies used in most PCS standards in order to measure the characteristics in a FDD system. The carriers at these two frequencies are each modulated by the same pseudo-noise (PN) sequence at a clock rate of 5 Mbps. The length of the PN sequence is 255 bits.

The transmitter is mounted on a mobile cart that can be wheeled about just like a mobile user. A monopole antenna is mounted on the cart at a height of about 1.6 m above the ground.

A.2 Receiver

The receiver is made up of an 8-element circular antenna array. The array elements are 8 identical dipole antennas. The signal received from each element is down-converted coherently to produce In-phase (I) and Quadrature (Q) baseband signals. The Baseband signals are then sampled at a clock rate of 10MHz by an A/D convertor and stored by a Sun Sparc workstation.

A.3 Data Collecting and Processing

Data are collected at a number of places around the McMaster Campus, including indoor environments such as the CRL building. By wheeling the transmitter about the McMaster Campus and placing the receiver at various locations, such as the rooftop of the Engeering Building and CRL building, the front of CRL (Lamp post heigth), a large amount of data have been collected.

One of the main goal of this measurement campaign is to collect a large amount of vector channel impulse responses that can later be used for smart antenna simulation and analysis. As described in Section 2.4.5, the vector channel impulse response can be obtained by correlating the baseband signals recorded by the Sparc workstation with the same PN sequence used by the transmitter.

For the purpose of multibeam smart antennas, the vector channel impulse response has to be further processed to simulate the channel response seen by each beam of the multibeam antenna. To achieve this, as shown in Figure 4.8, different weights are generated which in effect give us the desired multibeam antenna patterns. Figure A.1 shows an 8-beam pattern which was used in processing the collected data.

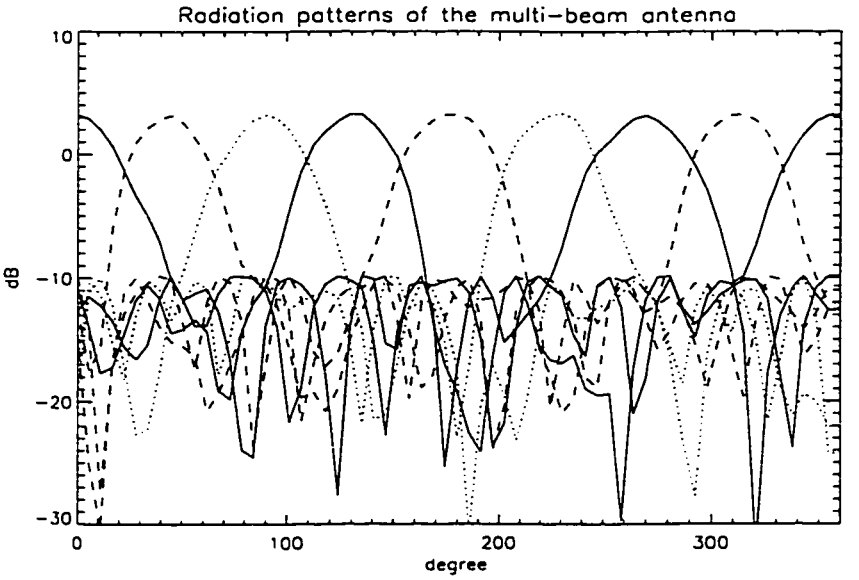

Figure A.1: The patterns of a simulated 8-beam multibeam antenna

Appendix B

The Proof of Eqn. (6.34) Having Lower Probability of Error Than Eqn.(6.29)

Since $\mathbf{H}$ is a cross correlation matrix, $\mathbf{H}$ is positive definite. [1] From the property of positive definiteness it follows that the inverse of a positive definite matrix is also positive definite [72]. Thus from Eqn. (6.35) we can see that $\mathbf{G}$ is also positive definite. Because $\mathbf{C}$ is a principle minor of $\mathbf{G}$,[2] it follows from the properties of positive definiteness that $\mathbf{C}$ is also positive definite. Since the inverse of a positive definite matrix is positive definite, $\mathbf{C^{-1}}$ is also positive definite. This proves m_{11}, the $(1,1)th$ element of $M = (\mathbf{FC^{-1}F}^T)$, is positive. Thus we have proven $g_{11} < e_{11}$ which means Eqn. (6.34) always gives lower probability of error than Eqn.(6.29).

[1] Definition of positive definite: A real, non singular matrix A is called a positive definite matrix if and only if the corresponding quadratic form $\mathbf{X^T AX}$ is positive, where $\mathbf{X}$ is any column vector.

[2] If we strike out equal numbers of rows and columns from a square matrix, the remaining elements form a minor of the original matrix. When the struck out rows and columns also have the same indices, the resulting minor matrix is located symmetrically with respect to the main diagonal of the original matrix, we call the corresponding minor a principle minor.

Bibliography

[1] Richard A. McGinn, "Possible Futures for the Global Network," *Networked Economy Conference*, March 1997.

[2] John Litva and T. Lo, *Digital Beamforming in Wireless Communications.* 685 Canton St., Norwood, MA 02062: Artech House, Inc., 1996.

[3] S. P. Applebaum and D. J. Champman, "Adaptive Arrays with Main Beam Constraints," *IEEE Trans. on Antenna and Propagation*, vol. AP-24, pp. 650–662, September 1976.

[4] B. Widrow, P.E. Mantey, L. T. Griffiths, and B. B. Goode, "Adaptive Antenna Systems," *Proc. IEEE*, pp. 2143–2159, December 1967.

[5] L. J. Griffiths, "A Simple Adaptive Algorithm for Real-Time Processing in Antenna Arrays," *Proc. IEEE*, vol. 57, pp. 1696–1704, October 1969.

[6] B. Widrow et al, "Adaptive Noise Canceling: Principles and Applications," *Proc. IEEE*, vol. 63, pp. 1692–1716, December 1975.

[7] O. L. Frost III, "An Algorithm for Linear Constrained Adaptive Array Processing," *Proc. IEEE*, vol. 60, pp. 926–935, August 1972.

[8] L. J. Griffiths and C. W. Jim, "Alternative Approach to Linearly constrained Beamforming," *IEEE Trans. on Antenna and Propagation*, vol. AP-30, pp. 27–34, January 1982.

[9] G. V. Tsoulos, M. A. Beach, and S. C. Swales, "On the Sensitivity of the Capacity Enhancement of a TDMA System with Adaptive Multibeam Antennas," *Sixth IEEE International Symposium on Personal, Indoor and Mobile Radio Communications*, pp. 165–169, September 1995.

[10] Simon C. Swales, Mark A. Beach, David J. Edmards, "The Performance Enhancement of Multibeam Adaptive Base-Station Antennas for Cellular Land Mobile Radio Systems," *IEEE Trans. on Vehicular Technology*, vol. 39, pp. 56–66, February 1990.

[11] Y. Ogawa, Y. Nagashima, and K. Itoh, "An Adaptive Antenna System for High Speed Digital Mobile Communications ," *IEEE Trans. on Communications*, vol. E75-B, pp. 413–421, May 1992.

[12] William C. Y. Lee, "Capacity and Trunking Efficiency of Smart Antenna," *IEEE Vehicular Conference*, pp. 612–616, 1997.

[13] William C. Y. Lee, "An Optimum Solution of the Switching Beam Antenna Systems," *IEEE Vehicular Conference*, pp. 170–172, 1997.

[14] Jack H. Winters, "Adaptive Antennas for Wireless Systems," *Wireless 97 Tutorial*, July 1997.

[15] Jack H. Winters, "Signal Acquisition and Tracking with Adaptive Arrays in the Digital Mobile Radio System IS-54 with Flat Fading," *IEEE Trans. on Vehicular Technology*, vol. 42, pp. 181–188, Nov. 1993.

[16] Yingjie Li, Martin J. Feuerstein, and Douglas O. Reudink, "Performance Evaluation of a Cellular Base Station Multibeam Antenna," *IEEE Trans. on Vehicular Technology* , vol. 46, pp. 1–9, February 1997.

[17] Joseph T. Mayhan, "Adaptive Nulling with Multiple-Beam Antennas," *IEEE Trans. on Antenna and Propagation*, vol. AP-26, pp. 267–273, March 1978.

[18] B. Friedlander and B. Porat, "Performance Analysis of a Null-Steering Algorithm Based on Direction-of-Arrival Estimation," *IEEE Trans. on Acoustics, Speech, and Signal Processing*, vol. 37, pp. 461–466, April 1989.

[19] William C. Y. Lee, "An Optimum Solution of the Switching Beam Antenna Systems," *Sixth IEEE International Symposium on Personal, Indoor and Mobile Radio Communications*, pp. 170–172, September 1995.

[20] T. Matsumoto, S. Nishioka, and D. J. Hodder, "Beam-Selection Performance Analysis of a Switched Multibeam Antenna System in Mobile Communications Environments," *IEEE Trans. on Vehicular Technology*, vol. 46, pp. 10–19, February 1997.

[21] J. T. Mayhan, "Nulling Limitations for a Multiple-beam Antenna," *IEEE Trans. AP*, vol. AP-24, pp. 769–779, November 1976.

[22] Xiaoming Yu and John Litva, "Low Computational Complexity Multiuser Detection Using Multibeam Antennas," *IEEE Proceedings of VTC'98* , vol. 1, May 1998.

[23] Xiaoming Yu, Zaonian Li, Chen Wu and John Litva, "An Adaptive Multibeam Microstrip Antenna Array for PCS," *IEEE 1997 APS International Symposium and URSI Radio Science Meeting*, July 1997.

[24] Xiaoming Yu and John Litva, "A New Adaptive Antenna Array Structure for CDMA Wireless Communications," *IEEE 1996 APS International Symposium and URSI Radio Science Meeting*, pp. 172–175, July 1996.

[25] Ziaonian Li, Xiaoming Yu, Chen Wu and John Litva, "A 4-element Multibeam Microstrip Smart Antenna Array System," *IEEE 1997 APS International Symposium and URSI Radio Science Meeting* , July 1997.

[26] M. Lu, T. Lo, J. Litva, "A Physical Spatio-Temporal Model of Multipath Propagation Channels," *IEEE Vehicular Technology Conference*, pp. 108–184, 1997.

[27] S. Y. Seidel, T. S. Rappaport, "Site Specific Propagation Prediction for Wireless In Building Personal Communication System Design," *IEEE Trans. on Vehicular Technology*, vol. 43, Nov. 1994.

[28] Benjamin Rulf and Gregory A. Robertshaw, *Understanding Antennas for Radar, Communications, and Avionics.* New York, NY 10003: Vann Nostrand Reinhold Company Inc., 1987.

[29] Mischa Schwartz, William R. Bennett, and Seymour Stein, *Communication Systems and Techniques.* : McGraw-Hill Book Company, 1966.

[30] Theodore S. Rappaport, *Wireless Communications: Principles and Practice.* Upper Saddle River, NJ 07458: Prentice Hall, 1995.

[31] Jorgen B. Andersen, Theodore S. Rappaport, and Susumu Yoshida, "Propagation Measurements and Models for Wireless Communications Channel," *IEEE Communications Magazine*, pp. 42–49, January 1995.

[32] Richard C. French, "The Effect of Fading and Shadowing on Channel Reuse in Mobile Radio," *IEEE Trans. on Vehicular Technology*, vol. VT-28, pp. 171–181, August 1979.

[33] Fumio Ikegami and Susumu Yoshida, "Analysis of Multipath Propagation Structure in Urban Mobile Radio Environments," *IEEE Trans. on Antennas and Propagation*, vol. 4, pp. 531–537, July 1980.

[34] Nadia S. Adawi, Henry L. Bertoni, Joseph R. Child, William A. Daniel, John E. Dettra, Robert P. Eckert, Earl H. Flath, Robert T. Forrest, William C. Y. Lee, Samuel R. Mcconoughey, John P. Murray, Herbert Sachs, George L. Schrenk, Neal H. Shepherd, and Floyd D. shipley, "Coverage Prediction for Mobile Radio Systems Operating in the 800/900 MHZ Frequency Range," *IEEE Trans on VTC*, vol. 37, pp. 3–72, February 1988.

[35] J. D. Parsons, *The Mobile Radio Propagation Channel.* New York: Halsted Press, 1992.

[36] Simon Haykin, *An Introduction to Analog and Digital Communications.* : John Wiley & Sons, Inc., 1989.

[37] J. J. Blanz, Al Klein, and W. Mohr, "Measurement-Based Parameter Adaptation of Wideband Spatial Mobile Radio Channel Models," *IEEE Fourth International Symposium on Spread Spectrum Techniques and Applications*, pp. 91–97, 1996.

[38] J. Fuhl, J.P. Rossi, and E. Bonek, "High Resolution 3-D Direction-of-Arrival Determination for Urban Mobile Radio," *IEEE Trans. on Antennas and Propagation*, vol. 45, pp. 672–681, April 1997.

[39] A. Klein and W. Mohr, "A Statistical Wideband Mobile Radio Channel Model Including the Direction of Arrival," *IEEE Fourth International Symposium on Spread Spectrum Techniques and Applications*, pp. 102–106, 1996.

[40] Q. Spencer, M. Rice, B. Jeffs, M. Jensen, "Indoor Wideband Time/Angle of Arrival Multipath Propagation Results," *IEEE Vehicular Technology Conference*, pp. 1410–1414, 1997.

[41] R. A. Valenzuela, "A Ray Tracing Approach for Predicting Indoor Wireless Transmission," *IEEE Vehicular Technology Conference*, pp. 214–218, 1993.

[42] William C. Jakes, Jr., et al, *Microwave Mobile Communications.* : John Wiley & Sons, Inc., 1974.

[43] Joseph C. Liberti and Theodore S. Rappaport, "A Geometrically Based Model for Line-of-sight Multipath Radio Channels," *IEEE Conference on Vehicular Technology*, pp. 844–848, 1996.

[44] Joseph C. Liberti and Theodore S. Rappaport, "Analysis of CDMA Cellular Radio Systems Employing Adaptive Antennas in Multipath Environments," *IEEE Conference on Vehicular Technology*, pp. 1076–1080, 1996.

[45] Michael C. Lawton and J. P. McGeehan, "The Application of a Deterministic Ray Launching Algorithm for the Prediction of Radio Channel Characteristics in Small-Cell Environments," *IEEE Trans. on Vehicular Technology*, vol. 43, pp. 955–968, November 1994.

[46] K. R. Schauback, N. J. Davis, and T. S. Rappaport, "A Ray Tracing Method for Predicting Path Loss and Delay in Microcellular Environments," *Proc. 1992 IEEE Vehicular Technology Conference*, pp. 932–935, May 1992.

[47] D. C. Cox, "Delay Doppler Characteristics of Multipath Propagation at 910 MHz in a Suburban Mobile Radio Environment," *IEEE Trans. Antennas and Propagation*, vol. 20, pp. 625–634, September 1972.

[48] W.C.Y.Lee, *Mobile Communications Engineering.* : New York: McGraw-Hill, 1982.

[49] R. Price and P.E. Green, "A Communication Technique for Multipath Channels," *Proc. of the IRE*, vol. 46, pp. 555–570, March 1958.

[50] R. C. Hansen, *Phased Array Antennas.* : John Wiley & Sons, Inc., 1997.

[51] Barry D. Van Veen and Kevin M. Buckley, "Beamforming: A Versatile Approach to Spatial Filtering," *IEEE ASSP Magazine*, pp. 4–24, April.

[52] S. Haykin, Editor, *Array Signal Processing.* : Prentice-Hall, Inc., 1985.

[53] R. Valentin, H.-G. Giloi, and K. Metzger, "More on Angle Diversity for Digital Radio Links," *Proc. of IEEE Globecom 90*, pp. 812–816, December 1990.

[54] G. D. Alley, C. H. Bianchi, and W. A. Robinson , "Angle Diversity and Space Diversity Experiments on the Salton/Brawley Hop," *Proc. of IEEE Globecom 90*, pp. 778–790, December 1990.

[55] Thomas Eng, Ning Kong, and Laurence Milstein, "Comparison of Diversity Combining Techniques for Rayleigh-Fading Channels," *IEEE Trans. on Communications*, vol. 44, pp. 1117–1128, September 1996.

[56] Rodney Vaughan and J. Bach Andersen, "Antenna Diversity in Mobile Communications," *IEEE Trans. on Vehicular Technology*, vol. VT-36, pp. 149–172, November 1987.

[57] S.S. Jeng, H.P. Lin, G. Xu and W.J. Vogel, "Measurements of Spatial Signature of an Antenna Array," *Sixth IEEE International Symposium on Personal, Indoor and Mobile Radio Communications*, vol. 2, pp. 669–672, September 1995.

[58] Ayman F. Naguib, "Adaptive Antennas for CDMA Wireless Networks," *PhD dissertation, Standford University*, 1996.

[59] A. J. Paulraj and C. B. Papadias, "Space-Time Processing for Wireless Communications," *IEEE Signal Processing Magazine*, pp. 49–83, November 1997.

[60] D. Gerlach and A. Paulraj, "Adaptive Transmitting Antenna Arrays with Feedback," *IEEE Signal Processing Letters*, vol. 1, pp. 150–152, October 1994.

[61] A.M. Saleh and R.A. Valenzuela, "A Statistical Model for Indoor Multipath Propagation," *IEEE Journal on Selected Areas in Communications*, vol. SAC-5, Feb. 1987.

[62] John G. Proakis and Masoud Salehi, *Communication Systems Engineering.* Englewood Cliffs, New Jersey 07632: Prentice-Hall, Inc., 1994.

[63] Shahid U. H. Qureshi, "Adaptive Equalization," *Proceedings of the IEEE*, vol. 73, pp. 1349–1387, Septemberr 1985.

[64] Philip Balaban and Jack Salz, "Optimum Diversity Combining and Equalization in Digital Data Transmission with Applications to Cellular Mobile Radio – Part I: Theoretical Considerations," *IEEE Trans. Communications*, vol. 40, pp. 885–894, May 1992.

[65] W.C.Y. Lee, "Overview of Cellular CDMA," *IEEE Trans. Vehic. Tech.*, vol. 40, pp. 291–302, May 1991.

[66] K. S. Gilhousen et al., "On the Capacity of a Cellular CDMA System," *IEEE Trans. Vehic. Tech.*, vol. 2, pp. 303–12, May 1991.

[67] ITU, "IMT 2000 [Online]," *http://www.itu.int/imt/1-info/articles/brochure/index.html*, 1999.

[68] Alexandra Duel-Hallen, Jack Holtzman, and Zoran Zvonar, "Multiuser Detection for CDMA Systems," *IEEE Personal Communications*, pp. 46 – 58, April 1995.

[69] Shimon Moshavi, "Multi-User Detection for DS-CDMA Communications," *IEEE Communications Magazine*, pp. 124 – 136, October 1996.

[70] Subramamian Vasudevan and Mahesh K. Varanasi, "Optimum Diversity Combiner Based Multiuser Detection for Time-Dispersive Rician Fading CDMA Channels," *IEEE Journal on Selected Areas in Communications*, vol. 12, pp. 580–592, May 1994.

[71] Richard C. Johnson, *Antenna Engineering Handbook (Third edition).* : McGraw-Hill, Inc., 1993.

[72] Franz E. Hohn, *Elementary Matrix Algebra.* New York: The Macmilian Company, 1957.

[73] John R. Rice, *Matrix Computations and Mathematical Software.* : McGraw-Hill Book Company, 1981.

[74] Ruxandra Lupas and Sergio Verdu, "Near-Far Resistance of Multiuser Detectors in Asynchronous Channels," *IEEE Trans. on Communications*, vol. 38, pp. 496 – 508, April 1990.

[75] S. Verdu, "Minimum Probability of Error for Asynchronous Gaussian Multiple-Access Channel," *IEEE Trans. Information Theory*, vol. 32, pp. 85–96, January 1986.

[76] L. Bigler, H. P. Lin, S. S. Jeng, and G. Xu, "Experimental Direction of Arrival and Spatial Signature Measurements at 900 MHz for Smart Antenna Systems," *Proceedings of IEEE 47th Vehicular Technology Conference*, pp. 55–58, 1995.

[77] Simon Haykin, *Adaptive Filter Theory (Third Edition)*. Upper Saddle River, NJ: Prentice Hall, 1996.

[78] Gregory A. Clark, Sanjit K. Mitra, and Sydney R. Parker, "Block Implementation of Adaptive Digital Filters," *IEEE Trans. on Circuits and Systems*, vol. CAS-28, pp. 584–592, June 1981.

[79] Philip E. Gill, *Numerical Linear Algebra and Optimization*. Readwood City, CA: Addison-Wesley Publishing Company, 1991.